

RSC Advances



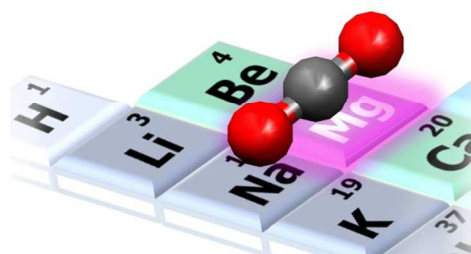
This is an *Accepted Manuscript*, which has been through the Royal Society of Chemistry peer review process and has been accepted for publication.

Accepted Manuscripts are published online shortly after acceptance, before technical editing, formatting and proof reading. Using this free service, authors can make their results available to the community, in citable form, before we publish the edited article. This *Accepted Manuscript* will be replaced by the edited, formatted and paginated article as soon as this is available.

You can find more information about *Accepted Manuscripts* in the [Information for Authors](#).

Please note that technical editing may introduce minor changes to the text and/or graphics, which may alter content. The journal's standard [Terms & Conditions](#) and the [Ethical guidelines](#) still apply. In no event shall the Royal Society of Chemistry be held responsible for any errors or omissions in this *Accepted Manuscript* or any consequences arising from the use of any information it contains.

Graphical abstract



Magnesium is used as leitmotif in this review in order to explore the systems involved in natural and artificial CO₂ cycles.

5

Cite this: DOI: 10.1039/c0xx00000x

www.rsc.org/xxxxxx

REVIEW

Magnesium-based systems for carbon dioxide capture, storage and recycling: from leaves to synthetic nanostructured materials

Jenny G. Vitillo*^a

Received (in XXX, XXX) Xth XXXXXXXXX 20XX, Accepted Xth XXXXXXXXX 20XX

DOI: 10.1039/b000000x

Steep rise of carbon dioxide level in the atmosphere is one of the main causes of global warming. This increase is ascribed to the fact that, since the beginning of industrial revolution, natural processes for CO₂ sequestration are no more able to cope with the excess of CO₂ produced by anthropogenic activities. In the recent years, research has been focused on defining artificial CO₂ cycles to support the natural one.

Element magnesium is used in this review as *leitmotif* to explore the majority of systems involved in any step of natural and artificial CO₂ cycles (separation, storage, sequestration or recycling). Magnesium is in fact ubiquitous, being present in the mesosphere as global layers, on the Earth surface in the most important enzyme for carbon fixation (Rubisco) and in silicates, that constitute the most part of rocks, where CO₂ is sequestered through natural weathering. For what concerns synthetic materials, zeolites, metal-supported particles and metal-organic frameworks are only few of the systems considered in literature. The intent of this review is to connect different fields of study to create an interdisciplinary review in the chemistry domain. Research outlooks are suggested for the different fields. In the end, a qualitative analysis of the advantages and limits of different processes and a rough estimate of their potential are given in terms of the time needed to reduce the atmospheric CO₂ level. Although economical, political and health evaluations would be also necessary, this analysis indicates that forestation could be the possible winning solution in the short-middle term for lowering atmospheric CO₂ concentration.

1. Introduction

Carbon dioxide is the most abundant greenhouse gas in the terrestrial atmosphere. Its presence keeps the Earth from being a cold rock in space. Moreover, CO₂ is also of paramount importance being at the basis of essential processes such as photosynthesis. Since 1750 (that is at the beginning of the Industrial Revolution) a steep and continuous increase of its atmospheric level has occurred, after 10,000 years of constant concentration (see Figure 1).^{1, 2} This phenomenon has a well established anthropogenic origin and can be mainly related to fossil fuels combustion (73.8%), agriculture and deforestation (22.6%) and other sources (3.6%).³ In 265 years, CO₂ concentration in the atmosphere increased from pre-industrial 280 to the present day 400 ppmv, corresponding to an excess of about $9 \cdot 10^{14}$ kg of CO₂ (900 metric gigatons).⁴ It is noteworthy that the last part of the plot reported in Figure 1b shows an almost linear dependence of CO₂ level with time. If a linear fitting of those data is performed, the following relationship is obtained:

$$[\text{CO}_2] = 17.084t - 2615.0$$

($r^2 = 0.98$), where [CO₂] is the atmospheric CO₂ concentration in

ppmv and t is the time expressed as the AD year. This allows to predict a value as high as 445 ppmv in 2050. If the data reported in Figure 1b are compared with the ones reported in part a of the same figure, it would be evident that in the past 420,000 years such a high value was never reached, being [CO₂] values always lower than 300 ppmv.¹ Figure 1a also reports the surface temperature profile of the past 420,000 years in Antarctica, as in Ref. 1. The temperature values are referred to the average temperature in 1950. A strong and direct correlation between the concentration of CO₂ and the temperature is evident,^{1, 5} with a short delay between the variation in [CO₂] and the corresponding change in temperature ΔT . Linear fitting of those data gives the phenomenological equation:

$$\Delta T = 0.092 [\text{CO}_2] - 25.7$$

($r^2 = 0.75$), where [CO₂] is in ppmv and ΔT in °C (referring to the value recorded in 1950). According to this equation, the actual [CO₂] value (400 ppmv) would correspond to a huge increase of 11.1°C in the Earth's average temperature, eventually with an unknown time delay.

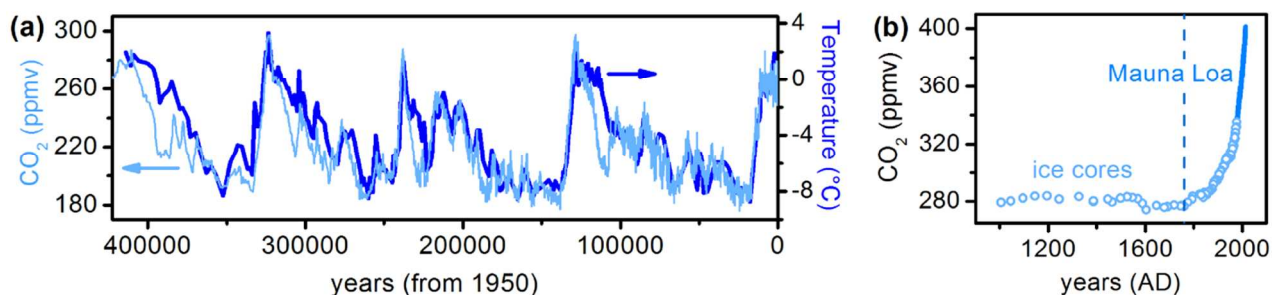
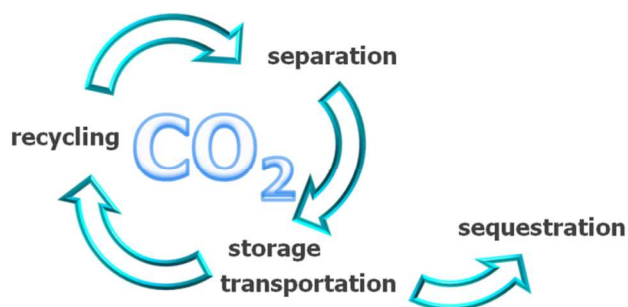


Figure 1 (a) Atmospheric CO₂ profile and surface temperature change with respect to the value recorded in 1950 in the past 420,000 years in Antarctica, accordingly to the Vostok ice cores recording. Data as reported in Ref. 1. (b) Atmospheric CO₂ concentration dependence with time accordingly to data recorded on Vostok ice cores¹ (light blue circles) and directly measured from atmosphere at the Mauna Loa observatory (blue solid line).² The perfect accordance between the two sets of data is evident. The dashed vertical line indicates the beginning of the industrial revolution.

More precise climate model simulations, although differing in the absolute value of ΔT , all accordingly predict an increase in the planet temperature, as already occurring. Contemporaneously, other related global changes have been verified in a cause-effect cascade, e.g. the raise in global sea level ($3.18 \pm 0.4 \text{ mm} \cdot \text{year}^{-1}$),⁶ and an increase in the frequency of extreme weather events (floods, hurricanes, ...).⁷ It is evident that a further increase in carbon dioxide concentration would make these events even more drastic. On the other hand, the immediate stop of the anthropogenic CO₂ emissions would require a drastic technological downgrade that is neither possible, nor acceptable. In order to help in the visualization of the enormity of the CO₂ amount already present in excess in the atmosphere, three different pictorial representations are reported in Figure 2 (see ESI for details). This amount would correspond to about: (i) 255 000 bottles of liquid CO₂ having the size of the Empire State Building (Figure 2a); (ii) the CO₂ fixed in the wood of a forest covering the entire Earth surface (Figure 2b); (iii) twenty mountains of magnesium carbonate having the size of Monviso (Figure 2c). It is evident that just the capture of this amount would represent a pharaonic project. The ineluctable dependence of humankind from fossil fuels which is likely to continue in the future decades makes the prospect even worse. *Adapt, mitigate or ignore?* was the provocative question made by Sir David King in one of its famous articles,⁷ as the three possible alternative in front of a problem that seems without an easy solution. Following the need to *mitigate*, the research community is deeply engaged in the search for substitute energetic routes or more efficient energy management aimed to lower or eliminate the equation implicit in the use of fossil fuels: Energy = CO₂ emission. At the same time, research addresses the definition of efficient artificial flows in the CO₂ cycles, aimed to support the natural ones (see Scheme 1).

This artificial CO₂ cycle is constituted by three steps: (i) separation, where CO₂ is separated from air⁸ or from flue gases of stationary point sources (e.g. coal-fired power plants); (ii) short term storage and/or transportation of CO₂,⁹ (iii) long term storage (sequestration) in general in a subterranean or submarine storage site (CCS process).¹⁰ However, an excess of 900 Gtons of CO₂ can be also taken as an opportunity, considering carbon dioxide as a C1 feedstock, cheap and everywhere abundant. CO₂ recycling (CCU process), as an alternative to sequestration, constitutes an appealing strategy, allowing the transformation of a “problem” in valuable chemicals, e.g. the transformation of CO₂

in fuels. It is evident that it is mandatory in this case differentiating the number of possible CO₂-based reactions (and then of products). In fact, the amount of available CO₂ is so large that any single chemical would fast saturate the market.¹¹ This is a very important research field, being at present only a small fraction of the CO₂ recycled.¹¹⁻¹⁶



Scheme 1. CO₂ cycle.

It is crucial to keep in mind that the amount of the materials that will be employed significantly in the CO₂ cycle would have to be approximately of a similar order of magnitude of the excess of CO₂ itself. Systems composed in large part of rare or costly elements will not be applicable on a global scale. Magnesium is the fourth most common element in the Earth's crust, making up 13.9% of the planet mass. It is then a good choice as fundamental constituent for materials to be used with this aim. In literature, magnesium based systems have been reported for each of the CO₂ cycle steps. Some of them showed superior performances with respect to any other material of their class, especially in applications that require a high affinity of the material for CO₂, such as gas separation and catalysis. It should be noted that Rubisco, the enzyme at the basis of the most important carbon dioxide recycling process on Earth, that is carbon fixation in plants, is a Mg-based enzyme.

In the following, a general description of the CO₂ molecule and of the different strategies adopted in CO₂ separation and recycling will be presented. Mg-based representatives of the different classes of materials will be reviewed along with their applications in the different steps of the CO₂ cycle: enzymes, Grignard reactants, metal-organic frameworks (MOFs), metal surfaces, Mg-O based oxides, zeolites, clays, hydroxides, silicates, and hydrides.

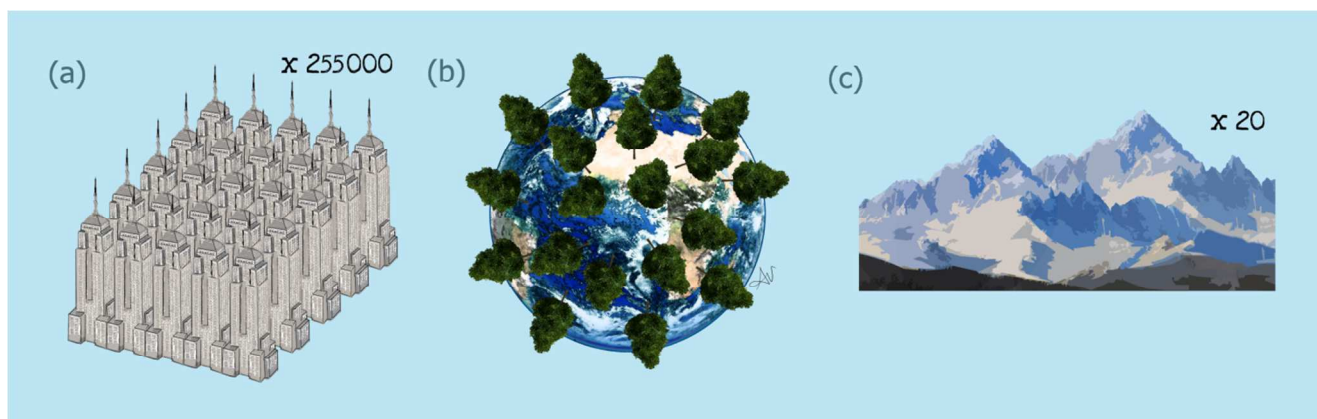


Figure 2. Pictorial representations aimed to help in the visualization of the excess amount of CO₂ present in the atmosphere in 2015: (a) 255 000 bottles of CO₂ liquid having the size of the Empire State Building; (b) the CO₂ fixed in the wood of a two years old forest covering the entire Earth surface; (c) twenty mountains of magnesium carbonate having the size of Monviso (height 3842 m).

For each of these systems, a description of their structure and of the mechanism and energetics of the interaction with CO₂ will be presented, when possible, along with a review of their performances. The factors at the basis of the suitability of Mg²⁺ materials for interaction with CO₂ will be also discussed. In the conclusions, outlooks on the future research on materials have been reported. A qualitative analysis of the systems proposed for the capture of atmospheric CO₂ is also shown, with the aim to individuate a possible solution for the mitigation of CO₂ level in the short-middle term.

2. CO₂

2.1. The CO₂ molecule

Carbon dioxide is a linear molecule characterized by a significant quadrupolar moment (see Table 3). Its electrostatic potential can be qualitatively described like a positive doughnut in the C plane with two negative lobes on the molecular axis (see Figure 9a). CO₂ can then act both as a Lewis acid and Lewis base on pure electrostatic basis, interacting in a side-on geometry through a direct interaction with C with negative charges,¹⁸ whereas in the case of positive charges end-on adducts through one O are formed.¹⁷ However, experiments and calculations converge in indicating that adsorption is a complex interplay of dispersion forces and electrostatics, favoring cooperative adsorption based on the interaction through both the C and O atoms with the material. This means that CO₂ adsorption and activation are favored on surfaces where strong Lewis acid-base couples are present, as for example on oxide surfaces. It is then evident that favoring intermolecular interactions between CO₂ molecules (that is between quadrupoles) is beneficial on the CO₂ capacity of materials.¹⁹

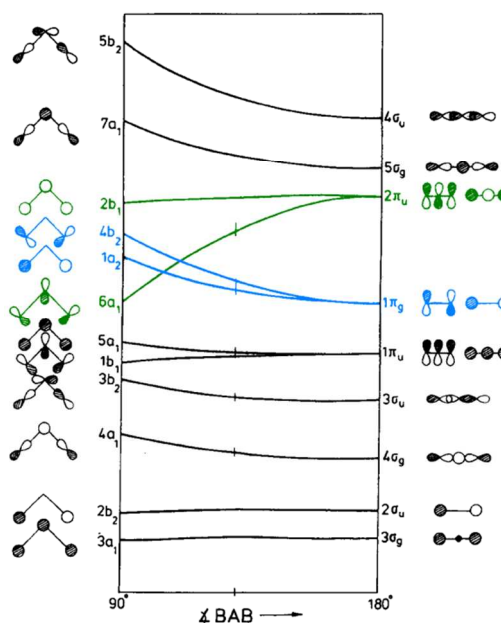
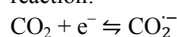


Figure 3. Walsh diagram of CO₂ orbital energies in linear (right) and bent geometries (left). HOMO and LUMO levels have been signaled by light blue and green colors, respectively. Adapted from Ref. 12. Reproduced with permission. Copyright Elsevier 1996.

Several geometries of coordination on surfaces are possible (see for example Figure 12 and Section 4.6 for further details), which nature can determine different reaction paths. These species can be identified through the use of spectroscopies, such as ¹³C nuclear magnetic resonance (NMR),^{20, 21} and infrared (IR) spectroscopies.²² For what concerns IR spectroscopy, carbon dioxide is characterized by three vibrational modes: the IR-inactive symmetric stretching mode $\tilde{\nu}_1$ (1388.3 cm⁻¹ for ¹²CO₂ gas),²³ the doubly degenerated bending vibration $\tilde{\nu}_2$ (667.3 cm⁻¹)²³ and the asymmetric stretching mode $\tilde{\nu}_3$ (2349.3 cm⁻¹).²³ Upon interaction with the materials, these modes are only slightly shifted, even when highly charged species are present.²³ The shift of the CO₂ vibrations upon adsorption gives some insight into the adsorption geometry and the nature of the adsorption site. The

presence of a negative charge, although leaving identical (and elongated) the two C=O bonds, causes a change in the $\angle\text{OCO}$ angle: this corresponds to the decrease of the $\tilde{\nu}_3$ mode and to the removal of the degeneracy for the $\tilde{\nu}_2$ mode. On the contrary, in the case of adsorption on a positive charge the molecule is still linear but the two C=O bond are no more identical: the C-O bond adjacent to the cation lengthens slightly whereas the other C-O bond shortens of almost the same amount.²³ This spectroscopically corresponds to an increase of the asymmetric stretching mode frequency.²⁴ It is important to remind at this point that if the adsorption in a microporous material is considered, a strong matrix confinement effect is observed on the vibrational modes of CO₂ because of its significant quadrupole moment.²³ A shift in the $\tilde{\nu}_3$ mode to 2338 cm⁻¹ has been estimated for the unperturbed molecule in microporous materials due to confinement.¹⁷ If chemical bonded species are formed, signals in the 1800-800 cm⁻¹ region are observed, the position of which bands is indicative not only of the nature of the formed species but also of the geometry of coordination.^{12, 22} A comprehensive review of the characterization by infrared spectroscopy of CO₂ surface species on oxide surfaces is reported in Ref. 22.

First step in reactions involving CO₂ is its activation, that in all cases asks for the formation of a CO₂⁻ anion with a change from the linear to a bent geometry.¹² More precisely, dissociation of CO₂ likely happens through the formation of a Freund-Messmer anionic complex (CO₂⁻...CO₂), that is through an intermediate CO₂^{δ-} state. The factors that influence the formation of chemisorbed CO₂ species are: (i) the electronic configuration of the system; (ii) its work function (as a measure for the ease electron transfer); (iii) the influence of local geometry.¹² The change in the CO₂⁻ geometry from the linearity of the neutral CO₂ can be explained by considering the qualitative scheme reported in Ref. 12, showing the molecular orbitals of CO₂ for both the linear and bent configurations (Figure 3). The HOMO (light blue) and the LUMO (green) orbitals are indicated with colors to facilitate their identification. It is clear that moving from linear to bent configuration, π -orbitals show the most pronounced alterations in energies with a split of all the degeneracies.¹² The perturbation is particularly important for HOMO and LUMO: upon bending, the inversion in stability of one of LUMO orbitals (the $2\pi_u-6a_1$ one) with respect to the HOMO ones is observed. The occupation of this $2\pi_u-6a_1$ orbital by the electron transferred from the surface determines the bond angle.¹² Gas phase measurements indicate that the average C-O bond order in CO₂⁻ is only 1.5 as compared to 2 in neutral CO₂.¹² This is in line with the larger C-O distance (1.24 versus 1.15 Å in neutral CO₂) and the smaller bond enthalpy of C-O in CO₂⁻ with respect to CO₂, making the anionic form more unstable upon dissociation.¹² The formation of this anionic species is a strong rate determining step in reactions involving CO₂. The potential associated to the reaction:



is estimated to be of -2.1 V versus normal hydrogen electrode.¹⁵ It is evident that in absence of promoters (as protons in the solution¹⁵ or basic agent on surfaces) this electron transfer will unlikely happens.²⁵

2.2. CO₂ recycling

The use of CO₂ as chemical feedstock was¹² in 1996, and still nowadays is limited to few industrial processes:¹⁴ synthesis of urea and its derivatives, salicylic acid and carbonates. Only 128 Mt per year of CO₂ are in fact utilized in industry.¹⁴ This low exploitation of CO₂ as reagent is due to two main factors: the low efficiency of the catalysts and the high CO₂ cost. In fact, although it is in general claimed in academic literature that CO₂ is a highly abundant and cheap reactive, it is important to remind that it is rarely present as pure in nature and the separation cost is energetically demanding.¹⁵ Actually, CO₂ is expensive because its separation cost is high and this is the main reason for the absence of a particular interest on CO₂ on the industrial point of view.¹⁵ Nevertheless the CO₂ emission restrictions due to Kyoto protocol can push towards the use of CO₂ as reagent, by creation of a market for the separated CO₂.

Table 1. Review of some important reactions involving CO₂ as reagent for which Mg-based materials have been reported as catalysts or as co-reagents.

Reactions	name	ΔH (kJ mol ⁻¹) ^a	Ref.	n.
CO ₂ + H ₂ ⇌ CO + H ₂ O (g)	reverse water gas shift (RWGS)	+41.2	14	[1]
CO ₂ + H ₂ ⇌ CO + H ₂ O (l)		-2.8	12	[1]bis
CO ₂ + 4H ₂ ⇌ CH ₄ + 2H ₂ O	methanation of carbon dioxide or Sabatier reaction	-164.9	26	[2]
CO ₂ + 3H ₂ ⇌ CH ₃ OH + H ₂ O	synthesis of methanol	-49.5	14	[3]
CO ₂ + H ₂ ⇌ HCOOH	formic acid synthesis	-31.8	27	[4]
CH ₄ + CO ₂ ⇌ 2CO + 2H ₂	dry reforming of methane	+247	28	[5]
CH ₄ + CO ₂ ⇌ CH ₃ COOH	carboxylation of methane	-16.6	15	[6]
C ₆ H ₆ + CO ₂ ⇌ C ₆ H ₅ COOH	carboxylation of benzene	-40.7	15	[7]
2 MeOH + CO ₂ ⇌ CH ₃ COCH ₃ + H ₂ O	carboxylation of methanol	-27.9	29	[8]
Mg(OH) ₂ + CO ₂ ⇌ MgCO ₃ + H ₂ O	carbonation	-19.7	30	[9]
MgO + CO ₂ ⇌ MgCO ₃	carbonation	-100.9	30	[10]
MgSiO ₃ + CO ₂ ⇌ MgCO ₃ + SiO ₂	carbonation of pyroxene	-81	31	[11]
$\frac{1}{3}\text{Mg}_3\text{Si}_2\text{O}_3(\text{OH})_4 + \text{CO}_2$ ⇌ MgCO ₃ + $\frac{2}{3}\text{SiO}_2 + \frac{2}{3}\text{H}_2\text{O}$	carbonation of chrysotile	-35	31	[12]
$\frac{1}{3}\text{Mg}_3\text{Al}_2\text{Si}_3\text{O}_{12} + \text{CO}_2$ ⇌ MgCO ₃ + SiO ₂ + $\frac{1}{3}\text{Al}_2\text{O}_3$	carbonation of pyrope (garnet)	-92	31	[13]

^aReaction enthalpies at 298 K.

In addition to that, CO₂ is often described as a molecule with a low reactivity. This is not always the case, being for example, a selective oxidant towards hydrocarbons.¹⁵ Moreover, most of the reactions are favorable on the thermodynamic point of view (see Table 1: the entropic term gives a little contribution to the Gibbs free energy so that ΔH is a good guide to thermodynamic feasibility of those reactions).¹² The reason of the low reactivity

reputation has a kinetics origin and relies on the high energy needed for the formation of the intermediate anionic species.¹² Additionally, if the reaction requires the breaking of a C-O bond, substantial energy has to be supplied for its cleavage,¹² making the activation of CO₂ the main rate determining step in both natural and artificial processes.

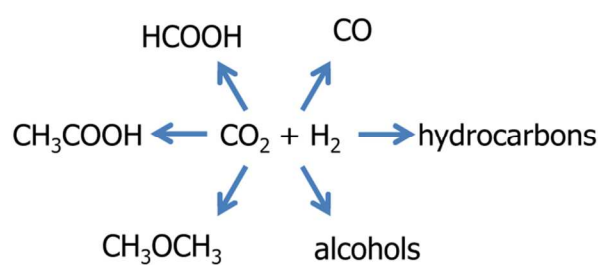
All the reactions involving CO₂ can be divided in two groups: (ia) reactions where CO₂ is inserted as a whole in the products and (iia) reactions that require to break one or more carbon-oxygen bond. Another classification, only in part coincident with the previous one, separates the reactions between (ib) reactions leaving unchanged the oxidation state of carbon and (iib) reactions where CO₂ reduction is required. In both cases, the second group of reactions asks more energy than the first group.

It is interesting to notice that the most important reactions aimed to carbon fixation in nature, that is the ones catalyzed by Rubisco and PEPC enzymes, belong to the (ia) group (see Section 4.1). Moreover, in general larger the change in the oxidation state, larger the activation energy (E_a), and then slower kinetics of reaction are expected.¹⁵ For example, in methanation reaction (that requires the largest change in the oxidation state of carbon from +4 to -4) an E_a of 106.9 ± 0.5 kJ mol⁻¹ has been reported for the reaction catalyzed by Pd/Mg-SiO₂,³² whereas CO formation (change from +4 to +2) has an apparent activation energy of only 52.7 ± 0.2 kJ mol⁻¹. This last statement is not always true: for example in gas phase complexes of CO₂ with Ti the insertion of the metal in one C=O bond was observed without energetic barrier.³³ CO₂ is also dissociatively chemisorbed with the formation of surface carbide and oxide on Mo surfaces already at RT.¹²

Among all the possible reactions involving CO₂,^{13, 15} the discussion will be restricted in the following to hydrogenation reactions (reactions [1]-[4] in Table 1), methane reforming (reaction [5]), carboxylation of methanol (reaction [8]) and inorganic carbonation (reactions [9]-[13]). It is important to stress that the reactions involving CH₄/CO₂ and CO₂/H₂ mixtures can represent alternatives to separation processes, when possible.

2.2.1. Hydrogenation reactions

Reaction of CO₂ with H₂ can bring to the formation of very different products:¹⁴ CO, methane, alcohols, formic acid, hydrocarbons, dimethyl ether, etc. (see Scheme 2). Although free H₂ is not available in significant amounts on Earth, H₂ can be produced in several processes. Among them, particularly interesting are those related to renewable sources. CO₂/H₂ mixtures can be produced by biomass gasification (see also Section 2.3). Moreover, in order to guarantee a continuous electricity supply, electricity excess generated in solar and wind stations is converted to hydrogen by water electrolysis. Hydrogen is then stored as hydride and converted back to electricity when needed. The possibility to exploit the hydrogen so obtained for fuel production through reaction with CO₂ constitutes a new and hot topic in the metal hydride field.²¹



Scheme 2. Hydrogenation reactions.

The formation of one among all the possible products is obviously determined by the CO₂/H₂ ratio in the gas feed and, because of the different reaction enthalpies (see Table 1), by the temperature and pressure conditions adopted. Additionally, the nature of the catalyst and any detail of its composition and preparation (calcination procedure, reduction temperature) determine the formation of one or another reaction product (see Section 4.6).¹⁴ This sensitivity can represent a big advantage for the CO₂/H₂ systems: in principle it is possible to vary the reaction path and then the products by small changes in the reaction conditions. Also the presence of small pollutants in the gas feed can be determinant on the reaction path.¹⁴ Nevertheless, this also clearly indicates that each of these reactions can constitute a side reaction for each of the others. Both homogeneous and heterogeneous catalysts have been reported to be active in CO₂ hydrogenation,¹⁴ allowing the formation of very different reaction products. Among the heterogeneous catalysts, metals, crystalline oxides (perovskite and pyroclones) and metal particles supported on oxides and carbons have been reported. Although for all these reactions, the reaction mechanism is nowadays unknown, the combination of the results reported so far in literature allows to identify some common points, that are here summarize in the following ten bullet points.

(i) The rate determining step in all these reactions is the CO₂ activation. For example, activation energies for reactions [1] and [2] on Ni(100) surface have very similar values:³⁴ 88.7 for [2] and 72.8-82.4 kJ mol⁻¹ for [1]. This allows to suppose that their rate determining step is common. Moreover, hydrogenation/dehydrogenation on metal particles is known to be a relatively fast process. The formation of methane or CO will be then determined by the mobility of the H species on the surface. The reaction would proceed to the formation of methane if hydrogen is fast dissociated and can move easily on the surface towards the carbonate species (and/or viceversa).³⁵ On the contrary CO is released (see Section 4.6.2 and 4.9).

(ii) Catalysts for these reactions are in almost the totality of the cases, metal particles supported on oxides, where the metals are transition metals active in hydrogen splitting.

(iii) On supported metal particle catalysts, the reaction is a dual site one if the oxidic support is acidic or basic in nature, whereas it is single site one if the support is inert (e.g. SiO₂, carbon). In dual site reactions, hydrogen is dissociated on the metal particles, whereas CO₂ is activated on the oxidic system through the formation of formate (acidic oxides) or carbonate/carboxylic species (basic oxides). The recombination of the two units happens at the boundary between the metal particle and the oxide surface. The metal particles participate significantly to the

decomposition of CO₂ only if supported on inert support and if they are suitable for doing it: e.g. Rh is able to activate CO₂, whereas Ni and Pt are not.²⁸

(iv) Ni, Cu and Fe-based catalysts are the most widely used catalysts in industry, although they suffer of a large sensitivity to impurities in the gas feed and to side products. Noble metals are on the contrary more active and characterized by a larger stability but their high cost makes impractical their large use. This means that, although largely academical studied, their large application on the industrial point of view would be hindered by economical issues.

(v) Addition of small amount of basic ions as promoters to the catalyst composition facilitates the activation of CO₂ and reduces coke formation.

(vi) The catalyst preparation strongly influences the dimension and distribution of the metal particles, parameters that have a direct influence on the reaction path. To truly compare the different supports and metals by using literature results, attention have to be paid to the different preparation methods that can originate different aggregation of the metal particles making difficult or even impossible the evaluation.

(vii) Often a catalyst able to work for one of the hydrogenation reaction can be used for another.

(viii) High dispersion of the metal particles is suitable to enhance reaction kinetics. Nevertheless, dimensions lower than 100 Å have to be avoided because they can be more easily poisoned by impurities in the gas feed and by coke formation.

(ix) Choice of the suitable support is very important *in primis* because it determines the particle size, composition and dispersion. CO chemisorption and EXAFS study³⁶ on supported 0.5% Rh on TiO₂, MgO, SiO₂, MCM-41 and γ -Al₂O₃, showed that the metal dispersion strongly depends upon support, increasing in the order: TiO₂ < La₂O₃ < CeO₂ < ZrO₂ < MgO < SiO₂ < MCM-41 < γ -Al₂O₃. Moreover, in the same study a change in the oxidation state of Rh was observed from metallic to cationic on TiO₂ and γ -Al₂O₃, respectively.³⁶

(x) Supports with a high oxygen mobility are preferred because they facilitate coke oxidation.

Among all the hydrogenation reactions, the most important ones can be identified in the reverse water gas shift¹⁴ (RWGS, reaction [1] in Table 1), the methanation of CO₂ (Sabatier reaction, [2]), the methanol synthesis [3]³⁵ and hydrocarbon synthesis.

Sabatier reaction. The hydrogenation of CO₂ can proceed through further steps of hydrogenation or can have as only product the fully hydrogenation product of CO₂, that is methane. Sabatier reaction is a highly efficient and highly exothermic reaction ($\Delta H_{298K} = -165 \text{ kJ mol}^{-1}$), when carried out at temperature lower than 200°C in an industrial process.³⁷ This because of catalysts that allow to efficiently overcome the kinetic limitations due to the change from +4 to -4 in the oxidation state of carbon. Research in this field is concentrated on how to increase the lifecycle of the largely used Ni-based catalysts, that are easily deactivated by the formation of stable carbonyls. The economic issue for the synthetic methane is however represented mainly by the hydrogen production cost.³⁵ Nevertheless, the huge and increasing availability of methane from natural sources would make more valid (on the environmental point of view) to

purify methane from these sources or to reform it than to synthesize it (see Section 2.2.2 and 2.3). A concrete application of the Sabatier reaction could be instead to use it to increase the methane concentration in biogas by using hydrogen from renewables.³⁵ Other applications are related to space program for Mars colonization, where the Sabatier reaction would allow the easy production of a fuel and water.^{14, 38, 39}

Reverse water gas shift. RWGS, being an endothermic reaction,¹⁴ is often present as side reaction wherever CO₂ and H₂ are present together in the reaction mixture. Its efficiency increases at high temperature (about 600°C) or in presence of highly exothermic reactions, causing the poisoning of the catalysts, e.g. of Ni supported catalysts in methanation reactions. The most widely used catalysts in RWGS are copper based catalysts. However, Cu particles have a strong tendency to sinter, particularly at high temperature easily causing the deactivation of the catalysts. Addition of small amounts of other metals (e.g. Fe) have shown to increase the stability of the catalysts, also up to 120 h.¹⁴

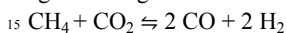
Synthesis of methanol. Methanol is a fuel and a very versatile reagent. Synthesis of methanol from CO₂/H₂ gas mixture can be obtained through the use of low reaction temperatures (250-350°C) and high pressures.¹⁴ This reaction has in general a low selectivity being accompanied by the formation of almost all the other possible products.⁴⁰ Cu/ZnO catalysts are considered the most effective catalyst for methanol formation, although the low activity and stability of Cu particles create major problems for practical applications as observed for RWGS. For this reason, new supports that allow to increase Cu particle stability (as perovskites) and the use of bimetallic metal particles are the directions followed in the research. New supports able to facilitate Cu reduction are also expected to increase the reaction yields.⁴⁰ In fact, Cu is likely reduced to Cu⁰⁺ species during the reaction⁴⁰ and this is thought to be a crucial step in the reaction mechanism.⁴⁰ Formation of Cu⁺ would increase on the contrary the selectivity for the formation of CO, that is RWGS yields.⁴⁰ For this reaction, beside Cu sintering, an important cause of deactivation is due to coke formation. Although outside the scope of the present review, it is important to stress as in the studies reported on these catalysts, the ability of ZnO to split hydrogen also at RT⁴¹ is often not taken into account.

Synthesis of hydrocarbons. Synthesis of hydrocarbons from CO₂ is a two steps reaction that can involve CO or methanol as intermediates. In CO mediated reactions, Co and Fe-based catalysts are the most widely used, whereas in methanol mediated ones the catalysts adopted are the same used for methanol synthesis. For what concerns the CO-mediated synthesis, after CO formation the process continues as a classical Fisher Tropsch process. Nevertheless, direct hydrogenation of CO₂ brings to the formation of very short chain hydrocarbons with a strong preference for methane. This is due to the slow adsorption rate of CO₂ on the surface with a contemporaneous and fast dissociation and mobility of hydrogen, that favors the successive hydrogenation of intermediates.

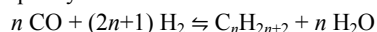
2.2.2. Methane reforming

Methane is an important renewable fuel with well know problems of storage and transportation with respect to other hydrocarbons. Moreover, in automotive it has lower performances than other

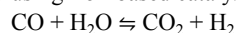
fuels as for example LPG (liquefied petroleum gas).¹⁵ Several processes have been envisaged to convert it to higher value products. Conversion to syngas (mixture of CO and H₂) is particularly interesting because it represents the feed for the Fischer-Tropsch process. For example, the conversion of natural gas (main component: methane) to syngas and then to LPG (main components: propane and butane) would be particularly appealing.¹⁵ Various technologies exist for the conversion (reforming) of methane to syngas, differing in terms of oxidant used, kinetics and energetics of the reaction but also in the final H₂/CO ratio. Among the different reforming strategies, dry reforming of methane has a 20% lower operating cost compared to other reforming processes.²⁸ This process uses CO₂ as oxidant agent through the reaction:²⁸



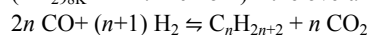
For this reason, in principle it can be directly applied to biogas, coal-seam, landfill gases or low quality natural gas, converting to syngas both the largest abundant greenhouse gases present (see Section 2.3). The syngas so obtained has in general a H₂/CO ≤ 1. A syngas with this ratio increases the selectivity of Fischer-Tropsch towards long chain hydrocarbons, that is towards higher quality fuels.²⁸ In fact if for the reaction:



the needed H₂ is produced through the water gas shift reaction using iron-based catalyst:

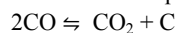


($\Delta H_{298\text{K}} = -41.2 \text{ kJ mol}^{-1}$)²⁸ the overall reaction is then:

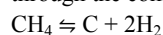


having actually a H₂/CO ≤ 1 for $n \geq 2$.²⁸ For alkanes having $n \geq 5$, pure CO₂ can be also easily recovered at the end of the reaction. The H₂/CO ratio of the syngas obtained by reforming can be tuned in the 0.5-2 range²⁸ by changing the operational conditions and the composition of the feed gas, or including the presence of H₂O and O₂ (mixed methane reforming).²⁸

Although promising, dry reforming of methane suffers of several problems: (i) high presence of side reaction products (RWGS and coke formation); (ii) endothermicity of the reaction ($\Delta H_{298\text{K}} = +247 \text{ kJ mol}^{-1}$); (iii) deactivation of the metal particles (due to sintering, reaction with the support, reaction with impurities in the gas stream, with oxygen and side reaction products). Among all these problems, coke formation is the major obstacle in dry methane reforming.^{28, 42} Coke formation is predicted by thermodynamic models to cover a very wide temperature range (black curve in Figure 4). The formation of this deposit can be due to different processes, as the Boudouard reaction:



($\Delta H_{298\text{K}} = -171 \text{ kJ mol}^{-1}$)²⁸ that is most likely to occur for temperature lower than 700°C (see Figure 4).²⁸ For these reasons, methane reforming reaction are in general carried out at high temperature (> 700°C) also in order to facilitate the oxidation of the carbon residue. Nevertheless carbon can be also formed through the complete dissociation of methane:



($\Delta H_{298\text{K}} = +75 \text{ kJ mol}^{-1}$).²⁸ In this case, the coke formation would be significant for temperature higher than 557°C (see Figure 4).²⁸

From these models it is clear that carbon formation is unavoidable for $T < 900^\circ\text{C}$. The models also indicate how low pressures of operation (about 1 bar) are essential to obtain high

conversion and high H₂/CO yields.⁴³ Nevertheless, it is interesting to notice that it has been clear since the first reports that for any catalyst and CO₂/CH₄ ratio it is possible to select appropriate temperature and pressure conditions to avoid the formation of coke.²⁸ In particular, larger CO₂/CH₄ ratio means larger concentration of the oxidant CO₂ that would allow an easier removal of the formed coke. Moreover, the use of basic promoters as Mg, facilitating CO₂ decomposition, promotes carbon oxidation. It is also important to remind that not all the carbon types are stable in the same way, being some of them more easily oxidized. Besides, the carbon formed increases in stability with the reaction time. Unfortunately Ni, the most widely used catalyst for methane dry reforming, is also an important catalyst in the synthesis of nanotubes, that are a very stable form of carbon (low H/C ratio). Ni atoms are also able to form very strong bonds with C atoms, further hindering carbon removal. For this reason, although Ni-based catalyst are widely used, they can be fast deactivated,^{28, 42} and strategies aimed to increase their stabilities are the aim of the research in this field. On the contrary, noble metal catalysts are found to be particularly resistant to carbon deposition,²⁸ but they are generally uneconomical. Because of this, in the practical use, they are only added as dopants in order to form bimetallic particles with Ni in order to hinder catalyst poisoning.²⁸ Improvements in catalysts stability have been observed upon the addition of small amounts of oxidants as O₂ and H₂O to the CO₂/CH₄ feed. The addition of O₂ showed to be particular beneficial causing contemporaneously the partial or the total combustion of methane lowering the high energy requirement for the reforming.

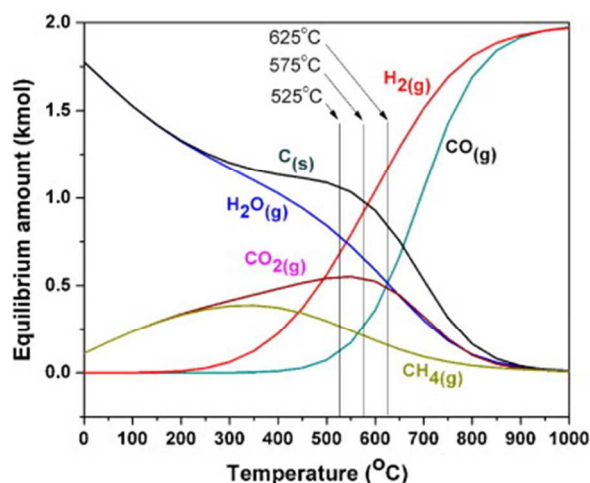


Figure 4. Thermodynamic equilibrium composition for dry methane reforming considering 1 kmol of CH₄ and 1 kmol CO₂ at 1 atm, from 0–1000°C and at inlet feed ratio of CO₂/CH₄ = 1 and including the formation of coke. These plots were created by using Gibbs free energy minimization algorithm on HSC Chemistry 7.1 software. Reproduced with permission from Ref. 44. Copyright 2013 Elsevier.

All the considerations made in Section 2.2.1 for hydrogenation catalysts are also valid for the dry reforming ones. The main difference relies in the fact that the rate determining step in dry methane reforming is the adsorption and activation of methane, that is even less reactive than CO₂ (see Table 3). In fact, the difference between the activation energies of CH₄ and CO₂

amounts to about 12 kJ mol⁻¹ in several systems. Rh is the metal for which the dissociation of CH₄ is most favorable, being observable from 150°C, that is at significantly lower temperature than other transition metals.⁴⁵ Also in this case, on a 1%Rh/MgO catalyst at 500°C, E_a of 97 kJ mol⁻¹ for CH₄ and 85 kJ mol⁻¹ for CO₂ were obtained.^{28, 45} Two mechanisms have been proposed for methane activation on metal surfaces: CH₄ direct and indirect dissociation. In both cases, the formation of intermediates as formyl or CH_x species is hypothesized, with the oxygen coming then from the support (direct) or from the oxidant (indirect).²⁸ In the first case, the surface oxygen would come from hydroxyls on acidic support and from carbonates on basic support.⁴⁶ Likely both direct and indirect processes happen depending on the temperature, being the direct process favored for $T > 550^\circ\text{C}$.⁴⁷ At $T < 550^\circ\text{C}$, CH_x species can be formed as testified by the formation of C₂H₆.⁴⁵ Activation of methane is carried out on the metal particles or at the interface between the metal and the support.^{28, 48} Activation of CO₂ happens exclusively on the support (if Rh catalyst are not used) whereas the recombination of the intermediates at the metal/support interface.²⁸ In particular it has been proposed by pulse reactions, as CH₄ would be dissociated in the first step of the reaction at the metal-oxide interface with formation of CO (in low amount) and H₂ by leaving carbon species and oxygen vacancies on the support. The reaction would then proceed on the oxygen vacancies through CO₂ dissociation to CO and oxidation of the left superficial carbon species to CO.^{49, 50}

As in hydrogenation reactions, also in this case the support plays a crucial role in the activation of CO₂, important process for both the methane reforming reaction itself and for the coke removal.²⁸ CO₂ inert supports have then to be avoided for dry reforming of methane. Both acidic (formation of formate) and basic oxides (formation of carbonate/carboxylic/bicarbonate) have been successfully adopted. Solids characterized by a high bulk oxygen conductivities and high thermal stabilities ($> 1000^\circ\text{C}$), as perovskite materials, have shown to be highly suitable catalysts, actually bringing to an efficient oxidation of the coke formed in dry methane reforming.^{28, 28}

2.2.3. Carboxylation of methanol

Every organic carbonate can be in principle transformed in any other organic carbonates.¹⁵ Among them, dimethyl carbonate is especially interesting to be a versatile reagent, used as precursor for resins and fuel additives and also as methylating and carbonylating agent.^{51, 52} Unfortunately, at present time dimethyl carbonate is synthesized by using phosgene or a highly flammable and toxic reactant mixture (CH₃OH/CO/O₂/CuCl_{cat}).^{52, 53} The most interesting route to reach linear carbonates would be the direct carboxylation of alcohols.¹⁵ There is then an important ongoing research on new catalytic systems for the direct reaction between CO₂ and alcohols in order to synthesize the corresponding carbonate compound.⁵² It has been outlined as the presence of both acidic and basic sites on the catalysts surface is an important factor in selective dimethyl carbonate synthesis (see Section 4.7.2).⁵² The proposed reaction mechanism asks for the formation of two reaction intermediates: methyl carbonate and methyl cation where the former would be formed by activation of CO₂ and MeOH on basic sites.⁵⁴ Methyl cation would instead be

formed by MeOH activation on acidic sites.^{52, 54} Dimethyl carbonate would then be formed through recombination of the intermediates. It is interesting to notice that the dimethyl carbonate synthesis gives often dimethyl ether as by products, due to decomposition of the carbonate itself. This is quite interesting being dimethyl ether, a good quality fuel for internal combustion engines.¹⁴ In particular it has been reported as the relative amount of carbonate/ether is strongly dependent upon the reaction conditions, allowing to switch from one to the other.

2.2.4. Inorganic carbonation

Carbonation is a process exploited for CO₂ separation (see Section 2.3), sequestration and recycling. Synthesis of inorganic carbonates is considered the safest and the most permanent method for carbon disposal,^{24, 31, 55} by formation of value added materials in the form of solid carbonates.²⁴ This synthetic procedure can couple the separation with the synthesis of products, lowering the cost of the process. Oxides (Section 4.6), hydroxides (4.7), carbonates⁵⁶ and silicates (4.8) have been studied in this field. Silicates (and in particular magnesium silicates) are largely natural abundant materials (they are the main constituents of the Earth's crust) and for this reason they are indicated as one of the few realistic choices between materials to be employed in the artificial CO₂ cycle.⁵⁵ They are the main constituents of the geological disposal sites walls. Unfortunately, carbonation reactions are in general characterized by very slow kinetics and by low conversion yields.^{57, 58} For separation purposes, carbonation should be carried out at high temperatures ($T > 300^\circ\text{C}$),^{11, 59} because of the high stability of the formed carbonates (see Section 4.6). Regeneration of the sorbents is then carried out by calcination at even higher temperatures. For carbon dioxide mineralization purposes, on the contrary, higher yields and lower reaction temperatures (80-150°C) are observed for reactions conducted in slurries and by the use of promoters.^{24, 57} Similar strategies aimed to enhance carbon fixation in geological sequestration sites have been also reported. Nevertheless, these methods rapidly increase the cost of the process, considered on the contrary the cheapest among the sequestration technologies (see Section 4.8.3 and Ref. 52).⁵⁵

It is noteworthy that carbonate formation is an exothermic reaction (see reactions [9]-[13] in Table 1), where the amount of heat depends strongly on the reagent used. This heat can be a large fraction (up to 46% for⁶⁰ CaO and 25% for MgO)^{61, 62} of the heat released during the combustion process forming CO₂ (393.8 kJ mol⁻¹ CO₂ for combustion of elemental carbon).^{31, 60} This means that substantial heat is liberated in the overall chemical reaction, increasing the kinetics of the carbonation process. Moreover, for sufficiently fast processes, this heat can be efficiently recovered, further lowering the overall cost of the CCS process. For example, calcium looping technologies are at present one of the most efficient technologies for CO₂ capture, although the very high temperature of reaction ($T > 700^\circ\text{C}$).⁶³⁻⁶⁵

Carbonation of dry carbonates has been also reported as a strategy to obtain chemical selective sorption of CO₂ by maintaining a low regeneration temperature.⁵⁶ In this case, separation process is carried out in presence of substantial amount of moisture in order to allow the formation of the

corresponding bicarbonate species. Bicarbonates are in general less thermally stable than the corresponding carbonates, allowing the regeneration of the system at $T < 200^\circ\text{C}$. In literature, the most studied systems are K_2CO_3 and Na_2CO_3 that are CO_2 sorbents with suitable adsorption temperatures in the 60-100°C range with the possibility to fully regenerate the system at temperatures as low as 120-200°C.⁶³ Nevertheless, analogously to what observed for the other classes of materials, the carbonation yields are far from the stoichiometric amount.⁶⁶ Dispersion on supports has been shown to be beneficial on the reaction yields.⁶⁷

2.3. CO_2 separation

CO_2 separation processes are thought to be applied to four main gas mixtures: (i) air ($\text{N}_2/\text{O}_2/\text{CO}_2$), (ii) natural gas (CO_2/CH_4), (iii) post-combustion flue gases (CO_2/N_2) and (iv) pre-combustion ones (CO_2/H_2). These separation processes differ significantly in the nature of the gases involved and in the CO_2 partial pressure, besides on the temperature and (total) pressure conditions (see Table 2). Other separation processes (e.g. CO/CO_2), having more restricted applications, would not be covered in this review.

The importance of atmospheric CO_2 capture, although its high cost (not only on the energetic point of view), will be often stress in this review. Separation from air is decidedly the most challenging among those processes, being the concentration of CO_2 very low (0.04%). Nevertheless, an efficient air capture would allow on one hand to mitigate the increase in the planet temperature and on the other, the existing fossil fuel based infrastructure to remain unaltered⁵⁵ (at least until consumption of the fossil fuel stocks). Moreover, CO_2 is three times as heavy as fuel⁵⁵ and therefore cannot be stored in cars or airplanes. CO_2 from these sources has then to be released in the atmosphere and recaptured later.⁵⁵ Methane from natural sources (biogas, coal-seam, landfill gases, cow breeding) is rarely pure. The most important impurity (amounting also to the 60% on volume) is carbon dioxide. CH_4 purification is then needed not only because CO_2 decreases the heating value of methane but essentially because CO_2 concentration higher than 5 vol.% hinders even the catalytic oxidation of methane.⁶⁸ Moreover, CO_2 concentration in natural gas has to be below 3% in volume, in order to avoid pipeline corrosion. This restriction is less important existing several materials able to store high volumetric quantities of methane at RT.^{69, 70} The huge and increasing availability of methane from natural sources and the important methane global warming potential (twenty-one time the CO_2 one) make mandatory its use. In order to understand the amount of gas coming from these natural sources, in US the methane produced in landfill gas per year amount to about the 13-20% of total US CH_4 production.²⁸ Besides the possibility to chemically convert it in syngas (see Section 2.2.2), CO_2/CH_4 mixtures can be enriched in CH_4 through the Sabatier reaction (by using renewable hydrogen, see Section 2.2.1)⁷¹ or by separation processes.

Post-combustion CO_2 separations indicate those processes that can retrofit large stationary CO_2 sources as coal-fired plants. In these case, flue gases resulting from the fuel combustion are predominantly containing N_2 with CO_2 concentrations of about 15%. Coal is currently the dominant fuel in the power sector and coal-fired plants are at present the most important CO_2 sources. Any breakthrough system in the post-combustion class would be

of paramount importance in the short middle term because it can retrofit the most largely abundant emission sites. Pre-combustion strategies, on the contrary, are thought to be applied to hydrocarbons/coal gasification plants, aimed to remove CO_2 from H_2 -rich streams before energy conversion. This process, besides lowering CO_2 emissions, enhances also the efficiency of the combustion. These processes are particularly interesting if applied to methane as in Integrated Gasification Combined Cycle plants (IGCC). It is important to stress as for what concerns post-combustion and pre-combustion processes, the temperatures reported in Table 2 are the lowest at which the separation can be carried out, being the ones at the smokestack exit. However, this does not imply that these are the most favorable temperatures if the efficiency of the whole process is taken into account. Efficient recovering of the heat evolved during the capture processes is in fact more difficult at this low temperatures. Post combustion separation processes are traditionally carried out by using aqueous solutions of amines, in particular monoethanolamine.¹¹ These systems are characterized by high CO_2 selectivities and capacities (0.5-1 mol CO_2 per mol of amine, corresponding to about 2-4 mmol g^{-1})¹¹ and by an intrinsic stability to moisture. Nevertheless, they present several problems, in primis the energy penalty that have to be paid for their regeneration, estimated as 25-40% in a coal-fired power station.¹¹ Minimum energy required for CO_2 separation in post-combustion systems would be only 3.5%, as estimated on pure thermodynamic basis.¹¹ This large difference is in great part ascribed to the presence of water: regeneration of amines is in fact carried out at 100-140°C. It is then evident that the most part of the heat provided would be spent for solvent heating and boiling. Amines have also other important drawbacks: these compounds are in fact costly, corrosive, carcinogenic and they easily undergo to thermal degradation.¹¹

For these reasons, parallel to the research aimed to improve the performances of amine process, solid sorbents are deeply investigated in order to find a valid alternative as CO_2 scrubbers. Because of the absence of solvents, solid sorbents have also the advantage of a wider temperature range of operation than liquid ones.⁶³

Wang et al.^{59, 63} have classified CO_2 sorbents/scrubbers according to their working temperatures in (i) low temperature ($< 200^\circ\text{C}$), (ii) intermediate temperature (200-400°C) and (iii) high temperature ($>400^\circ\text{C}$) sorbents. They have also identified the important parameters to fully characterize a CO_2 scrubber in: (i) working T and P conditions; (ii) working capacity (the actual reversible capacity of the system in the working conditions: see for example Ref. 72); (iii) selectivity; (iv) durability; (v) kinetics; (vi) recycling stability; (vii) cost; (viii) regeneration cost.

Table 2. Summary of the different compositions and operational temperature and pressure conditions of the principal gas mixtures interesting for CO_2 separation processes. In the gas compositions, besides CO_2 , only the main components are indicated.

gas mixture	composition (vol.%) ^{2, 3, 11, 68}	T (°C)	P (bar)
air	78% N_2 , 21% O_2 , 0.04 % CO_2	25	1
natural gas	30-60% CH_4 , 40-70% CO_2	25	1-10
post-combustion	70-77% N_2 , 15-16% CO_2	50-75	1
pre-combustion	61% H_2 , 35% CO_2	40	30

In Table 3, the properties of the different gases involved in the separation processes reported in Table 2 are shown. For what concerns the geometrical point of view, CO₂ has the smallest kinetic diameter with respect to all the other gases. Moreover, on the electrostatic point of view, CO₂ would be characterized by the strongest interaction energy. Presence of high polar sites in materials would then increase their affinity towards the most polar molecule in the mixture (that is toward CO₂) and then their selectivity.

On thermodynamic and molecular sieving basis, separation of CO₂ from other gases would be then not a so difficult task in principle. Nevertheless, if high purity of CO₂ after separation and low CO₂ concentration in the gas feed are considered, this statement is no more true. Unfortunately, for CO₂ recycling to different products from carbonates, high purity of the gas is requested.¹⁵ In this case, the production cost of CO₂ is so high to limit its use as feedstock in industrial processes.¹⁵

Table 3. Kinetic diameter (*d*), critical temperature (*T_c*) and electrostatic components of different gases (*α*, polarizability; *μ*, dipole moment; *Θ*, quadrupole moment) as in Ref. 73.

gas	<i>d</i> (Å)	<i>α</i> (Å ³)	<i>μ</i> (D)	<i>Θ</i> (D · Å)	<i>T_c</i> (K)
CO ₂	3.30	2.507	0.000	4.30	304
CH ₄	3.80	2.448	0.000	0.02	190
N ₂	3.64	1.710	0.000	1.54	126
H ₂ O	2.65	1.501	1.850	2.30	647
CO	3.76	1.953	0.112	2.04	133

The presence of water has to be also considered in real processes. It is evident from the properties reported in Table 3 that water presence can strongly lower the efficiency in sorption and separation of CO₂. A quantum mechanical calculation considering a Mg²⁺ ion in gas phase indicates a larger binding energy for H₂O (BE^c = 326.5 kJ mol⁻¹, MP2/aug-cc-pVTZ level) than for CO₂ (247.7 kJ mol⁻¹). Moreover, Mg²⁺ interaction with CO₂ mediated through water would be characterized by a decidedly lower binding energy (80 kJ mol⁻¹) at the same level of calculation. Strong and specific chemical interactions are then needed in order to increase the selectivity of the materials and their stability in operational conditions. Nevertheless, effective systems for CO₂ removal must combine high selectivity and capacity with minimal energetic input to liberate the captured CO₂ that means low interaction energies. In fact, the energy consumed per cycle is directly related to the sorption heat, if efficient heat recovery systems are not present. Stability in presence of moisture of the materials themselves is also an issue for example for metal-organic frameworks (see Section 4.3). Besides water, more corrosive contaminants as H₂S are often present bringing to a further lowering of the cyclability of the separation system.

Summarizing, the ideal material for carbon dioxide capture from real flue gases and from atmosphere requires low synthetic cost, high stability, low heat of adsorption, long-term adsorption cycling, stability to contaminants and oxidative and high selectivity in presence of water. This means that on one hand the material need to be stable in presence of moisture and that the completion between CO₂ and H₂O is minimized.⁷⁴

Separation technologies can be distinguished in four groups differing in the way the regeneration is performed: (i) PSA (pressure swing adsorption), (ii) VSA (vacuum swing

adsorption), (iii) TSA (temperature swing adsorption) and (iv) ESA (electric swing adsorption). Other systems that have been reported can be seen as a combination of those processes. PSA and VSA differ on the pressures adopted. For PSA, the separation is conducted at about 5-6 bar, whereas the regeneration is performed by flushing the column with an inert gas at lower pressure (about 1 bar). For VSA, the pressures involved are lower, being the inlet at 1-1.5 bar and the outlet 0.1 bar. In TSA, the column is also heated during the regeneration by passing a hot gas through the column.⁷⁵ For ESA, the desorption is achieved by heating the fixed bed using electricity,⁷⁵ and it is then more effective than TSA if the adsorbent itself is a good electric conductor (e.g. graphitic carbons). Among those processes, TSA is particularly promising, owing to difficulties with compressing or applying a vacuum to large volumes of a low pressure flue gas stream, that would be required for pressure-swing or vacuum-swing adsorption.⁷⁶

At this point, it is important to stress that on the applicative point of view, volumetric CO₂ densities are more significant than CO₂ gravimetric densities.⁷⁷ Nevertheless, in general these data are not available in the articles. For this reason, in the following only the gravimetric densities are reported in order to allow the comparison with the different materials. It would be useful that in future publications, the volumetric capacities will be reported along the gravimetric ones.

Another important consideration derives by reminding that three factors are at the basis of any separation process: thermodynamics; (ii) molecular sieving and (iii) kinetic effects. For these reason, separation properties of materials would be accurately characterized only in studies performed in dynamic conditions. Nevertheless, those measurements require the use of reactors, mass spectrometers and large quantities of sample, making them trickier measurements the static volumetric measurements. For these reasons, in most part of the articles only the selectivities derived from static measurements are reported (adsorption selectivity, *S_{ads}*).⁷⁶ In the following, selectivity will be then often synonym of adsorption selectivity. Nevertheless, I am aware that the permeation selectivities *S_{per}* are the correct parameter to be considered, defined as the product of the adsorption (*S_{ads}*) and the diffusion (*S_{diff}*) selectivities.⁷⁸ *S_{ads}* are almost coincident with *S_{per}* only when high correlation effects in molecular jumps from one adsorbed site to another are present for the different species (*S_{diff}* = 1).⁷⁸ This is true for example in materials characterized by 1D channel pores or by small pore openings.⁷⁸ If the correlation effects are negligible (*S_{diff}* being the quotient of the Maxwell-Stefan diffusivities of the pure components in the material), then *S_{ads}* represents only an approximation of *S_{per}*. The relative scale of material performances can be then different in dynamic conditions. In fact, higher *S_{ads}* is not directly correlated with high *S_{diff}* being the former enhanced by high energetic of interactions whereas the second decreases, if high correlations are not present. Diffusion have to be enhanced (by adopting higher operational temperatures, larger intercorrelation and pore openings) if a large difference in the adsorption strength of the two gas components is present.

Computer simulations aimed to predict selectivities of materials have shown to be a particularly accurate and easier tool in some cases with respect to the experimental counterpart. Nevertheless,

in this case the use of rigid framework has to be carefully avoided, constituting a higher approximation with respect to more negligible factors as dimensions of the particles and defects.⁷⁹ This is particularly true in the case of metal organic frameworks, materials that can be characterized by drastic structural changes upon adsorption.^{80, 81}

3. The Mg²⁺ ion

Besides few exceptions, magnesium is in general in its ionic form Mg²⁺. The ions reactivity or, more generally, the ions ability to polarize adsorbate can be predicted through their charge/radius ratio but also through their electrostatic effects on the chemical properties of ligands to which they are coordinated. A fairly clear concept of the magnitude of this effect can be acquired by considering the acid strengthening effect of a divalent metal ion on a coordinated water molecule.⁸² In Table 4, the pK_a for water coordinated to different divalent ions is reported. Ionic radii for the same ions in tetra- (*r*_{tetr}) and hexacoordinate complexes (*r*_{hexa}) are also presented.⁸² If the pK_a values are compared with that of pure water (15.7), it is evident that all of them are lower than this value and in most cases the smaller *r*_{hexa}, the lower the pK_a, i.e. larger the ion reactivity. For water molecules coordinated to ions in four coordination, an even lower pK_a is then expected for all the ions. It is noteworthy that, if the Be²⁺ ion is excluded, Mg²⁺ has a pK_a value very close to the median of the values reported in Table 4. This suggests as catalysts involving Mg²⁺ in the active site would have a good reactivity but also a relatively low stabilization of the reaction products. For what concerns separation processes, a lower regeneration energy of the Mg-based systems with respect to other M²⁺-based systems can be predicted on these basis.

Table 4. Values of pK_a ($K_a = \frac{[H^+][Mg(H_2O)_5OH]^+}{[Mg(H_2O)_6^{2+}]}$) for water hexacoordinated to divalent ions and the ions radius in hexacoordinate (*r*_{hexa}) and tetra-coordinate complexes (*r*_{tetr}), as from XRD measurements. Data from Ref. 82 and references therein.

	pK _a	<i>r</i> _{hexa} (Å)	<i>r</i> _{tetr} (Å)
Ba ²⁺	13.1	1.49	—
Be ²⁺	4.3	0.59	0.41
Ca ²⁺	12.5	1.14	—
Cd ²⁺	9.8	1.09	0.92
Co ²⁺	9.4	0.89	0.72
Fe ²⁺	8.4	0.92	0.77
Mg ²⁺	11.4	0.86	0.63
Mn ²⁺	10.1	0.97	0.8
Ni ²⁺	9	0.83	0.69
Zn ²⁺	9.6	0.88	0.74

Nevertheless, CO₂ is a quadrupolar molecule and, for this reason, it would be more sensitive to the polarity of the bond involving Mg²⁺ than to the polarizing ability of the ion alone when Mg²⁺ is part of a material. In this case the difference in electronegativity between the ions involved in the bond is a more precise indication of the polarity of the materials surfaces.⁶¹ The large electronegativity difference between Mg and C, N and O (the most common Mg²⁺ ligands in materials) allows to predict a high

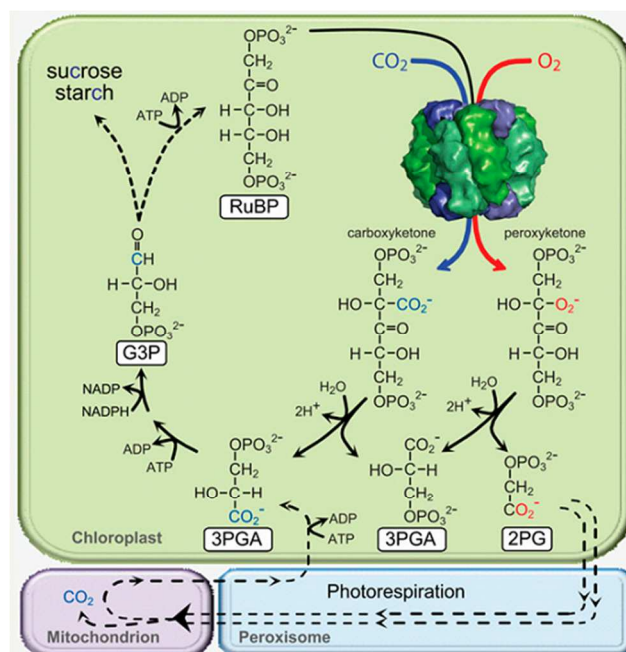
polarity in the bond involving Mg and then a high affinity towards CO₂. This has been actually verified in comparative studies on oxides⁶¹ and metal-organic frameworks.⁸³

4. Mg-based materials involved in the CO₂ cycles

4.1 Enzymes

Mg²⁺ is present as essential cofactor in many enzymatic reactions going from methylation, phosphorylation and carboxylation.^{15, 82} Its large presence is likely related to its large abundance in nature but also to its small ionic radius (see Table 4), making it an essential factor in electrophilic catalysts.⁸² In enzymatic reactions, in fact, the electrostatic effect of the metal on the chemical properties of the ligands to which it is coordinated⁸² plays a crucial role firstly in determining the acidity of the coordinated water. Carboxylases are enzymes that allows carboxylation, that is carbon dioxide fixation. In general, carbon dioxide is present as bicarbonate (HCO₃⁻) in cells.⁸² Nevertheless, bicarbonate is unreactive as a carboxylating agent, whereas carbon dioxide is electrophilically reactive.⁸² For this reason, the first step in the carboxylation reactions is often constituted by the conversion of bicarbonate to carbon dioxide through the mediation of adenosine triphosphate (ATP).

Among carboxylases, six of them can present Mg²⁺ as metal cofactor in the active site:¹⁵ Rubisco, PEPC, PEP carboxykinase, Acetyl-CoA carboxylase, Propionyl-CoA carboxylase and Pyruvate carboxylase.¹⁵ In particular, Rubisco and PEPC are the two most important carboxylases enzymes. They differ also in the form in which is CO₂ at the beginning of the reaction: Rubisco uses dissolved CO₂, whereas the one used by PEPC is originating from the dehydration of bicarbonate.



Scheme 3. Simplified scheme illustrating how CO₂ fixed to RuBP by Rubisco is distributed among the resulting two molecules of 3PGA that feed into the photosynthetic Calvin cycle to produce triose phosphates (glyceraldehyde 3-phosphate [G3P]) for carbohydrate synthesis or RuBP regeneration. The contrasting oxygenation reaction of Rubisco produces 2-phosphoglycolate (2PG), which requires the photorespiratory pathway

to recycle it back to 3PGA. Photorespiration is a complex pathway that involves four subcellular compartments and multiple enzymatic steps (represented by dashed lines), requires additional energy (ATP), and results in a loss of fixed CO₂ in the mitochondria. Reproduced with permission from Ref. 84. Copyright 2011 American Society of Plant Biologists.

4.1.1. Rubisco

Ribulose 1,5-bisphosphate carboxylase/oxygenase (EC 4.1.1.39), also known with the abbreviation Rubisco, is an enzyme responsible of the main route for carbon dioxide fixation from the atmosphere (through the Calvin cycle, see Scheme 3).⁸² In particular it catalyses the reaction of ribulose 1,5-bisphosphate (RuBP) with CO₂ and water to obtain two 3-phosphoglycerate molecules (3-PGA), to feed the Calvin cycle. Being the 3-PGA a three-carbon compound, the plants where the Rubisco uses directly atmospheric CO₂ without previous transformation are called C3 plants. Rubisco is estimated to be responsible of the CO₂ fixation for about 100 Gtons per year⁸⁵⁻⁸⁷ and it is the most abundant enzyme (if not the protein)^{87, 88} on Earth. This abundance is related to the slow and unspecific enzymatic activity of Rubisco, recognized as one of the most inefficient enzymes in general:⁸⁷ its turnover frequency (k_{cat}) amounts^{82, 84} to only $<0.1-14 \text{ s}^{-1}$ at 25°C (for comparison, enzymes often have k_{cat} of 10^3-10^4 s^{-1}).⁸² It is in fact indicated as the rate determining step in the Calvin cycle. Rubisco phylogeny started in fact 3.5 billion years ago, in an atmosphere where oxygen was present only in traces and the carbon dioxide concentration was also up 20 times the present value.^{84, 89-91} For this, it is very low efficient at the actual CO₂ levels: the energetic efficiency of C3 plants is only

1%.⁸⁷ Moreover, Rubisco has a low ability to discriminate O₂ from CO₂. Because of this and of the higher concentration of oxygen in the present atmosphere with respect to CO₂ (21% versus 0.04%), Rubisco can catalyze decarboxylation reactions (photorespiration).^{82, 92, 93} This effect is even larger at temperatures higher than room temperature⁸⁴ and in dark conditions, being RuBP not produced in absence of light.⁸⁴ On the contrary, it is well known that any increase in CO₂ atmospheric concentration, brings to an increase in the plant growth rate.^{84, 94-98} Because of its importance, since its discovery⁹⁹ the structure of this enzyme has been deeply investigated by means of both experimental and computational studies, with the aim to understand how genetically modify Rubisco to increase its catalytic efficiency.⁸⁷

The structure of Rubisco as in *Spinacia oleracea* is described in Figure 5a and b while in part c only the 8 pockets and corresponding active sites of the enzyme are reported. In part d, a scheme of the active site is reported, with bound to the Mg²⁺ ion and CABP, an isomer of the reaction transition state. An atomistic representation of part d, aimed to have a closer view on the Mg²⁺ coordination, is reported in parts e and f of the same figure. In plants and cyanobacteria,⁸⁸ this enzyme has a mass of about 550 kDa and it is constituted by eight large (L) and eight small (S) subunits, with each couple differentiated in Figure 5 by means of different colors. Each of the eight L subunits hosts an active site (Figure 5c) situated on the external surface of the enzyme. Among all the species present in the pockets, only four residues and the Mg²⁺ ion are responsible of the enzyme activity.

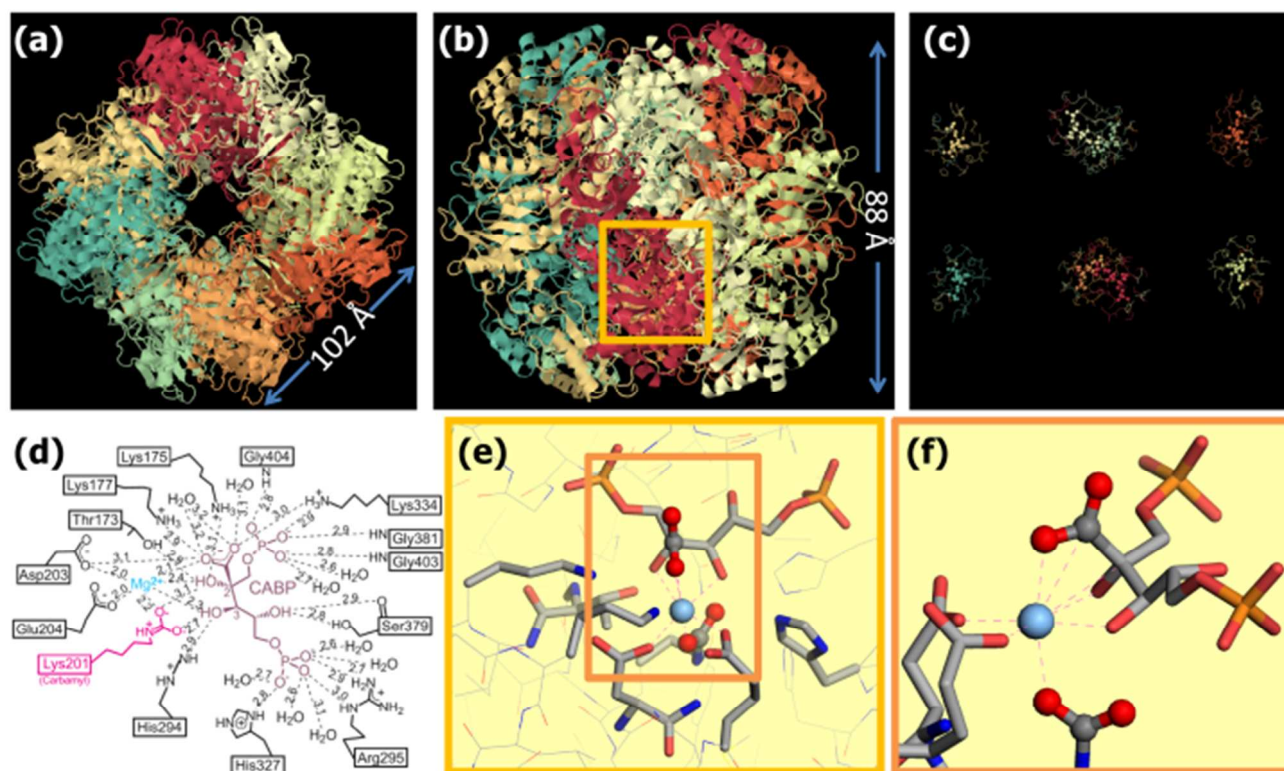


Figure 5. Rubisco with Mg²⁺ and the transition state analog CABP bound to the active site from *Spinacia oleracea* (Protein Data Bank ID: 8RUC, resolution of 1.6 Å)⁸⁸ shown from two perspectives: (a) looking down the fourfold axis of symmetry and (b) rotated 90°. The eight subunit couples L-S (large and small) are represented with different colors (images obtained by the Jmol software).¹⁰⁰ (c) The eight pockets (one per L unit) with the ligands are represented using the same orientation as in part (b). (d) Schematic 2D representation of the active site complex, showing Mg²⁺, CABP, and all of the

active site contacts, including the carbamyl-Lys201, with interatomic contact distances given in angstroms as in the 1RXO structure (PDB ID). Adapted from Ref. 82, Figure 8.23D from p. 423. By permission of Oxford University Press, USA. (e,f) Atomistic view of the coordination around the Mg^{2+} ion in two different orientations and magnifications. The CO_2 units (that is the one directly involved in the carboxylation reaction and the one incorporated in the carbamyl unit of lysine) are represented as ball and stick atoms. The atoms at a distance lower than 3 Å from Mg^{2+} are linked to the ion through dashed lines. The atoms are represented according to following color code: oxygen (red), carbon (grey), sulfur (yellow), phosphor (orange), magnesium (light blue), nitrogen (dark blue). Hydrogen atoms, being absent in the XRD structure, were omitted.

In the reaction catalyzed by Rubisco, a minimum of two carbon dioxide molecules are needed: one associated to the activation of the enzyme, while the second one participating to the carboxylation reaction. The activation of the enzyme would proceed through a two step mechanism: in the first step, one CO_2 molecule reacts with the ϵ -amino group of a lysine residue¹⁰¹ (Lys201 in spinach enzyme) causing its carbamylation. In this part, Mg^{2+} would assume a rare pseudotetrahedral coordination, with three water molecules and the fourth position occupied by CO_2 . During the second step, Mg^{2+} is then bound to the enzyme, through the N-carbamyl group formed in most part of the complexes.¹⁰¹ Mg^{2+} is in an octahedral coordination at this point, coordinating a water molecule that plays an important role in the whole reaction. Since this step, Mg^{2+} would maintain an octahedral coordination, although differently distorted.⁸⁶ The carboxylation and cleavage of RuBP then take place through a six step reaction (extensively discussed in the literature, see in particular Ref. 86): (i) coordination of RuBP; (ii) coordination of CO_2 ; (iii) carboxylation of RuBP; (iv) hydration; (v) RuBP cleavage to a 3-PGA molecule and a carbanion intermediate and (vi) protonation of the carbanion with the formation of a second 3-PGA molecule. Recent calculations indicate that the coordination and activation of CO_2 would happen through an acid base mechanism given by a concerted action of the RuBP and the water molecule coordinated to Mg^{2+} .^{86, 102} The Gibbs free energy of CO_2 coordination (solvated system) in the (i) step has been calculated to be of 21 $kJ\ mol^{-1}$ by means of quantum mechanics calculations (PBE-D).¹⁰² The structure around Mg^{2+} in the transition state that precedes the RuBP cleavage (step v) is reported in Figure 5d, e and f. This transition state is estimated to be about 100 $kJ\ mol^{-1}$ higher in energy with respect to step (i). In these figures, it is evident that Mg^{2+} is in a distorted octahedral coordination. Each vertex of the octahedron is occupied by an oxygen atom, where the two apical positions are occupied by one oxygen of the two pristine CO_2 molecules. The other four oxygens are due to two O of the CABP molecule and the remaining two are belonging to two carboxylate groups (Asp204, Glu203 residues).⁸² All these oxygens are at distances between 2.3 and 2.4 Å from Mg^{2+} . It is interesting to notice that the CO_2 molecule is strongly bent ($\angle O-C-O = 118^\circ$) and that both the C and one O are at a distance lower than 3 Å from Mg^{2+} .⁸⁸ The importance of Mg^{2+} in the reaction is evidenced by the fact that removing it or exchanging it with a Ca^{2+} ion, the enzyme loses completely its catalytic activity.⁸² This is likely related to the importance of the coordinated water in the reaction: Mg^{2+} has the ability to polarize water more than Ca^{2+} (see Table 4) without having the ability to favor its reaction with CO_2 , as for example a Zn^{2+} ion would do (the active site in the carbonic anhydrase enzyme).

4.1.2. PEPC

In order to enhance Rubisco catalyst efficiency, in some plants two metabolic strategies have been adopted aimed to concentrate CO_2 around the enzyme:¹⁰³ the Crassulacean Acid Metabolism

(CAM, 7% of plant species: e.g. succulent plants)¹⁰⁴ and the C4 carbon fixation (3% of plants: e.g. maize, sugar cane and sorghum).^{87, 105, 106} These two mechanisms were the results of plant evolution to adapt to difficult environmental conditions as drought or salinity and to the lower CO_2 atmospheric concentration in the recent geological history.⁸⁹⁻⁹¹ In both mechanisms, the carbon dioxide is previously stored in a four-carbon organic acid as malic ($HO_2CCH_2CHOHCO_2H$) or aspartic acid ($HOOCC(NH_2)CH_2COOH$) and then recovered for the Calvin cycle through decomposition of this precursor. This decomposition is often carried out in closed and CO_2 impermeable environments to further concentrate CO_2 (Kranz anatomy). The formation of the organic acid is obtained through the reaction of bicarbonate with phosphoenolpyruvate (PEP, $[C_3H_2O_6P]^{3-}$) to oxaloacetate ($[O_2CCCH_2CO_2]^{2-}$) and an inorganic phosphate. The enzyme at the basis of this process is the phosphoenolpyruvate carboxylase (PEPC, EC 4.1.1.31). This reaction is very important being involved also in the citric acid cycle. For this reason, PEPC enzyme is present in all plants (C3- and C4-plants) and in some bacteria. PEPCs can then have different kinetics and regulatory properties that correlates with their respective roles in cellular metabolism.¹⁰⁷⁻¹⁰⁹ These differences are achieved by small structural differences. For example, the high efficiency of C4-PEPC enzyme is related to the presence of a glycine unit in the active site that sterically hinders a strong binding with feedback inhibitors as aspartic or malic acids.¹⁰⁸ In any case, PEPCs turnover number is comprised between 30-150 s^{-1} ,^{110, 111} that is 1-2 orders of magnitude higher than Rubisco's. Moreover, decarboxylation reactions are not catalysed by PEPCs: this is related to the highly exothermicity of the overall mechanism bringing to the formation of oxaloacetate, characterized by a Gibbs free energy change of 30 kJ/mol .¹⁰³ Further, PEPC has a high affinity towards bicarbonate and then it is not inhibited by O_2 .¹⁰⁷ The efficiency of the process is evidenced by the fact that, although their scarcity, C4 plants account for the 30% of the terrestrial carbon fixation.¹¹²

All known PEPC are tetrameric enzymes: a PEPC can be described as a dimer of dimers with respect to the subunit constant (see Figure 6a),¹¹⁰ having a molecular weight of about 440,000 Da. PEPC activity is controlled in an allosteric manner, through the presence of activator or inhibitor molecules. In the activation step, PEPC binds firstly the metal cofactor, constituted by a divalent cation, either Co^{2+} , Mn^{2+} or Mg^{2+} .^{82, 92, 103, 105} This metal center will be necessary firstly in PEP coordination but it plays also a leading role in the last part of the reaction process, coordinating contemporaneously the enolate intermediate and CO_2 bringing to the formation of oxaloacetate. After coordination of the metal by the enzyme, PEP is bound through a bidentate coordination to the metal. In Figure 6b, the PEPC structure around the metal center of the enzyme from *Escherichia coli* (Protein Data Bank ID: 1JQN, resolution of 2.35 Å)¹⁰⁷ is reported. In this structure, PEPC is bound to Mn^{2+} (metal cofactor), to a PEP analog (3,3-dichloro-2-

dihydroxyphosphinoylmethyl-2-propenoate, DCDP), and aspartate (allosteric inhibitor). It is evident that the metal ion is in a roughly tetragonal bipyramidal coordination with all the vertex at an average distance of 2.1 Å. This distance is significantly shorter than the one observed in Rubisco structure. As for the Rubisco metal center, all the first neighbours are six oxygen atoms: two of them belonging to the PEP moiety, two to water molecules and two oxygens due to two different COO⁻ units (that is the ones relative to Asp603 and Glu566 residues in the inactive form of *Escherichia coli* PEPC). This is schematically represented in step 2 of Figure 6c. Then the carboxylation

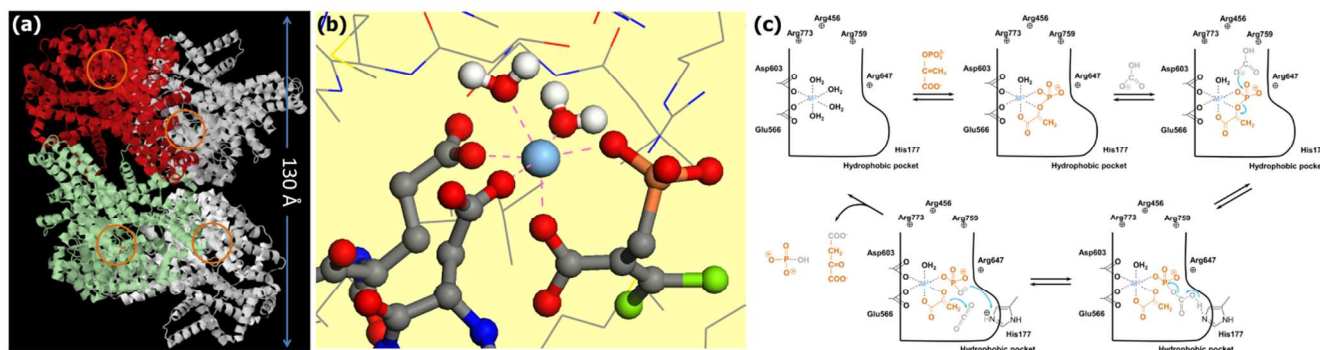
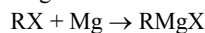


Figure 6. PEPC from *Escherichia coli* with Mn²⁺, phosphoenolpyruvate analog (3,3-dichloro-2-dihydroxyphosphinoylmethyl-2-propenoate, DCDP), and aspartate (allosteric inhibitor) bound to the active site (Protein Data Bank ID: 1JQN, resolution of 2.35 Å).¹⁰⁷ (a) Ribbon diagram of PEPC view along the front C₂ axis. The two subunits of one of the two dimers are differentiated by green and red colors (image obtained by the Jmol software).¹⁰⁰ The position of the four active sites is indicated by orange circles. (b) Atomistic view of the coordination around the Mn²⁺ ion in interaction with DCDP. The atoms at a distance lower than 2.4 Å from Mn²⁺ are linked to the ion through dashed lines. The atoms are represented according to following color code: hydrogen (white), oxygen (red), carbon (grey), sulfur (yellow), phosphor (orange), manganese (light blue), nitrogen (dark blue), chlorine (green). Hydrogen atoms not belonging to water molecules are omitted. (c) PEPC enzymatic mechanism as in Ref. 107 converting bicarbonate and PEP to oxaloacetate and phosphate.

4.2. Grignard reagents

Grignard reagents are obtained from the reaction of an alkyl, alkenyl or aryl halide (RX, X = Cl, Br or I) with elemental magnesium:



and constitute the single most important organometal reagent used in laboratory synthesis of organic compounds since their discovery.¹¹³ It is thought that the versatility, ease of preparation and high selectivity of Grignard reagents¹¹³ delayed the interest in organo-transition metal chemistry.¹¹⁴

The preparation of a Grignard reagent requires in general an ether solvent (usually diethyl ether or tetrahydrofuran). The reagent is then solubilized through the coordination to Mg by ether oxygens (see Figure 7a). Completely anhydrous conditions need to be adopted because of the high Grignard reagent reactivity with water. Also oxygen presence has to be carefully avoided. In ether solution, Grignard reagents are better represented through the Schlenk equilibrium mixture:

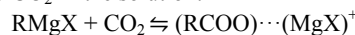


where the equilibrium of the reaction is dramatically affected by the solvent. Although in low concentration, dimeric and polymeric structures are also present in solution.¹¹⁵ It is interesting to notice that in both the mono- and dimeric form, Mg is in tetrahedral coordination (see Figure 7), that is in its most active form (see Table 4). Moreover, the large electronegativity difference of carbon and magnesium makes the bond between

reaction proceeds through a three step mechanism (step 3-5 in Figure 6c). (i) Firstly, bicarbonate anion is coordinated by three arginine units in the pocket¹¹⁰ and acts as a nucleophile to attack the phosphate group in PEP dissociating it in a carboxyphosphate and in the very reactive enolate form of pyruvate; (ii) histidine (H177 in *Escherichia coli*) then modulates the proton transfer on the carboxyphosphate through its diazolate ring bringing to its dissociation in a phosphate group and in a CO₂ molecule; (iii) the reaction of CO₂ with enolate happens with the formation of oxaloacetate and the protonation of the phosphate group [PO₄]²⁻ to [PO₃OH]⁻.^{103, 107}

them highly polar and C a strong nucleophilic center. Reactions of Grignard reagents with an enormous variety of substrates has been reported.¹¹⁴ Although the reaction mechanism is far to be settled,¹¹⁶ several evidences seem to indicate dimeric species as important intermediates.^{115, 116}

The strong separation in charge of C and Mg in Grignard reagents is expected to be particularly suitable to activate CO₂. In fact, the reaction of these compounds with CO₂ is a well known two step reaction and it is among the simplest reactions to form new C-C bonds. The synthesis is performed by using dry ice or bubbling CO₂ in the solution:



with the formation of carboxylates, that are then converted to the corresponding carboxylic acids after addition of an aqueous acid solution (HA):



This reaction allows to fix the whole carbon dioxide in an organic compound analogously as in Rubisco and PEPC enzymes by consumption of a reagent. Once formed, the newly affixed carbon of the carboxyl group can be modified to give a plethora of other substituents. Nevertheless, in ideal conditions a stoichiometric amount of Grignard reagents is consumed in the reaction. Life cycle assessments of this process would be particularly interesting to state if this reaction is actually having a positive carbon footprint or a negative one.

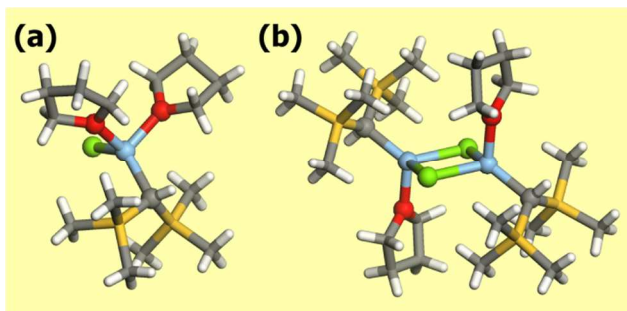


Figure 7. Mono- (a) and dimeric forms (b) of the Grignard reagent chloro-bis(trimethylsilyl)methyl-bis(tetrahydrofuran)-magnesium. Structures from Ref. 117. The atoms are represented according to following color code: hydrogen (white), oxygen (red), carbon (grey), silicon (yellow), magnesium (light blue), chlorine (green).

4.3. Metal organic frameworks

Metal organic frameworks (MOFs) are a relatively new class of crystalline materials which structure is constituted by the linking of metal oxide/metal clusters through organic linkers. At difference of many organometallic structures, in these materials a strong bond exists between the organic and the inorganic parts, allowing the retaining of the material architecture also upon solvent removal. The materials so obtained are in general highly porous and the possibility to easily tailor them toward specific applications has been often stressed in the literature on the subject.^{118, 119} Their conceptual design has been compared to the Geomag toy (a toy construction system consisting primarily of metal spheres and short connecting sticks). In fact, several organic and inorganic parts (called secondary building units) with different coordination and functionalities can be in principle freely combined.^{120, 121} The possibility to change their pore width, dimensionality of the structure and chemical compositions is relatively easier for this class of compounds with respect to anyone else. Their applications are spread from catalysis,^{122, 123} gas adsorption and separation, fuel cells, proton conductivity, protein adsorption,^{74, 124} ... The first report about a MOF structure date in 1971.¹¹⁹ Nevertheless, only after the report of the first structure able to retain its porosity upon solvent removal, a big exploit has been experienced by MOFs¹²⁵ with the creation of more than 20 000 different materials.^{119, 124} Most of the guinness materials among crystalline ones belong to the MOF class: NU-110 (the largest surface area material, 7140 m² g⁻¹),¹²⁶ IRMOF-74-XI (the largest pore aperture, 98 Å)¹²⁴ and MOF-399 (the lowest density, 0.126 g cm³).¹²⁷ However, there are still some open challenges due to their large synthetic cost and their low stability, both on the thermal and chemical point of view. For what concerns this last point, most of MOFs are highly sensitive to water, also at atmospheric concentrations, hindering their practical use.^{118, 128, 129} MOFs have been subjected to several studies for CO₂ storage and separation in different pressure and temperature conditions.^{3, 63, 129, 130} Their structure makes MOFs ideal subjects for combined experimental and theoretical studies, allowing to couple the ability to fast screening of the possible structures of computational techniques with a direct application of the indications obtained in experiments.^{17, 72, 78, 131, 132} By using this strategy, materials with superior performances with respect to

any component of other materials classes have been reported for both CO₂ separation and storage.¹³¹⁻¹³³

Most part of MOFs materials are based on transition metals. The use of s-block metal centers to construct the metal oxide units in MOFs is comparatively rare.¹³⁴ This fact is related to the predominance of ionic forces and absence of well defined metal-oxide secondary building units making more difficult the prediction of the coordination geometry and then the rational design of MOFs with respect to transition metal-based ones.¹³⁴ Nevertheless, the high abundance of these elements, and they cheap and non toxic nature makes the exploratory synthesis of the corresponding MOFs a worthwhile endeavour.¹³⁴ Moreover, the larger ionicity of the metal-oxygen bond for s-block material with respect to transition metal centers is expected to be beneficial on interaction with a quadrupolar molecule as CO₂. Among the s-block metals, magnesium is the most commonly used.¹³⁴ The Mg-based MOFs tested as CO₂ adsorbents/separators are reported in Table 1. A comprehensive list of the Mg-based MOFs reported in the literature so far is present in the ESI (Table S1). It is important to notice that the most part of them has been reported only after the synthesis in 2005 of the first Mg-based MOF with permanent porosity.¹³⁵

The relative abundance of Mg-MOFs is due to the structural chemistry of Mg²⁺, that is very close to the that of Zn²⁺, one of the most common metal in MOFs.¹³⁴ Nevertheless, the lower atomic mass of Mg²⁺ with respect to transition metals confers to the Mg analogues higher surface areas and lower densities with expected larger performances on the gravimetric gas densities achievable in storage and separation. Volumetric gas densities (a more important parameter in CO₂ separation, see Section 2.3)⁷⁷ are instead expected to be lower. Another important point that hinders the practical use of Mg-based MOFs is related to their low stability in presence of water due to the large ionic character of Mg-O bonds.¹²⁸ Mg²⁺ has a high affinity for oxygen donor atoms of water and other polar solvents, that can represent competitive ligands with respect to the organic linkers, facilitating material degradation.¹³⁶ Although some Mg-MOFs have been claimed to be water resistant,¹³⁷ a standardize method to evaluate the water resistance parameter is actually lacking and at the basis of contradictory observations reported in literature,^{129, 138} likely related to different operation conditions. For what concerns catalytic reaction involving CO₂, they are quite rare in MOFs¹²² and they are completely absent for Mg-MOFs materials.¹²³

In all the structures reported for Mg-MOFs, Mg²⁺ is six-coordinated (see Table 5 and Table S1). Nevertheless, in most of them at least one of the ligands is represented by a solvent molecule (e.g. H₂O, DMF) that can be in principle removed upon activation, that is upon thermal treatment of the material in vacuum or in inert gas flow. If the thermal stability of the structure is higher than the temperature needed to remove the solvent, at the end Mg²⁺ would show a coordination vacancy that represents a high energetic site for molecule adsorption. The possibility to create open metal sites in MOFs structure by activation has been reported in several cases.^{3, 83, 119, 128, 132, 135, 139-142} In this regards, particularly interesting are the isomorphous materials [M₂(dobdc)(H₂O)₂] with H₄dobdc = 2,5-dihydroxyterephthalic acid and M = Ni, Co, Zn, Mg, Mn or Fe.^{3, 83,}

¹⁴¹ These materials have been reported in literature with several acronyms, as CPO-27-M, M-MOF-74, IRMOF-74-I or M/DOBDC. Their structure is an honeycomb-like with the vertex of the hexagon occupied by filars of M-O units linked between
 5 them by dobdc units (see Figure 8a). The metal center is in an octahedral coordination in the as-synthesized material, with one of the positions occupied by a water molecule. This molecule is removable upon degassing at 120°C, so leaving open the metal center.
 10 Mg have been compared for their CO₂ adsorption performances.⁸³

MOFs represent ideal systems to systematically study the roles of different open metal sites or functional groups on materials properties. The isotherms obtained in Ref. 83 at 23°C are reported in Figure 9b (see also Table 5). It is evident that the CO₂ uptake of
 15 IRMOF-74-I-Mg is twice larger than in any other member of the series.^{3, 11, 83} This is true in the whole 0-1 bar range, with significant uptakes also at pressures close to 0.39 mbar (0.22 mmol g⁻¹).⁸³

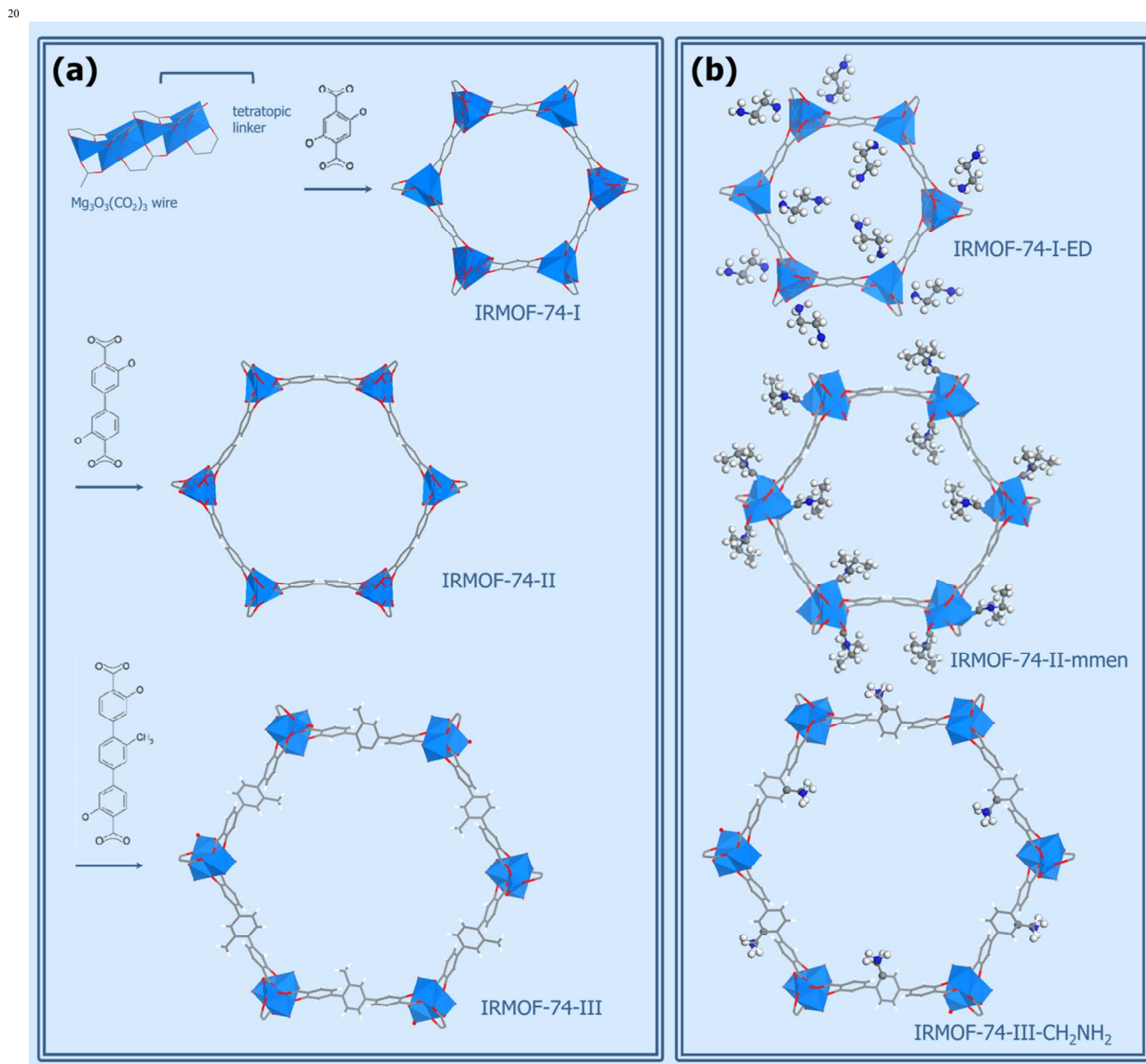


Figure 8. (a) Structures of the isomorphous IRMOF-74 materials for increasing dimension of the linker (from top to bottom, IRMOF-74-I, IIb and III) as from Refs. 118, 120, 147. (b) Exemplificative structures of amino-functionalised IRMOF-74 reported in literature.^{118, 147, 148} The atoms are represented according to following color code: hydrogen (white), oxygen (red), carbon (grey), magnesium (light blue), nitrogen (dark blue). Please notice that the
 25 structure reported in the top of part b as in Ref. 148 is likely biased by symmetric constraints in the calculations.

Although characterized by a larger surface area, the exceptional CO₂ uptake of IRMOF-74-I-Mg is more related to the higher adsorption energy measured in this material with respect to the others of the series (47 versus 41 and 37 kJ mol⁻¹ for Ni and Co

30 analogues, respectively).⁸³ This may be attributed to the larger ionic character of the Mg-O bond.⁸³ A detail of the electrostatic potential map in the pores of the MOFs as obtained at the B3LYP-D*/TZVp level is reported in Figure 9a. The high

ionicity of this structure in the region around the metal site is well evident. This map shows in fact that there is a strong positive potential (blue regions) on Mg^{2+} site and a strong negative potential around the oxygen belonging to the carboxylate group of the organic ligand (red regions).¹⁴⁴ Quantum mechanical calculations indicated that $\text{Mg}^{2+}\cdots\text{OCO}$ complex would not possess a linear but an angular geometry in this material in order to maximize the lateral interaction between the CO_2 molecule and the oxygen atom of the carboxylic group O_{carbox} ($\text{C}\cdots\text{O}_{\text{carbox}}$ distance 2.975 Å, see Figure 9b).¹⁴⁴ The calculations allowed also to indicate the remarkable role played by the dispersion contribution, which roughly accounts for one-half of the total gas-solid interaction energy.¹⁴⁴ A similar finding was reported in a combined DFT/CC and IR spectroscopic study on carbon dioxide adsorption on the zeolite H-FER.¹⁴⁵ Accordingly, also dynamic separation measurements performed in flow for CO_2/CH_4 and CO_2/N_2 indicated clearly higher performances of the Mg^{2+} -based material with respect of the other IRMOF-74-I.¹³⁸

Similar results were obtained considering MOFs where the cations are hosted as extra-framework species (rho-ZMOF).¹⁴⁶ It was computationally predicted that the isosteric heat of adsorption at the lowest coverage increases with the charge-to-diameter ratio of the cation for CO_2 adsorption and separation, being Mg^{2+} rho-ZMOF the best performing material after Al^{3+} rho-ZMOF. Moreover, because of its larger pore volume, Mg^{2+} rho-ZMOF would possess the highest total capacity of the whole series also in this case.

IRMOF-74-I-Mg represents the most investigated MOF for CO_2 storage and separation.^{3, 11, 83, 141, 144, 149} This is due to its superiority in performances in the $p < 1$ bar range not just with respect to its isomorphous materials, but also with respect to all the other MOFs. It is also characterized by a very high CO_2/N_2 selectivity (175 at 0.15 bar CO_2 , with a purity of CO_2 in the adsorbed phase of 97%),⁷⁶ although lower than CaA zeolite (250).⁷⁶ Moreover, in this range its CO_2 volumetric capacity is very close to the one reported for NaX,^{3, 10} the reference material in CO_2 separation studies (see Table 5 and Table 7). To explore

the effect of the pore size of the material on the CO_2 capacities, IRMOF-74-I analogues have been synthesized by using larger linkers, exploiting the peculiar property of MOFs to allow easy tailoring and modification of the materials: the structure of IRMOF-74-I isomorphous having biphenyl (two isomorphs: IRMOF-74-IIa,¹²⁴ and IRMOF-74-IIb,¹⁴⁷) and triphenyl (IRMOF-74-III)¹¹⁸ linkers are reported in Figure 8a. The corresponding CO_2 isotherms obtained at 25°C for pressure ≤ 1 bar are reported in Figure 9c, where they are compared with the IRMOF-74-I one. Although the larger pore volume of IRMOF-74-IIb and IRMOF-74-III, their CO_2 capacity is lower and decreases with the pore size. This effect was expected because of the low pressure considered and the importance of dispersion forces in CO_2 interaction with material surfaces, also in presence of highly polarizing sites.^{17, 144, 145} The potential of two opposite pore walls is additional only up to a limit pore dimension. A glance to Figure 9c seems to indicate that whereas for IRMOF-74-IIb (light blue triangles) such an effect is still present, in IRMOF-74-III (light blue stars) it is completely lost. In fact, this material stores only 2.95 mmol g^{-1} of CO_2 at 25°C and 1 bar, that is about one fourth of IRMOF-74-I in the same conditions. The strong effect of pore dimension on CO_2 adsorption has been observed also for frameworks which combine the properties of interpenetration with the presence of coordinatively unsaturated sites¹⁵⁰ as N' -tetrakis-(4-carboxyphenyl)-biphenyl-4,4'-diamine).¹⁵⁰ Although promising, IRMOF-74-I needs still some improvements: first of all, it has been proven to be difficult to regenerate, being only the 87% of its capacity recovered after flushing with CH_4 at RT.¹³⁸ Moreover, it has been theoretically predicted¹⁴⁹ (and then experimentally verified)^{128, 148} that it rapidly loses its CO_2 capacity under humid conditions. Presence of other trace flue contaminants such as SO_2 and SO_3 fast poison open metal sites.¹⁰ Regeneration in presence of moisture causes the hydrolyzation of the material. Even more important for applications, its CO_2 adsorption capacities degraded by long term storing the material under both dry or humid conditions.¹⁴⁸

Cite this: DOI: 10.1039/c0xx00000x

www.rsc.org/xxxxxx

REVIEW

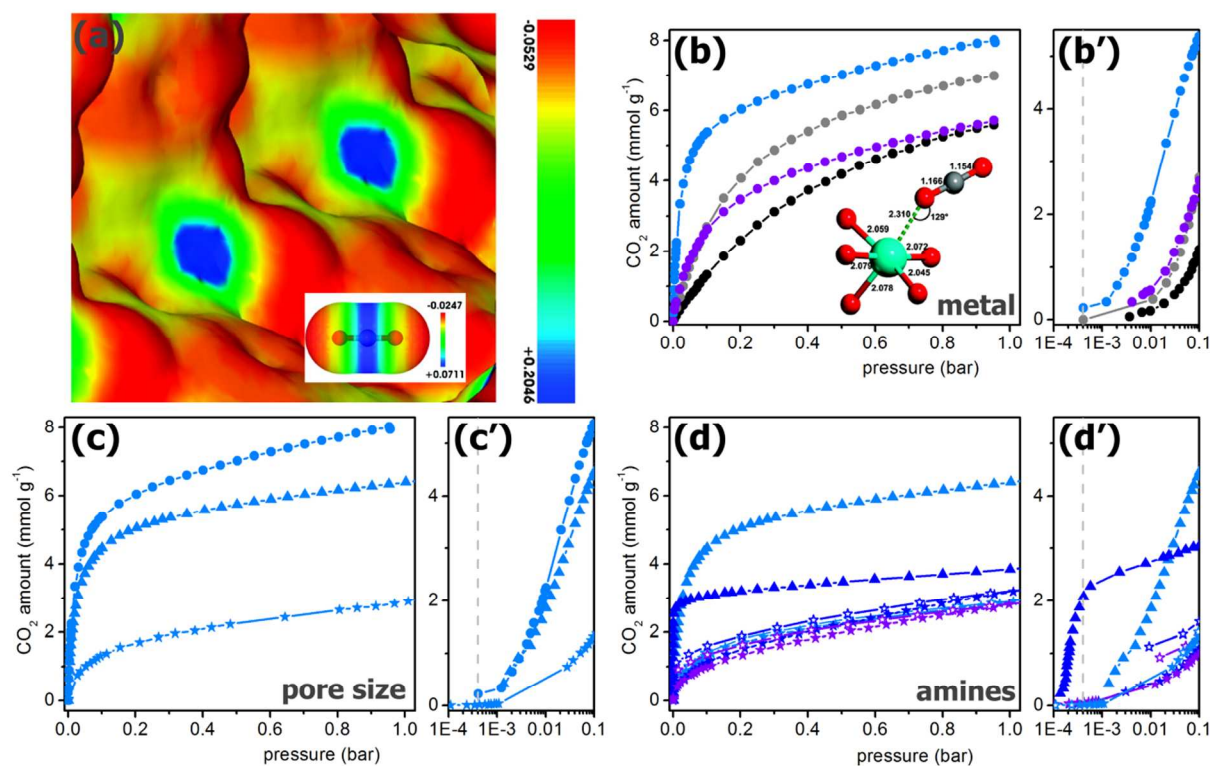


Figure 9. (a) Detail of the electrostatic potential of IRMOF-74-I mapped on the electron charge density isosurface (0.003 au) together with the electrostatic potential of CO₂. Red, green, and blue represent negative, zero, and positive values of the potential (a.u.), respectively. In the inset the electrostatic potential map obtained for CO₂ is reported. Adapted from Ref. 144. Reproduced with permission. Copyright 2010 American Chemical Society. (b-d) CO₂ adsorption isotherms obtained at 25 °C on IRMOF-74 materials. The three plots compare the curves obtained for materials differing in (b) the metal center, (c) the dimension of the linker or (d) in the presence and nature of aliphatic amines groups. Full and empty scatters refer to the adsorption and desorption branch of the isotherm, respectively. Plots obtained by digitalization of the data reported in Refs. 83, 118, 147 in order to allow a direct comparison. The scatters refer to the points of the original curves used for the digitalization. The legend is: (b) IRMOF-74-I-Mg (light blue scatters), Co (grey), Zn (black) and Ni (violet); (c) IRMOF-74-I (circles), IRMOF-74-IIb (triangles) and IRMOF-74-III (stars); (d) IRMOF-74-IIb (light blue triangles), IRMOF-74-IIb-mmen (dark blue triangles), IRMOF-74-III (light blue stars), IRMOF-74-III-CH₂-NH₂ (dark blue stars) and IRMOF-74-III-CH₂-NHMe (violet stars). (b', c', d') Inset in the 0-0.1 bar pressure region. The vertical dashed line marks the value of current partial pressure of CO₂ in the atmosphere (0.4 mbar).² The cluster reported in part (b) reports the geometry of the CO₂ adsorption on the metal site in IRMOF-74-I-Mg as obtained from periodic calculations (B3LYP-D*/TZVp). Reproduced with permission from Ref. 144. Copyright 2010 American Chemical Society. The atoms are represented according to following color code: oxygen (red), carbon (grey), magnesium (light blue).

15 Properties of porous solid materials can be easily modified by impregnating or tethering active groups onto their surface.¹¹ Analogously to silica-based materials, metal-organic frameworks properties have been improved in the CO₂ sorption by alkyl amines grafting. Alkylamines are able to chemisorbs CO₂,
 20 leading to higher adsorption enthalpies after grafting (see Table 5), facilitating CO₂ adsorption in the lower pressure regimes (see Figure 9d). The presence of water in this case is even beneficial on the adsorbed CO₂ instead of hindering its chemisorptions, because it allows to double the CO₂ uptake per metal site.¹¹
 25 Moreover, the presence of amines is expected to confer to the materials a higher stability to water because in presence of open metal sites they are grafted on those site hindering their accessibility to water and then the hydrolysis of the metal-oxygen bond.¹⁰ Also regenerability of the material/cyclability appears to
 30 be improved by their presence.¹⁴⁸ Amine grafting in MOFs was

reported to be possible either through post-synthetic modification of the framework^{130, 147, 148, 151-154} (analogously to silica-based materials),¹⁵⁵ or incorporating them during the synthesis by using an appropriate linker.¹¹⁸ In post synthesis methods, as stated
 35 above, the grafting happens through the bonding between the open metal site and the amine molecule. The high crystallinity of MOFs and the large separation between the metal sites, avoid overloading of the material and a more stable grafting on their surfaces than in silica materials, providing higher stability upon
 40 cycling.⁶³ Between the two methods, the second approach makes intrinsically more stable the grafting of amines improving the cyclability of the materials.

The presence of aliphatic amines in the framework has been actually proven to improve the material stability under air and
 45 moisture,^{118, 148} their regenerability and also their affinity toward CO₂, allowing MOFs to reach a degree of affinity toward CO₂

and stability close to amine-modified oxides.¹⁴⁸ Both the grafting approaches have been applied to representatives of Mg-IRMOF-74 family: IRMOF-74-I, IRMOF-74-IIb and IRMOF-74-III. In particular, for IRMOF-74-I and IRMOF-74-IIb effective post-synthesis grafting procedures were reported allowing a high dispersion of ethylenediamine (ED)¹⁴⁸ and tetraethylenepentamine¹⁵¹ (TEPA) in IRMOF-74-I and of N,N'-dimethylethylenediamine (mmem)¹⁴⁷ in IRMOF-74-IIb (see Figure 8b). On the contrary, in IRMOF-74-III different aliphatic amines have been introduced during the synthesis by using appropriate linkers: IRMOF-74-III-NH₂, -CH₂NHBoc, -CH₂NMeBoc, -CH₂NH₂, and -CH₂NHMe.¹¹⁸ It is evident from the comparison of part a and b of Figure 8 as the introduction of an amine functionality strongly compromises the free pore volume of IRMOF-74-I and -II whereas IRMOF-74-III, because of its large pore dimension, would maintain a high porosity (see Table 5). Correspondingly, a strong decrease in the CO₂ capacities at 1 bar for IRMOF-74-IIb-mmem with respect to IRMOF-74-IIb was observed (see Figure 9d), whereas the pristine and the modified IRMOF-74-III show essentially the same capacity at 1 bar. Nevertheless, IRMOF-74-IIb-mmem adsorbs at least twice the CO₂ amounts than the alkylamine-modified IRMOF-74-III. This is likely related to the nature of the alkylamine used. In fact, IRMOF-74-I-ED¹⁴⁸ showed completely comparable CO₂ adsorption than IRMOF-74-IIb-mmem for CO₂ partial pressures close to atmospheric one (1.51 vs. 1.8 mmol g⁻¹, respectively).^{147, 148} IRMOF-74-I-TEPA-40¹⁵¹ showed higher CO₂ capacities than any other MOFs for a flow containing 15% of CO₂, doubling the value reported for IRMOF-74-IIb-mmem (see Table 5).¹⁴⁷ Cao et al.¹⁵¹ evaluated also the influence of amine content on the adsorption capacity and they found as CO₂ capacities have a bell-bottomed dependence with respect to the concentration of the amine, likely associated to diffusion problems at high amine content. It is interesting to compare the shape of the isotherms reported in Figure 9d' in the 0-0.1 bar pressure range. Only for alkylamine modified materials, the isotherms show a S-shaped

behaviour that is particularly evident for IRMOF-74-IIb-mmem. Such a shape indicates that small drops in the CO₂ pressure are expected to cause a fast release of the CO₂ chemisorbed in the material and then an easy regeneration in pressure swing adsorption plants. The presence of amines is then beneficial on the CO₂ capacity only in the 0-0.1 bar pressure regime, making the material more selective for CO₂ capture from post-combustion flue gases (15% CO₂) or even from atmosphere (400 ppm). This effect is less evident for modified IRMOF-74-III materials, that shows essentially the same capacity of the unmodified material in the whole pressure range. Nevertheless, the difference between their adsorption (full scatters) and desorption (empty scatters) branches clearly indicates the formation of carbamates due to the reaction between the amine and CO₂ (see Figure 9d', violet and dark blue curves). Further, a larger stability of the separation performances in presence of water was observed for all the alkylamine modified materials. For example, the breakthrough time obtained for CO₂/N₂ separation in dry and moisture conditions was coincident for IRMOF-74-III-CH₂-NH₂, whereas the parent IRMOF-74-III-CH₃ showed a 80% decrease if water was admitted in the gas flow.¹¹⁸ This stabilization effect is obviously not verified if aromatic amines are introduced in the framework: in fact, although their introduction causes an increase of the energetic of adsorption because of cooperative effects,^{17, 156} they are not able to chemically react with CO₂.

Although the higher sorption heat (71 vs. 44 kJ mol⁻¹ for IRMOF-74-IIb with and without mmem, respectively)¹⁴⁷ due to the formation of carbamate/bicarbonate species, lower temperature for the full regeneration of the material were reported the amine modified IRMOF-I^{148, 151} and II.^{147, 152} Moreover, a comparison among different metal sites, allowed to verify that the larger electrostatic field of the Mg²⁺ is able to activate favorably the amine toward CO₂ more than any other metal.¹⁵² Some similarity with the Rubisco active site where claimed in this case.¹⁵²

Table 5. Review on CO₂ adsorption on Mg-based MOFs reporting the magnesium Coordination Number (CN), framework dimensionality, BET (S_{BET}) and Langmuir (S_{Langmuir}) surface area, pore volume (V_{por}), CO₂ capacity (n_{CO₂}) in different temperature and pressure conditions and isosteric heat of CO₂ adsorption (q_{iso}).

Material ^a	CN ^b	Framework dimensionality	S _{BET} ^c (m ² g ⁻¹)	S _{Langmuir} ^c (m ² g ⁻¹)	V _{por} ^c (cm ³ g ⁻¹)	n _{CO₂} @P,T (mmol g ⁻¹) ^g	q _{iso} (kJ mol ⁻¹)	Ref.
{[Mg(Hide)(H ₂ O) ₂]-1.5H ₂ O} _n	6 (2 H ₂ O)	1D	low	low	0.06	0.27@195 K, 0.93 bar (vol)	-	157
{[Mg ₃ (idc) ₂ (H ₂ O) ₅]-2 H ₂ O} _n	6 (3 H ₂ O)	3D	low	low	0.02	0.31@195 K, 0.93 bar (vol)	-	157
MgTTTP (PCN-72)	6 (1 DMSO)	3D	low	low	low	3.30@ 195 K, 1 bar 1.56@ 273 K, 1 bar 1.34@ 295 K, 1 bar	-	137
[Mg ₂ (HCO ₂) ₂ (NH ₂ -BDC)-(DMF) ₂] _n	6 (1 DMF)	2D	-	-	-	3.99@ 273 K, 1 bar (vol)	-	136
β-Mg(HCOO) ₂ ·2H ₂ O	6 (2 H ₂ O)	3D	-	-	-	0.30@298 K, 0.93 bar (vol) ^g	-	158
α-[Mg ₃ (O ₂ CH) ₆]	6 (0)	3D	150	-	0.11	1.69@298 K, 1 bar (vol)	-	159
γ-[Mg ₃ (O ₂ CH) ₆]	6 (0)	3D	120	-	24.7 vol.% ^d	2.01@298 K, 1 bar (vol)	-	160
Mg(HCOO) ₃ ⇌(CH ₃) ₂ NH	-	-	-	-	-	0.30@298 K, 1 bar	-	158
[(Fmd)Mg(HCOO) ₃]	6 (0)	3D	low	low	low	0.02@195 K, 1 bar	-	161
[(Gua)Mg(HCOO) ₃]	6 (0)	3D	low	low	low	0.01@195 K, 1 bar	-	161
{[Mg ₂ (H-3,5-PZDC) ₂ (H ₂ O) ₄]-H ₂ O} _n	6 (2 H ₂ O)	2D	low	low	low	0.36@298 K, 1 bar (vol)	-	123
[Mg(3,5-PDC)(H ₂ O)] (Mg-	6 (1 H ₂ O)	3D	-	-	38.7 vol.%	0.63@298 K, 1.01	-	162

MOF-1)							bar (tga/over N ₂)		
Mg ₂ (dobdc) CPO-27-Mg,	6 (1 H ₂ O)	3D	877 ¹⁶³	1030 ¹⁶³	0.37 ¹⁶³	5.36@298 K, 0.1	47 ⁸³	77, 83,	
MOF-74-Mg, IRMOF-74-I ^e			1495 ⁸³	1905 ⁸³	0.60 ¹²⁴	atm ⁸³	47 (-ΔH _{ads} , ¹⁴⁴	124,	
			1350 ¹²⁴	1600 ¹²⁴	0.21 ¹⁵¹	8.0@298 K, 1 atm ⁸³	VTIR ¹⁴⁴	141,	
			1542 ¹⁴¹	2060 ¹⁶⁴		14.32@298 K, 33	38-43 ¹⁴¹	144,	
			1800 ¹⁶⁴	886 ¹⁵¹		bar (vol) ¹⁴¹	42 ⁷⁷	151,	
			780 ¹⁵¹			15.66@278 K, 36		163	
						bar ¹⁴¹			
						9.04@313 K, 40			
						bar ¹⁶⁴			
						6.70@473 K, 40			
						bar (vol) ¹⁴¹			
						2.67@333 K in			
						15%CO ₂ /N ₂ (flow-			
						ms) ¹⁵¹			
Mg ₂ (dobpdc), IRMOF-74-IIb	6 (1 H ₂ O)	3D	2510 ^{e,124}	2940 ^{e,124}	1.04 ^{e,124}	0.17@298 K, 0.2	44 ¹⁴⁷	124	
						mbar ¹⁴⁷			
						6.6@298 K, 1 bar ¹⁴⁷			
IRMOF-74-III-CH ₃	6 (1 H ₂ O)	3D	2640	3940	1.37	2.95@298 K, 1.07	–	118	
						bar			
IRMOF-74-III-NH ₂	6 (1 H ₂ O)	3D	2720	4130	1.44	3.17@298 K, 1.07	–	118	
						bar			
IRMOF-74-III-CH ₂ NHBoc	6 (1 H ₂ O)	3D	2170	2720	0.95	2.08@298 K, 1.07	–	118	
						bar			
IRMOF-74-III-CH ₂ NH ₂	6 (1 H ₂ O)	3D	2310	3270	1.14	3.27@298 K, 1.07	Reversible	118	
						bar	@120°C		
IRMOF-74-III-CH ₂ NMeBoc	6 (1 H ₂ O)	3D	2220	2540	0.89	1.90@298 K, 1.07	–	118	
						bar			
IRMOF-74-III-CH ₂ NHMe	6 (1 H ₂ O)	3D	2250	3150	1.13	2.85@298 K, 1.07	Reversible	118	
						bar	@120°C		
IRMOF-74-I-ED	6 (1 ED)	3D	–	469	0.40	1.51@298 K, 400	Reversible at	148	
						ppm CO ₂ in Ar	110°C		
						(flow-tga)			
IRMOF-74-I-TEPA-30	6 (1 TEPA)	3D	312.63	410.68	0.19	4.49@333 K in	–	151	
						15%CO ₂ /N ₂ (flow-			
						ms)			
IRMOF-74-I-TEPA-40	6 (1 TEPA)	3D	132.24	230.5	0.15	6.06@333 K in	–	151	
						15%CO ₂ /N ₂ (flow-			
						ms)			
IRMOF-74-I-TEPA-50	6 (1 TEPA)	3D	23.54	54.21	0.05	3.48@333 K in	–	151	
						15%CO ₂ /N ₂ (flow-			
						ms)			
Mg(dobpdc) ₂ -mmen	6 (1 mmen)	3D	70 ¹⁰	–	0.02 ¹⁴⁷	1.8@298 K, 0.3	71 ¹⁴⁷	10,147	
						mbar (vol) ¹⁴⁷			
						3.9@298 K, 1 bar			
						(vol) ¹⁴⁷			
						3.14@313 K, 0.15			
						bar (vol) ¹⁴⁷			
						1.05@298 K, in 1 h			
						in Ar flow with 390			
						ppm CO ₂ (flow-			
						ms) ¹⁴⁷			
						2.52@313 K, in 15'			
						in 15%CO ₂ /N ₂			
						(flow-ms) ¹⁴⁷			
[Mg(TCPBDA)(H ₂ O) ₂]	6 (2 H ₂ O)	3D	low	low	low	1.49@298 K, 1.01	–	150	
·6DMF ·6H ₂ O (SNU-25)						bar			

^aNH₂-BDC = 2-amino-1,4-benzenedicarboxylate; DMF = *N,N*-dimethylformamide, H₂bdc = 1,4-benzenedicarboxylic acid, DMA = dimethylacetamide, H₂bpdc = 4,4-biphenyldicarboxylic acid, H₃btc = 1,3,5-tricarboxylic acid, H₂-3,5-PDC = 3,5-pyridine dicarboxylic acid, H₂-2,4-PDC = 2,4-pyridine dicarboxylic acid, H₃-3,5-PZDC = pyrazole-pyridine dicarboxylic acid; H₂NDA = 1,4-naphthalenedicarboxylic acid, phen = 1,10-phenanthroline, H₂hfpb = (hexafluoroisopropylidene)bis(benzoic acid); def = *N,N*-diethylformamide; ndc = 2,6-naphthalenedicarboxylate; D-H₂Cam = D-camphoric acid; DMA = dimethylacetamide; H₂tart = tartaric acid, dif = *N,N*-diisopropylformamide; H₂OBA = 4,49-oxybisbenzoic acid; H₄dobdc = 2,5-dihydroxy-1,4-benzenedicarboxylic acid; BPTC = 2,2',6,6'-tetracarboxybiphenyl; Boc = tertbutyloxycarbonyl; H₃idc = 4,5-imidazolecarboxylic acid; H₄TTTP = 2',3',5',6'-tetramethyl-[1,1':4',1''-terphenyl]-4,4''-dicarboxylic acid; formamidinium cation [Fmd⁺, (NH₂-CH⁺-NH₂)]; guanidinium cations[Gua⁺, C⁺(NH₂)₃]; TCPBDA²⁻ = *N,N,N',N'*-tetrakis(4-carboxyphenyl)-biphenyl-4,4'-diamine, ED = etilendiamine; TEPA = tetraethylenepentamine; mmen = *N,N'*-dimethylethylenediamine.

¹⁰ In parenthesis the number and the nature of solvent molecules coordinated to the most exposed Mg²⁺ species are reported.

^eSurface area and pore volume as obtained from N₂ adsorption, if not otherwise specified.

^fCalculated value upon manual removal of the solvent molecules from the solvated structure.

^gAr isotherm and pressure range adopted in the BET area calculation different from the standard one.

^hThe technique used for the measurement is indicated in parenthesis: vol = volumetry (static conditions), ms = mass spectroscopy, tga = thermal

¹⁵ gravimetric analysis.

ⁱConversion from original data in wt% made on the assumption that wt% = CO₂ weight/(CO₂ weight+sample weight)*100, if not otherwise specified.

4.4. Atmospheric Chemistry

The region of the terrestrial atmosphere extending from altitude between 75 and 110 km is referred as mesosphere/lower thermosphere and is of particular interest because it forms the boundary between the atmosphere and the space. The transition to space is in fact fixed at 105 km (turbopause) because of the change from a bulk to free molecular motion of the gas molecules.¹⁶⁵ Mesosphere is also the most sensitive region of the atmosphere to climate change.¹⁶⁶ It undergoes to a fast cooling due to the increased presence of molecular radiators like CO₂ and methane,¹⁶⁷ that have in that region an opposite effect with respect to what is observed in the troposphere (0-17 km). The upper atmosphere is characterized by temperatures between 170 and 250 K and by low pressures (10⁻⁶-10⁻³ bar in the mesosphere).¹⁶⁵ Because of these peculiar conditions, species (like atomic metallic species) and reactions very close to the gas phase conditions in the molecular quantum mechanics approximation are observed. For example, because of the low pressures, atomic oxygen is the major reactive species present there.¹⁶⁵ Also neutral metal atoms and metal ions are present in the upper atmosphere deriving from meteoric ablation. In fact, meteoroids, because of their high entry velocities (tens of km s⁻¹) undergo to rapid frictional heating by collision with air molecules and their constituent minerals subsequently vaporize with formation of atomic metallic species. This process has been estimated to provide daily a mass flux up to 130 t.^{165, 168} Magnesium is the most abundant metallic constituent of meteorites^{167, 169} and, therefore, meteoric ablation injects into the atmosphere large quantities of Mg and Mg⁺. Systematic

observation of global atomic magnesium layers in the atmosphere (Mg and Mg⁺ species) has become possible only since 2008 through satellite-born UV-visible spectroscopy.¹⁶⁵ Before this date, reaction of magnesium with the different reactive species present in the mesosphere were largely investigated in order to individuate the magnesium sink.

In the region between 75 and 110 km, magnesium is present in three main forms (see Figure 10b): Mg⁺, Mg and Mg(OH)₂, concentrated in three different global layers.¹⁶⁵ Mg⁺ layer peaks at heights between 90 and 100 km with a peak ion concentration of (1-5) · 10³ cm⁻³ during daytime, decreasing to 10⁻² cm⁻³ at night.¹⁷⁰ The Mg layer exhibits a peak at altitudes around 88 km and lower concentration than the ionic layer,¹⁷¹ for a total Mg⁺/Mg ratio between 4 and 12, unusually high with respect to what observed for other metals (e.g. Na). These species are fast converted to other molecular species by reaction with highly reactive species as atomic O and H, O₃ but also O₂, H₂O and CO₂. The third major gas phase magnesium species, Mg(OH)₂, would be formed through the subsequent reaction of Mg with O₃ (MgO), O₂ (OMgO₂) and H₂O (see Figure 10a). Molecular Mg(OH)₂ is concentrated in a global layer with a peak at about 85 km and its stability is due to the low reactivity toward atomic O (at difference of oxides and carbonates) and to the low concentration of atomic H at 85 km: in fact, although Mg(OH)₂ is destroyed significantly by atomic H, the low ratio [H]/[O] = 1% at 85 km makes the decomposition reaction quite improbable. All the other gas phase magnesium species (MgO, MgO₂, OMgO₂, MgCO₃, ...) are short lived and are dynamically and reversibly converted each other (see Figure 10a and c).¹⁶⁵

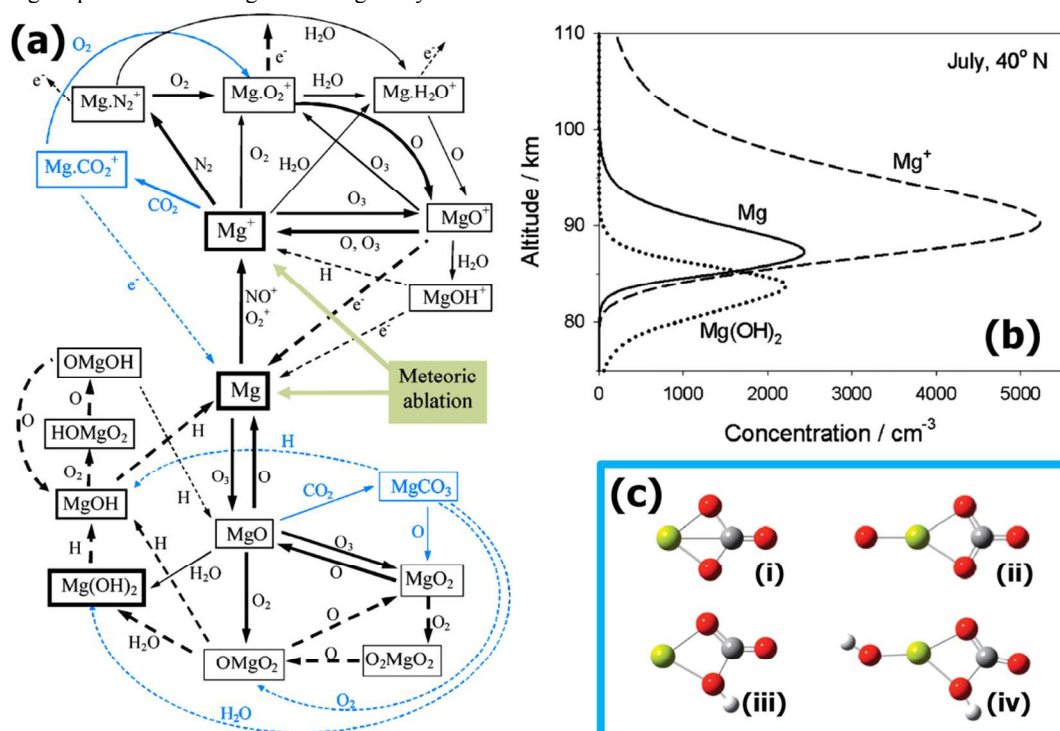
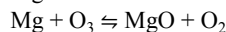


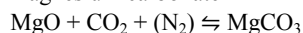
Figure 10. (a) Schematic diagram of magnesium chemistry in the upper mesosphere/lower thermosphere region. Major magnesium species are shown in boxes with bold outlines. Important reaction pathways are indicated with thicker arrows.¹⁶⁵ Reaction involving CO₂ or the products of CO₂ reaction with magnesium species are highlighted with blue color. (b) Vertical profiles of Mg⁺, Mg, and Mg(OH)₂ predicted by the 1D atmospheric model for July, at midlatitudes (40°N). These profiles are at midday.¹⁶⁵ (c) Optimized geometries (at the B3LYP/6-311+g(2d,p) level of theory) of magnesium-containing

molecules likely to form in the upper atmosphere: (i) $\text{MgCO}_3(^1\text{A}_1)$; (ii) $\text{OMgCO}_3(^3\text{A}'')$; (iii) $\text{Mg}(\text{OH})\text{CO}_2(^2\text{A}')$; (iv) $\text{HOMg}(\text{OH})\text{CO}_2(^1\text{A}')$. Color legend: Mg (yellow); O (red); C (gray); H (white). Parts (a-c) have been adapted from Ref. 165. Reproduced with permission. Copyright 2012 American Chemical Society.

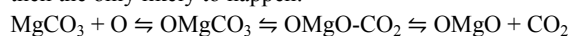
Among the possible reactions of magnesium species in the upper atmosphere, the ones involving CO_2 are very short living and are essentially based on neutral magnesium-derived molecular MgO .¹⁶⁵



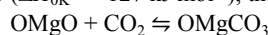
($\Delta H_{0\text{K}} = -147 \text{ kJ mol}^{-1}$), that after formation of molecular magnesium carbonate¹⁶⁵



would decompose in presence of atomic O or H. Decomposition with atomic H is largely favored on thermodynamic and kinetics basis ($\text{MgCO}_3 + \text{H} \rightleftharpoons \text{MgOH} + \text{CO}_2$, $\Delta H_{0\text{K}} = -277 \text{ kJ mol}^{-1}$) but the low concentration of atomic H at 80 km would make this reaction less likely to occur.¹⁶⁵ Decomposition in atomic O is then the only likely to happen.¹⁶⁵

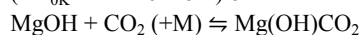
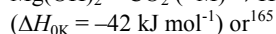
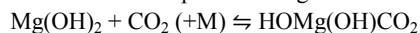


($\Delta H_{0\text{K}} = -127 \text{ kJ mol}^{-1}$), that can also react back to:¹⁶⁵



($\Delta H_{0\text{K}} = -118 \text{ kJ mol}^{-1}$), being the OMgCO_3 species more stable than $\text{OMgO} + \text{CO}_2$.¹⁶⁵

For what concerns Mg^+ and hydroxides, reactions with CO_2 are not favored with respect to others.¹⁶⁵ In particular, Mg^+ mostly reacts with O_3 giving MgO^+ for altitude larger than 90 km.¹⁶⁵ For altitude lower than 90 km, $\text{Mg}^+ \cdot \text{N}_2$ or $\text{Mg}^+ \cdot \text{CO}_2$ complexes will be present, but fast converted to $\text{Mg}^+ \cdot \text{O}_2$ (see Figure 10).¹⁶⁵ Reaction of CO_2 , with hydroxides on the contrary, is not likely to happen because of the low energetics and the high energetic barrier to the complex rearrangement.¹⁶⁵



($\Delta H_{0\text{K}} = -32 \text{ kJ mol}^{-1}$). The short life of magnesium carbonate and bicarbonate species is different for example with respect to atomic Na chemistry,¹⁷² for which NaHCO_3 represents its major reservoir species, likely involved in the phenomenon of noctilucent clouds.¹⁶⁷

4.5. Metal surfaces

Sorption of CO_2 on pure metallic magnesium is not largely studied being essentially of no practical use. Metallic magnesium is used only as dopant on metallic and oxidic catalyst to enhance their affinity toward CO_2 . The works present in the literature^{12, 173, 174} deal exclusively with single crystal surfaces with the aim to understand as Mg acts as promoter in CO_2 activation. The first report of a combined investigation of reactive CO_2 chemisorption was at $\text{Mg}(0001)$ surface by means of X-ray photoelectron (XPS) and high resolution electron energy loss (HREELS) spectroscopies.^{12, 173} This work showed that CO_2 is molecularly adsorbed on Mg only at 85 K; upon increasing the temperature, reactive chemisorptions occurs leading to surface carbonate and oxide. Carbonate was shown to be actually a surface species, whereas oxide is present as underlayer (thickness 0.4 nm). Also for chemisorptions on $\text{Mg}(0001)$ surfaces, the reaction showed all the characteristics associated with the participation of a precursor state through the Freund-Messmer mechanism ($\text{CO}_2^{\delta-} \cdots \text{CO}_2$

dimer).¹²

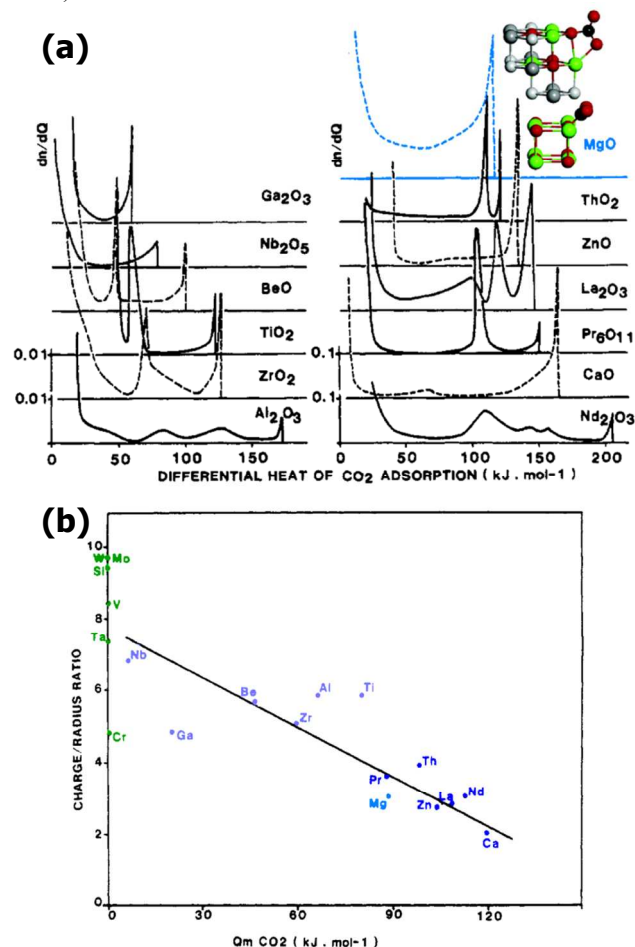


Figure 11. (a) Sites distribution as function of the differential heat of CO_2 adsorption as measured at 25°C on several metal oxides activated at 400°C as in Ref. 61. Cluster representations of monodentate CO_2

adsorption on MgO edges and bidentate adsorption on MgO corners (the major species) as obtained at the B3-LYP/6-31G(d) level are also reported. The atoms are represented according to following color code: oxygen (red/white), carbon (black), magnesium (green/grey). (b) Metal charge/radius ratio as function of the average isosteric heat of adsorption for CO_2 as in Ref. 61. Basic, acidic and amphoteric oxides have been signaled by blue, green and violet color, respectively. (a) and (b) adapted from Ref. 61. Reproduced with permission. Copyright 1990 American Chemical Society. Atomistic representations in part (a), adapted from Ref. 175. Reproduced with permission. Copyright 2005 American Chemical Society.

4.6. MgO-based oxides

Metal oxides are significantly employed in all the steps of the CO_2 cycles, such as for separation, adsorption, sequestration and recycling. In particular, their use as catalysts and catalyst supports have been reported, although between the two options, in almost the totality of the cases they are used as supports of catalytic particles, being both metal and oxidic species. This is due to their large surface area associated to a strong ionicity, that avoid the particles aggregation and then the lowering of the

catalytic efficiency. They have also a direct influence on the particles, determining their dimensions and distribution. On the other hand, oxides can show amphoteric, basic, neutral or acidic properties. According to Lewis definition, acidity and basicity indicate electron accepting and electron donating properties, respectively. The choice of the support can then change drastically the ability of the catalyst to activate CO_2 . Nevertheless, the problem of standardization of the acidity of solids is a difficult one and it has been addressed in the past,⁶¹ for example by means of microcalorimetry of adsorption⁶¹ and infrared spectroscopy.²² In particular, the possibility to use the average heat of adsorption of NH_3 and of CO_2 to compare the strength of acid and base surfaces respectively, has been reported.⁶¹ In Ref. 61, the materials were all treated at the same temperature (400°C) because of the importance of surface pretreatment in affecting the relative amount of surface OH (Brønsted acidity), overexposed metal cations (Lewis acidity) and oxygen anions (Lewis basicity) and then the mode of bonding of adsorbed molecules.⁶¹ From this statement, the complexity of the problem is clear only partially. In fact, only upon changing the temperature used to activate the material, a direct change in its basicity can be observed.¹⁷⁶ Nevertheless, from the comparison of 20 oxides, it was experimentally verified that the acidity is proportional to the charge/radius ratio of the metal (if the oxides are activated at the same temperature). In Figure 11b, the metal charge/radius ratio is reported as a function of the average isosteric heat of adsorption measured for these 20 oxides. It was evidenced as CO_2 affinity towards materials can be used as a measure of their basicity. It is evident that an oxide with a low value of charge/ratio is more ionic in nature and will present more basic sites.¹⁷⁶ A higher the charge/ratio would correspond to a greater degree of covalency of the oxide and then to a higher acidic character.¹⁷⁶

Differing on their basic/acidic character, oxides stabilize distinctively the particles and play an active role in the process, determining also the catalytic activity and selectivity.⁷¹ Actually, in many processes, the catalytic active site is not represented by the supported particles alone or by the support, but it is at the interfaces between the two species (see Section 2.2).^{14, 178} The broad use of metal oxides in the whole CO_2 cycle is due to their ability to form very different bulk and superficial carbonate and bicarbonate species, the relative percentage of which depends strongly on hydration.⁵⁷ This is exemplified for bulk phase in the ternary phase diagram for the $\text{MgO-CO}_2\text{-H}_2\text{O}$ system in Figure 12b. For what concerns superficial species, a picture of the different mechanism of adsorption of CO_2 on oxide is given in Figure 12a. The ability to form these superficial species is particularly important in the activation of CO_2 (see Section 2.1) and in determining electron donating properties.¹²

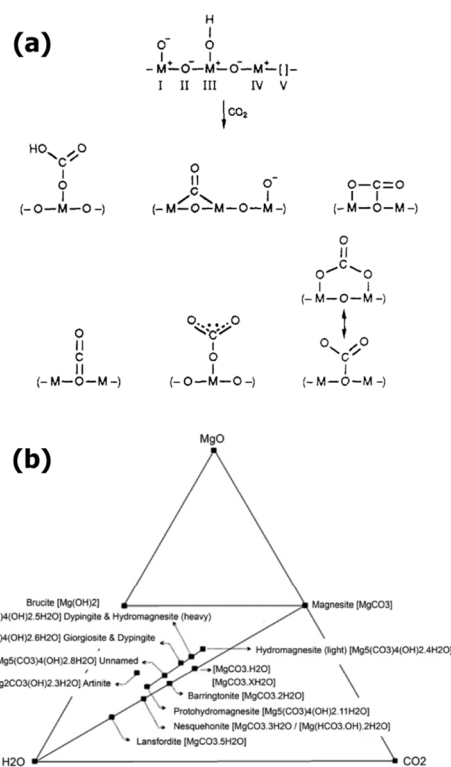


Figure 12. (a) Possible mechanisms of adsorption of CO_2 on the different types of adsorption sites present on the surface of metal oxides. Adapted from Ref. 61. Reproduced with permission. Copyright 1990. American Chemical Society. (b) Ternary phase diagram for the $\text{MgO-CO}_2\text{-H}_2\text{O}$ system with indicated the position of the hydrated and basic hydrates magnesium carbonate. Reproduced with permission from Ref. 177. Copyright 2012 Elsevier.

Among basic oxides, MgO is characterized by a medium-high basicity: its CO_2 isosteric heat of adsorption is in fact in the middle between CaO (high) and Ga_2O_3 (low basicity) in Figure 11a.⁶¹ MgO is then expected to facilitate the formation of CO_2^- species although not stabilizing them too much. CO_2 desorption from MgO is observed in fact in two temperature ranges: 60-320°C, where the most part of the carbonates are decomposed, and 500-800°C. MgO is an oxide with a rock-salt structure where each Mg^{2+} ion is octahedrally coordinated to six O^{2-} and viceversa. For the interaction with a perfect surface constituted by pentacoordinated ions O_{5c}^{2-} and Mg_{5c}^{2+} , it was theoretically shown as^{175, 179} CO_2 would be only weakly bound on MgO surface whereas chemically bound with formation of carbonate was observed on a similar surface of CaO . This difference in reactivity is explained by the larger stabilization in MgO of the O^{2-} ions at the surface by the Madelung potential, leading to a lower basicity and reactivity.¹²

Nevertheless, on the surface of real MgO particles, the landscape is in general more complicated (see Figure 13a-c). Different irregularities are present that can confer to MgO materials different basicity and reactivity. In particular, the distribution of the lower coordination O_{LC}^{2-} oxides ($\text{LC} = 3c, 4c$ for tricoordinated and tetracoordinated ions) and the hydroxyls coverage are important parameters in determining MgO basicity. Activation temperature and synthetic procedures have a drastic influence on these two parameters.¹⁸⁰⁻¹⁸² Surface area of MgO strongly varies

upon synthesis conditions from $10 \text{ m}^2 \text{ g}^{-1}$ of MgO “smoke” to several hundred $\text{m}^2 \text{ g}^{-1}$ (see Table 6).¹⁸² Each $\text{O}_{\text{LC}}^{2-}$ is accompanied by $\text{Mg}_{\text{LC}\pm 1}^{2+}$ ions, creating a vicinal acid-base couple that can more or less effectively coordinate CO_2 . The amount of $\text{O}_{\text{LC}}^{2-}$ sites depends not only on the particle size but also on outgassing the samples at increasing temperature.¹⁸³ Moreover (see Figure 13b and c), different OH species are present on the MgO surface,

distinguishable between “isolated” OH groups (identifiable by IR spectroscopy as a narrow band at 3749 cm^{-1} in Figure 13d) and “linked” OH groups, that is involved in hydrogen bonding (broad band at 3650 cm^{-1}). The hydroxyl coverage can be also changed by increasing the activation temperature or through water exposure.

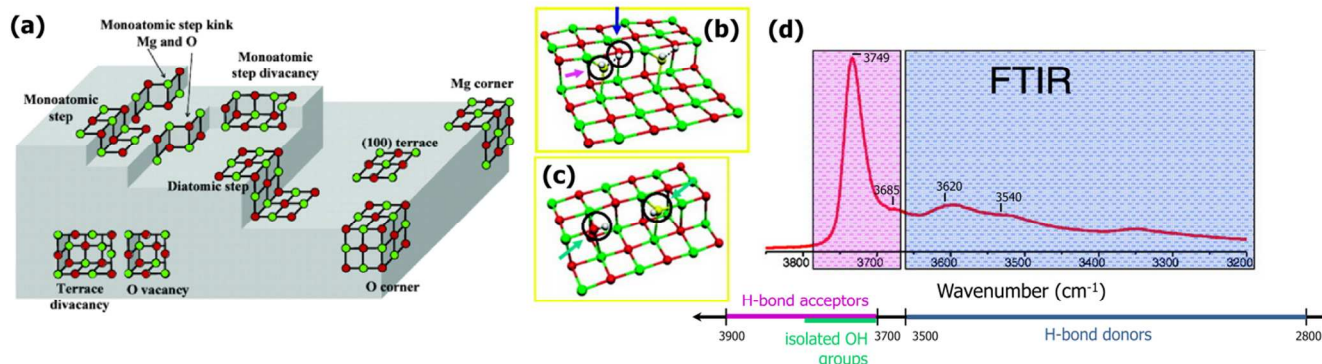


Figure 13. (a) Schematic representation of the irregularities on the MgO surface by using a modified steps and corners model. (b and c) Hydroxyl species on MgO defects. The arrows indicate the different hydroxyl species giving rise to the spectral features in part (d). (d) MgO infrared spectra after activation in vacuum at 300°C as in Ref. 184. Part (a), Adapted with permission from Ref. 183. Copyright 2006 American Chemical Society. Parts (b)-(d) Adapted with permission from Ref. 185. Copyright 2007 American Chemical Society. The atoms are represented according to following color code: hydrogen (white), surface oxygen (red), water oxygen (yellow), magnesium (green).

Contrary to what expected on the basis of its complicated surface structure,^{175, 181, 183, 185} microcalorimetric measurements of carbon dioxide conducted at 25°C on a high surface area MgO ($197 \text{ m}^2 \text{ g}^{-1}$, activation temperature 400°C)⁶¹ indicate an homogeneous adsorption behavior with two plateau at low ($0.0\text{--}0.6 \mu\text{mol} \cdot \text{m}^{-2}$) and high ($> 1.6 \mu\text{mol} \cdot \text{m}^{-2}$) coverage at 110 and 15 kJ mol^{-1} respectively, with a monotonic decrease for intermediate loadings. Accordingly, it has been shown by infrared spectroscopy studies¹⁸⁶ as chemisorption of CO_2 on MgO reveals mainly bidentate adsorbed species with a little part of unidentate. Quantum mechanical calculations suggest that monodentate species would be formed on edge sites (4c) and bidentate on corner sites (3c) of MgO.¹⁷⁵

4.6.1. Separation

For what concerns its use in CO_2 separation processes, MgO constitutes an interesting material being able to absorb CO_2 at relatively low temperature ($200\text{--}400^\circ\text{C}$) and showing the lowest temperature for regeneration among alkali oxides.⁵⁹ In fact, the decarbonation of MgCO_3 happens significantly already at $T = 385^\circ\text{C}$,¹⁸⁷ decidedly lower than $T > 700$ and 800°C required for Li- and Na-based systems, respectively.^{188, 189} MgO used in membranes for CO_2/N_2 separation allowed to reach very high values of selectivities (120 at 350°C).¹¹ Nevertheless, CO_2 capacities of MgO-based systems are still too low with respect to other oxides, although the intensive efforts made in literature (see

for example Table 6).⁶³ The main problems are the slow kinetics of absorption and the high sintering tendency during regeneration.⁵⁹ For what concerns the first point, it is essentially related to the fact that the produced MgCO_3 forms a passivating layer on the MgO surface hindering the reaction of the interior part of the particles.⁵⁸ Absorption of CO_2 in presence of water allows to obtain higher CO_2 capacities. The mechanism in this case is coincident with absorption on $\text{Mg}(\text{OH})_2$ and it is described in Section 4.7.1.

Several mesoporous MgO materials have been reported in literature, synthesized for example from sol-gel syntheses,⁶² through the use of surfactants or by structure replication of mesoporous carbon^{190, 191} and polymers.¹⁹² Nanosized crystal MgO have been also reported, synthesized through the use of surfactants^{62, 193}, hypercritical sol-gel drying¹⁹⁴ or MOF decomposition in air at high temperatures.^{195, 196} In these case higher CO_2 capacities were obtained with respect to commercial MgO ($0.2\text{--}0.5 \text{ mmol g}^{-1}$,⁶² see Table 6) although still far from the stoichiometric capacity (24 mmol g^{-1}). This increase is related to the higher surface/volume ratio of the particles and then to the higher number of tetraordinated and tricoordinated sites on the MgO surfaces, besides the fact that the smaller dimensions make the uptake less dependent on the diffusion of CO_2 in the bulk of the particles. MgO doping with other oxides does not bring significant increase in the CO_2 uptake (about 0.5 mmol g^{-1}).^{62, 63}

Table 6. Review of CO_2 sorption of some MgO-based materials reporting the precursors used in the synthesis, BET (S_{BET}) surface area, pore volume (V_{por}), crystal size of MgO particles, CO_2 capacity (n_{CO_2}) at 1 bar at different temperatures, regeneration temperature and number of cycles for which the cyclability of the material was tested.

Material	precursors	S_{BET}^a ($\text{m}^2 \text{ g}^{-1}$)	V_{por}^a ($\text{cm}^3 \text{ g}^{-1}$)	Crystal size ^a (nm)	$n_{\text{CO}_2}@P, 1 \text{ bar}$ (mmol g^{-1}) ^b	Regeneration T (K)	Cycles	Ref.
MgO	commercial				0.22-0.45@298 K (tga)			197

MgO	nitrate	7.6	0.02	40.4	0.08@100°C (vol)	600°C		198
MgO	Nitrate, CMK-3 carbon	250	0.52		1.82@298 K (tga) 2.27@373 K (tga) 1.64@298 K (tga, 15% CO ₂ /N ₂)	800°C in N ₂ (RT-200°C, > 70%)	3	190, 191, 197
MgO (FM1)	Nitrate, polyethylene oxide	101	0.24	10.2	1.93@100°C (vol)	600°C in N ₂ (RT-300°C, > 60%)	6	198
MgO (FM2)	Nitrate, polyethylene oxide	130	0.36	9.9	2.77@25°C (vol) 2.61@100°C (vol) 2.07@150°C (vol)	600°C in N ₂ (RT-300°C, > 60%)	6	198
MgO (FM3)	Nitrate, polyethylene oxide	121	0.29	10.4	2.18@100°C (vol)	600°C in N ₂ (RT-300°C, > 60%)	6	198
MgO (3DOM MgO)	Nitrate, PMMA, Pluronic F127, 20% ethanol	183	0.43	5-8	0.416@25°C (vol) no physisorbed	800°C in He (RT-400°C, > 50%)		199
MgO (3DOM MgO)	Nitrate, PMMA, Pluronic F127, 40% ethanol	243	0.45	5-8	0.568@25°C (vol) no physisorbed	800°C in He (RT-400°C, > 40%)		199
(Ca, MgO) (Ca/Mg = 1/50)		200 (fresh), 38 (after some days in air)			0.21@25°C (vol)			62
MgO-K ₂ CO ₃ MgO/C (Mg 21.1 wt%, MgO 42.6 wt%, mPC-MgO-773)	MgCl ₂ , sawdust	279	0.14	17.1	1.98@748 K 4.6@353 K (tga)	748 K	17	56 200
MgO/C (Mg 20.5 wt%, MgO 42.2 wt%, mPC-MgO-873)	chloride, sawdust	306	0.16	18.6	2.7@323 K (tga) 5.2@353 K (tga) 1.3@573 K (tga)	773 in N ₂ flow	19	200
MgO/C (Mg 19.4 wt%, MgO 41.4 wt%, mPC-MgO-973)	chloride, sawdust	298	0.15	17.8	5.1@353 K (tga)			200
MgO/γ-Al ₂ O ₃ (24wt% MgO, 5A3M)	Nitrate, Al(NO ₃) ₃ , P123 polymer	202	0.48		1.02@200°C (10% CO ₂ , 90% N ₂ , tga-ms) 2.11@200°C (10% CO ₂ , 80% N ₂ , 10% H ₂ O, tga-ms)	600°C in Ar flow (RT-350°C, > 50% for dry CO ₂ and > 70% for wet CO ₂)	6	192
MgO/γ-Al ₂ O ₃ (39wt% MgO, 5A5M)	Nitrate, Al(NO ₃) ₃ , P123 polymer	177	0.45		1.75@200°C (10% CO ₂ , 90% N ₂ , tga-ms) 2.98@200°C (10% CO ₂ , 80% N ₂ , 10% H ₂ O, tga-ms)	600°C in Ar flow (RT-350°C, > 50% for dry CO ₂ and > 70% for wet CO ₂)	6	192
MgO/γ-Al ₂ O ₃ (55wt% MgO, 5A7M)	Nitrate, Al(NO ₃) ₃ , P123 polymer	108	0.26		0.84@200°C (10% CO ₂ , 90% N ₂ , tga-ms) 1.91@200°C (10% CO ₂ , 80% N ₂ , 10% H ₂ O, tga-ms)	600°C in Ar flow (RT-350°C, > 50% for dry CO ₂ and > 70% for wet CO ₂)	6	192

^aSurface area and pore volume as obtained from N₂ adsorption.

^bThe technique used for the measurement is indicated in parenthesis: vol = volumetry (static conditions), ms = mass spectroscopy, tga = thermal gravimetric analysis.

Unfortunately, mesoporous and nanosized MgO fastly lose their capacity upon cycling. The sintering has been proven to rely on the necessity to heat up the system relatively fast.¹⁹⁴ Very slow heating rate would be necessary during the regeneration, that are impracticable in a plant. In these respect, a possible solution has been reported to be to support MgO on high surface area materials as zeolite,²⁰¹⁻²⁰³ mesoporous carbons,²⁰⁰ alumina¹⁹² and silica materials (SBA-15).²⁰⁴ One of the most interesting results in these area has been reported by Liu et al.²⁰⁰ MgO nanoparticles were in fact synthesized through fast pyrolysis of biomass waste (sawdust) preloaded with MgCl₂. A maximum capacity of 5.45 mmol g⁻¹ at 80°C and 1 bar was obtained with a good cyclability and a low regeneration temperature.²⁰⁰ This synthesis is particularly appealing being MgCl₂ largely abundant in seawater. Magnesium oxide has been also used as support for other CO₂ sorbent type as dry carbonates (see Section 2.2.4) with very low performances⁶⁷ and for CaO. Calcium looping technologies are at present one of the most efficient technologies for CO₂ capture between high temperature CO₂ sorbents,^{63, 64} especially if applied to cement industry.⁶⁵ Unfortunately, CaO suffers severely from sintering during regeneration.⁶³ MgO has been successfully used as supporting material for enhancing the sintering resistant properties of CaO.^{63, 205} If a CaO/MgO material with CaO/MgO = 0.4 is adopted, the starting CO₂ capacity of 15 mmol g⁻¹ was retained also after 50 cycles in a 100% CO₂ flow at 750°C.²⁰⁵

4.6.2. Catalysis

Besides as sorbents, magnesium-based oxides are also largely used like catalyst or catalyst supports in many reactions involving CO₂ as CO₂ hydrogenation,^{14, 206} dry reforming of methane,²⁸ and CO₂ copolymerization with epoxides. MgO activity as mild catalyst in formation of styrene carbonate with poor selectivity has been also reported.¹⁵ Use of MgO as photocatalyst for the reduction of CO₂ to CO in presence of H₂ and CH₄ has been also described.²⁵ It is also used as promoter in many oxidic catalysts for reactions involving CO₂.²⁸

Hydrogenation reactions. MgO,^{14, 207} Mg/SiO₂,^{14, 32, 208} and MgAl₂O₄^{14, 207} have been tested as support for Ru and Pd particles in catalyst both for CO₂ methanation (reaction [2] in Table 1) and reverse water gas shift (reaction [1]) reactions, for their ability to form carbonate and to strongly interact with the metal particles (see Section 2.2.1). The turnover frequency for CO₂ methanation obtained for high metal dispersion on these systems is in the order: Ru/Al₂O₃ (16500 s⁻¹) > Ru/MgAl₂O₄ (8800 s⁻¹) > Ru/MgO (7900 s⁻¹) > Ru/C (2500 s⁻¹),²⁰⁷ indicating as the strongest the interaction with CO₂, the faster the reaction kinetics. The apparent activation energy for MgO-based materials for CO₂ methanation has been also reported for Ru/MgO (74 kJ mol⁻¹)²⁰⁹ and Pd/Mg/SiO₂ (82.2 ± 0.2 kJ mol⁻¹).³² This value was found to strongly decrease upon mechanical milling of the catalysts:²⁰⁹ after vibrating milling the activation energy on Ru/MgO decreases to 41 kJ mol⁻¹ and an even lower value was obtained for Fe-Ni/MgO (39 kJ mol⁻¹).²⁰⁹

It was reported in Section 2.2.1 as small changes in the catalyst composition can also favor one of the hydrogenation reactions over the others. For example, it was found that adding a small amount of Mg to the silica precursor (amorphous Mg/SiO₂ oxide)

would favor the formation of methane over CO in Pd based catalyst by stabilizing carbonate species on the catalyst surface and then methanation over RWGS reaction.³² The importance to create stable carbonates is at the basis of the larger yields obtained by Al₂O₃ with respect to most part of oxides. On the contrary, MgO based catalyst are not largely used being easily poisoned by small pollutants in the gas feed (e.g. H₂S) more easily than other supports.¹⁴

CO₂ methanation mechanism has been computationally and experimentally investigated by Kim et al.²⁰⁸ on a Pd-MgO/SiO₂. This study confirmed the dual site reaction mechanism for methanation/RWGS reactions. It emerged as MgO initiates the reaction by binding CO₂ molecules with formation of an activated surface magnesium carbonate species. Pd species would dissociate hydrogen molecules that then hydrogenate the carbonates and residual carbon atoms. This mechanism agrees on qualitative expectations and on what often proposed on the basis of experimental evidences.³²

Dry reforming of methane. Basic oxides, and in particular MgO, are used as supports or as additives in metal-based catalysts for methane reforming because they enhance the mechanical strength of the catalyst⁴² but, even more important, they lower the coking rate,²⁸ that represent the main problem in this sector (see Section 2.2.2). Contemporaneously, they promote the activation of carbon dioxide, which both participates to the reaction and to the oxidation of coke.²⁸ MgO is an irreducible oxide and this guarantee a larger stability of the catalysts if used as support. For all these reasons, Ni-based catalysts obtained by coprecipitation of aluminium oxide and magnesium oxide, although proposed for the first time in 1974 by Rostrup-Nielsen,²¹⁰ are still under investigation.²¹¹ Nevertheless, the propensity of MgO-NiO to form solid solution is well known. This fact markedly affect the catalytic activity of Ni/MgO catalysts. In fact, if the calcination temperature and the Ni dispersion facilitate the diffusion of Ni²⁺ ions in the MgO lattice, solid solutions are formed with the result that the Ni species would not be reducible anymore.⁴² Too small Ni particles (< 100 Å) have been also to be avoided in these catalysts because too strong Ni-O bonds are formed with the support, resulting in lower activities and more sensitivity to coke deposit. The Boudouard reaction would be also inhibited only on larger Ni particles.

MgO has been also used as support for Rh and Ru-based catalysts with more promising results with respect to other supports.²⁸ The dependence upon CO₂ on the kinetics of the reaction increases with the basicity of the support being important for Rh/MgO system instead of what observed for Al₂O₃ supported catalyst where no dependence upon CO₂ concentration was observed.⁴⁵ In fact, Rh/Al₂O₃ resulted to have a higher reactant conversion with respect (in the order) Rh/TiO₂, Rh/SiO₂ and Rh/MgO.⁴⁵ Nevertheless, Rh/MgO showed the highest stability (100 h)²¹² because of the more effective carbon oxidation by CO₂ due to the higher basicity of the support. Completely different was the behavior for Ru-based catalysts, where at 1 bar, 2%Ru/MgO resulted the catalysts with the highest activity with respect to corresponding TiO₂, SiO₂ and Al₂O₃ supported system and a lower coke formation.²¹³

Mg has been also used as promoter in dry methane reforming

catalysts. The effect of the promoter was found to be strongly dependent on the ratio of the additive to the active metal.²⁸ For example, studies of Na, K, Mg as additive in Pt/Al₂O₃,²¹⁴ indicated as Mg causes the higher increase in the activity with respect to the doped Na and K catalysts for 0.02% and 0.1%Pt/Al₂O₃ systems, whereas for 0.5%Pt/Al₂O₃ the K-doped systems showed higher performances. Nevertheless, for the 0.5%Pt/Al₂O₃ no deactivation was observed in any case, suggesting also a difference in the particle aggregation in this case.²¹⁴

Synthesis of methanol. Two are the main common problems for catalysts to be used for the synthesis of methanol: Cu clustering and carbon deactivation (see Section 2.2.3). Perovskites are oxidic materials with a ABO₃ formula (A is the cation having the larger dimensions and B is the smaller one, e.g. CaTiO₃). They are characterized by interesting properties as high thermal stabilities and large oxygen mobility. The latter is a characteristic particularly interesting in the applications concerning CO₂ reactions, because it would facilitate coke oxidation and then increase the stability of the catalysts. The perovskite structure can be seen as an AO structure hosting the B ion. In the use of perovskites as catalysts, B constitutes the catalytic active site that results in this way very well dispersed.⁴⁰ For these reasons, although the surface areas of these materials are very low (0.5-2 m² g⁻¹) they allow to obtain large metal dispersion accompanied by a large thermal stability toward sintering. Perovskite type A₂BO₄ consist of alternating layers of ABO₃ perovskite and AO rock salt which exhibit variable oxygen stoichiometry.⁴⁰ For their particular oxygen structure, A₂BO₄ allowed the stabilization of Cu species with special valence.⁴⁰ La₂CuO₄ perovskite catalysts for methanol synthesis⁴⁰ have been prepared by sol-gel synthesis. It was observed as the addition of Ce, Mg and Zr leads to several benefits as a remarkable decrease in particle dimension, lowering of the reduction temperature, an increase in the Cu dispersion and in the basic sites. These catalysts have been reported to show high selectivity for methanol.⁴⁰ Also high turnover frequency and long term stability in operation conditions (312 h) were obtained.⁴⁰ For what concerns the Mg-doped material (La_{0.8}Mg_{0.2}Cu_{0.7}Zn_{0.3}O_x), high dispersion of Mg was reached (MgO particles were no detectable by XRD) because it can easily substitute Cu²⁺ and Zn²⁺ in the B site. On the reactivity point of view, the Mg based material showed the highest selectivity toward CH₃OH formation (65.2%) with respect to the pristine material and to the modified Ce and Zr ones.⁴⁰

4.7. Hydroxides

4.7.1. Mg(OH)₂

Structure of magnesium hydroxide (brucite) is reported in Figure 14a and b. Mg(OH)₂ is a layered material constituted by single layers of Mg exposing an ordered surface of hydroxyls on both sides of the sheet. Each Mg ion is in octahedral coordination with 6 OH, where each hydroxyl is shared between three Mg²⁺ (Figure 14a and b). The small distances between the layers (< 1 Å) makes it difficult the diffusion of molecules in the interlayer space.

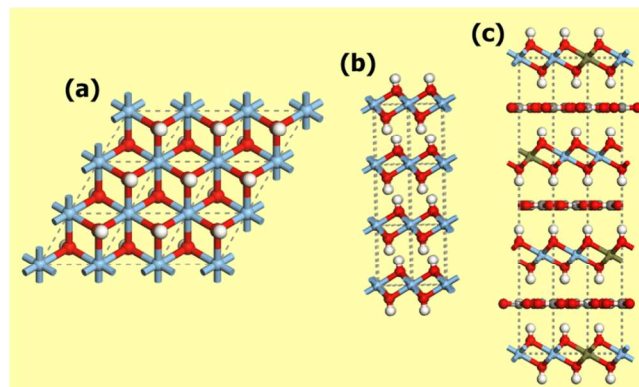
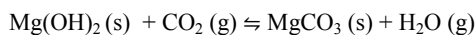
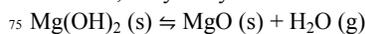


Figure 14. (a) Top view of the brucite layer in Mg(OH)₂ and (b) side view of Mg(OH)₂ layers as in the structure reported in Ref. 215. (c) Side view of hydrotalcite layers in the structure reported in Ref. 216. The atoms are represented according to the following color code: hydrogen (white), oxygen (red), carbon (grey), magnesium (light blue), aluminium (dark green).

Mg(OH)₂ is the product of hydration of MgO and it is characterized by a lower basicity than MgO.¹⁷⁶ For the disposal and separation of large amounts of CO₂ through the formation of carbonate, the carbonation of Mg(OH)₂ is of particular interest because of the relative easiness with it can be precipitated from sea water and dissolved minerals, and because it occurs naturally as brucite.⁵⁸ The carbonation process in Mg(OH)₂ is governed by the reaction:⁵⁸



(reaction [9] in Table 1) that is actually the result of two reactions, dehydroxylation:



($\Delta H_{298\text{K}} = +81.35 \text{ kJ mol}^{-1}$)³⁰ and MgO carbonation (reaction [10] in Table 1). Correspondingly, the regeneration process would be a two-step process, where MgCO₃ is decomposed to MgO, followed by its hydration to recover Mg(OH)₂. For reaction [9] a total uptake of 44.6 mass% is expected. This corresponds to 17.1 or 11.9 mol kg⁻¹ if the CO₂ uptake is normalized to the weight of Mg(OH)₂ or MgCO₃, respectively. It is interesting to notice that the overall reaction enthalpy for Mg(OH)₂ carbonation is significantly lower than for MgO (see Table 1) and with respect to many oxides and hydroxides (see Ref. 30). This indicates that the regeneration heat required for Mg(OH)₂ can be significantly lower than that required for the other processes, also with respect to MgO. This represent a significant advantage for Mg(OH)₂-based systems. The formation of bicarbonate species in this system is considered negligible in the literature of the subject, on one hand because these species are expected to be only surface species (in fact magnesium bicarbonate is stable only in solution). On the other hand, the most part of the studies are often conducted only by means of diffraction and gravimetric techniques whereas spectroscopic characterization would be necessary in order to identify all the species formed.

The kinetics of simultaneous dehydroxylation and carbonation of precipitated Mg(OH)₂ were studied by Butt et al. at 0.78 bar.⁵⁸ This Mg(OH)₂ sample was constituted by dense agglomerates of relatively spherical particle 28.7 μm in diameter formed by submicrometer-sized single crystals.⁵⁸ Dehydroxylation was conducted both in helium and in helium/CO₂ flow (He:CO₂ = 1:2). An activation energy of 146 kJ mol⁻¹ was determined for

dehydroxylation in pure helium in the $375 < T < 475^\circ\text{C}$ range.⁵⁸ The same reaction in vacuum was reported to have an E_a of only $53\text{--}126\text{ kJ mol}^{-1}$.⁵⁸ The mechanism of dehydroxylation was also determined: it appeared as a nucleation and growth process,⁵ accompanied by extensive crystallite cracking with the formation of a porous, pseudomorphic structure comprised of MgO crystallites of the order of $100\text{--}200\text{ \AA}$. Dehydroxylation in He/CO₂ flow, correspond to the reaction [9] in Table 1, that is to Mg(OH)₂ carbonation. This reaction in this system has an E_a about three times the one for the reaction in absence of CO₂ (304 kJ mol^{-1}). Carbonation was determined to start at 275°C , reaching the most rapid carbonation kinetics near 375°C and ending at 450°C . During carbonation, MgCO₃ precipitates on the surface of the crystals as $200 \times 750\text{ \AA}$ particulates acting as a passivating layer hindering both the outward diffusion of H₂O and the inward diffusion of CO₂. This layer would be then the cause of the increase in E_a observed for the reaction in He/CO₂ flow with respect to He flow. This experiment also validated the hypotheses to explain the low yields observed in carbonation of MgO. Correspondingly, the kinetics of reaction are very slow. In fact, after 12 h of reaction, the carbonation fraction was only between 6.7 and 16.7 wt% for isothermal reactions conducted at temperatures between 250 and 500°C . Interestingly, this needs that a significant amount of the specimen remains carbonated also at temperature higher than the dissociation temperature of MgCO₃ (385°C) in presence of high concentration of CO₂ gas in the flow. This observation indicates the suitability of this system for PSA process: at $T > 385^\circ\text{C}$, it would be sufficient to lower the CO₂ concentration in the feed to regenerate the adsorbent. Nevertheless, the presence of the passivating layer limits the CO₂ uptake to about 15% of the stoichiometric capacity at 250°C and 500°C and to the 37% at 375°C .

An increase in the temperature window of reactivity down to 200°C and a slight improvement in the absorption capacities of Mg(OH)₂ were obtained by dispersing it in amorphous silica by hydrolyzing a solid mixture of magnesium hydroxide and sodium orthosilicate, followed by simply drying at 100°C for 1 h.³⁰ XRD pattern conducted on the fresh material indicated the presence of Mg(OH)₂ and impurities of NaOH and Na. The siliceous fraction of the sample, being amorphous, was not detectable. Thermodynamic equilibrium data acquired for this system for the decomposition of 1 mol of MgCO₃ in the presence of 1 mol of H₂O at 1.01 and 20.3 bar are reported in Figure 15a and b, respectively.³⁰

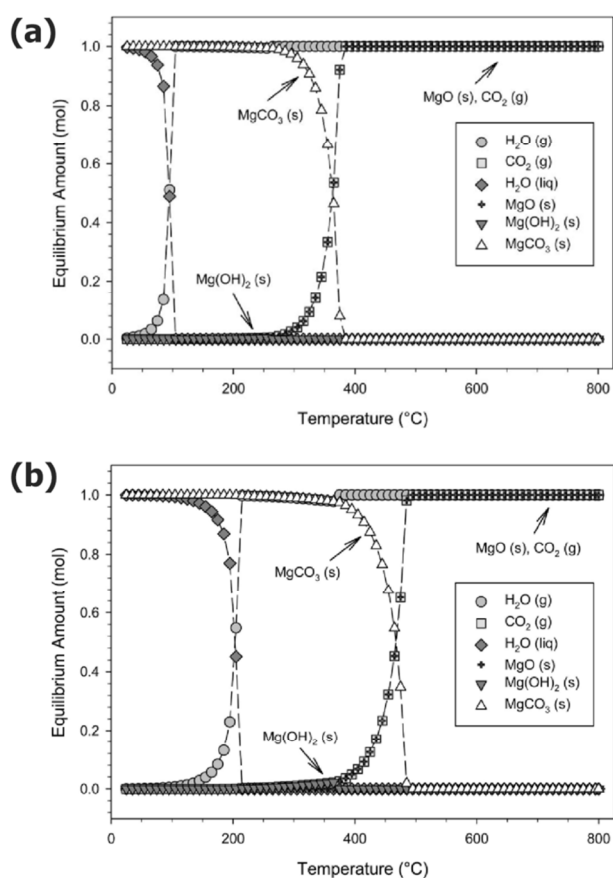


Figure 15. Thermodynamic equilibrium analysis as a function of temperature for a system of 1 mol of MgCO₃ (from Mg(OH)₂/SiO₂ system), 1 mol of H₂O, and 0.1 mol of N₂ at a pressure of (a) 1.01 and (b) 20.3 bar. Reproduced with permission from Ref. 30. Copyright 2009 American Chemical Society.

This Mg(OH)₂/SiO₂ system is an excellent candidate sorbent for CO₂ removal under integrated gasification combined cycle (IGCC) conditions ($200\text{--}315^\circ\text{C}$).³⁰ The compound has in fact a considerably higher CO₂ capture capacity than that of the commercial Selexol® process ($3\text{--}4$ versus 0.3 mmol g^{-1}),³⁰ and the energy required for the reverse carbonate decomposition was verified to be significantly lower than for other processes.³⁰ The system was fully regenerated for temperatures starting from 375°C at 20 bar, also in presence of water. Such a small difference in the temperatures for CO₂ removal and absorbent regeneration is particularly interesting for applications. High pressures for regeneration were considered in the study of Siriwardane et al.³⁰ because they allow to save the CO₂ compression costs required for CO₂ sequestration. The presence of water during regeneration was actually essential in order to allow a higher degree of rehydroxylation, condition necessary to guarantee high CO₂ capture and cyclability of the material. In fact, MgO at 200°C and 20 bar (CO₂/Ar/H₂O/N₂ = 28/28/10/34) showed uptake of only 0.25 mmol g^{-1} against 2.25 mmol g^{-1} of Mg(OH)₂-SiO₂ in same conditions, despite the higher carbonation enthalpy of MgO. These results suggest that the kinetics of CO₂ capture over MgO are much slower than those over Mg(OH)₂. Therefore the presence of Mg(OH)₂ is necessary for the CO₂

process in conditions interesting for IGCC. Moreover, sorbent capacity was observed to increase during cycles. This was associated to an increase degree of rehydroxylation. Nevertheless, the importance of $\text{Mg}(\text{OH})_2$ to carbonation can appear as a nonsense being the reaction of carbonation preceded by the dehydroxylation of the material. Moreover, the dehydroxylation is a process strongly endothermic and then cannot help locally the carbonation reaction, if not even hinders it. In my opinion, the beneficial effect of the presence in the starting material of $\text{Mg}(\text{OH})_2$ is related to the different nanostructure of the MgO that is formed. In particular, repeated cycles of hydroxylation – dehydroxylation would help keeping MgO as a finely divided, highly reactive, material. In fact, as verified by Butt et al.⁵⁸ the $\text{Mg}(\text{OH})_2$ dehydroxylation is a nucleation and growth process and the formed MgCO_3 crystal are significantly smaller than the starting $\text{Mg}(\text{OH})_2$ ones and concentrated only on the surface. The carbonation reaction has been verified by Butt et al.⁵⁸ to happens during the dehydroxylation. Likely, the surface of the formed nuclei of MgO outside the $\text{Mg}(\text{OH})_2$ crystals are very similar to the 3c species reported to exist in very special position on surface of bulk MgO (see Section 4.6). The high defectivity of the formed MgO would facilitate the activation of CO_2 and then the carbonation reaction of the material surface. This would also be another reason for the superficial nature of the carbonate formed, besides to rely on CO_2 diffusion problems. Moreover, it was found as CO_2 removal efficiency was higher if the regeneration was conducted at higher pressures (10 instead of 1 bar).³⁰ This was explained by the fact that significant rehydroxylation of MgO to $\text{Mg}(\text{OH})_2$ was observed at $T = 300^\circ\text{C}$ at 20 bar and $T = 275^\circ\text{C}$ at 10 bar, that is increasing the pressure increase the stability of the hydroxide and then the temperature window for the rehydroxylation process. Interestingly, CO_2 capture in $\text{Mg}(\text{OH})_2\text{-SiO}_2$ was observed up to 300°C at 1 bar and up to 400°C at 30 bar in a $\text{CO}_2/\text{Ar}/\text{H}_2\text{O}/\text{N}_2$ flow (10-30% H_2O , 10-30% CO_2). XRD analysis conducted³⁰ on $\text{Mg}(\text{OH})_2/\text{SiO}_2$ after exposure to CO_2 at 200°C and 20 bar, indicated a sample only partially carbonated being the pattern still dominated by $\text{Mg}(\text{OH})_2$ peaks, confirming that the capacity of the system was not fully exploited. Regeneration of the system at 400°C and 20 bar caused the formation of MgO , constituting the larger fraction of the sample, with some residual MgCO_3 and the appearance of forsterite (Mg_2SiO_4) and Na_2SiO_3 features. The fact that the absorption capacity of $\text{Mg}(\text{OH})_2$ also in $\text{Mg}(\text{OH})_2\text{-SiO}_2$ system was not fully exploited is likely imputable to its low surface area ($2.4\text{-}3.0\text{ m}^2\text{ g}^{-1}$).³⁰ An increase in the carbonation capacity can be reached by dispersing $\text{Mg}(\text{OH})_2$ on high surface area materials, as zeolites (see Table 7).²¹⁷ Hong et al.²¹⁷ precipitated $\text{Mg}(\text{OH})_2$ from a MgCl_2 solution on 13X and CaCHA zeolites and on a mesoporous CaCHA sample (CaCHA(M)).²¹⁷ X-ray diffraction showed that the pattern of 13X was maintained after the impregnation, whereas for the CaCHA samples only the peaks associated to $\text{Mg}(\text{OH})_2$ were observable, likely because a structure collapse due to the use of NH_4OH in the hydroxide synthesis. An uniform distribution of Mg^{2+} was observed for all the samples. For 13X, scanning electron microscopy images showed the formation of $\text{Mg}(\text{OH})_2$ nanoplatelets on the external surface of the zeolite.²¹⁷ For this

material, 99% of the hydroxide was carbonated at 200°C and 10 bar ($\text{CO}_2:\text{H}_2\text{O}:\text{N}_2 = 30:10:60$) whereas only 12.5% of pure $\text{Mg}(\text{OH})_2$ was reacted in the same conditions (2.16 mmol g^{-1}).²¹⁷ At 20 bar, 99.9% of the supported hydroxide was reacted (see Table 7).²¹⁷ Interestingly, although the zeolite structure of 13X- $\text{Mg}(\text{OH})_2$ collapsed after only 4 cycle, the CO_2 capture capacity was maintained because mainly related to the dispersion of $\text{Mg}(\text{OH})_2$.²¹⁷

4.7.2. Layer double hydroxides

In brucite structure, if Mg^{2+} is partially substituted by a M^{3+} cation, the layers result positively charged and the structure needs to be charge compensated by negative counterions, that are hosted in the interlayer space, in general with solvent molecules (see Figure 14c). This class of materials is named layer double hydroxides (LDH) and they have as general formula $\text{M}_{1-x}^{2+}\text{M}_x^{3+}(\text{OH})_2\text{A}_{x/m}^{m-} \cdot \gamma\text{H}_2\text{O}$.^{218, 219} They are also named synthetic hydrotalcites, being hydrotalcite one of the most abundant natural occurring LDH, with formula $\text{Mg}_6\text{Al}_2\text{CO}_3(\text{OH})_{16} \cdot 4(\text{H}_2\text{O})$ ($\text{M}^{2+} = \text{Mg}^{2+}$, $\text{M}^{3+} = \text{Al}^{3+}$ and $\text{A}_{x/m}^{m-} = \text{CO}_3^{2-}$). Mg-Al-CO represent also the most studied synthetic system in this class of materials. It is evident that the presence of species in the brucite interlayer is expected to facilitate the diffusion of reactive molecules (as CO_2) in the structure and then to enhance the reactivity of these materials with respect to brucite. The presence of negatively charged counterions is a very rare property in materials. This fact, with the very large flexibility in composition of LDH, makes them suitable for catalytic, ion exchange and separation applications.^{218, 219}

Moreover, LDH properties can be easily tuned by changing, among the others, the composition of their structure and the nature and the number of counterions (by changing the $\text{M}^{2+}/\text{M}^{3+}$ ratio). In particular, as other layered materials (e.g. clays, Section 4.8.2), the accessibility of the interlayer space is strongly dependent on the dimensions of the species hosted in the interlayer. The swelling can be facilitated as in clays by the use of counterions of appropriate size.²²⁰ Hydrotalcite surface area was varied by Fetter et al.²²¹ in the range $20\text{-}350\text{ m}^2\text{ g}^{-1}$ by changing the chemical composition. Wang et al.⁶³ recently reviewed the properties of LDH as CO_2 sorbents and state as they represent the most important intermediate temperature ($200\text{-}400^\circ\text{C}$ range) CO_2 sorbents, that is for precombustion processes.¹¹ Among the possible modifications aimed to tune their CO_2 capacities, intercalation of organic anions is particularly promising. For example, the use of stearate in Mg-Al LDH allowed to increase the CO_2 uptake from 0.5 (for $\text{A}_{x/m}^{m-} = \text{CO}_3^{2-}$) to 1.25 mmol g^{-1} at 200°C and 1 bar.²²⁰ This because the long chain hydrocarbon actually esfoliated completely the system, allowing to maximize the surface exposed to CO_2 . Also graphite oxide has been used as counterion in Mg-Al LDH with beneficial effects on both sorption capacities and recyclability.²²² Since their composition, It is evident that LDH present intrinsically anionic and basic sites and for this reason they are particularly suitable to activate carbon dioxide. Their acidic-basic properties can be modulated by changing the compensating anion, the amount and the nature of structural cations. For example, enhanced CO_2 adsorption properties have been reported if Al^{3+} is partially substituted by Ga^{3+} .²²³⁻²²⁵

Mg-Al hydrotalcites have been also used as support for Ru-Ni particles for dry methane reforming. Mg-Al hydrotalcites are very good reforming catalysts as they resist to carbon formation because of their basic properties, high surface area and thermal stability.²²⁶

Calcination of hydrotalcites allow to obtain mixed Mg-Al oxides having weak acid and basic properties that can be tuned by changing the calcination temperature.⁵² In fact, the calcination temperature has a strong influence on the number of active Mg-O species created and on the material structure (crystalline or amorphous).^{63, 227} Because of the presence of both basic and acidic properties (see Section 2.1), also these oxides have been tested as heterogeneous catalysts for CO₂ reactions and in particular in the direct carboxylation of methanol by Stoian et al.⁵² In order to increase the number of active sites, the hydrotalcites (Mg/Al = 3) were in turn supported on high surface area materials as silica lyogels (uncalcined silica xerogels, 1000 m² g⁻¹) before the calcination at 450°C (4.4 wt%). Surface areas as high as 646 m² g⁻¹ were obtained for the supported material. Both supported and unsupported Mg-Al oxide showed very high selectivity for temperatures comprised between 90 and 130°C (99.9%, CO₂/CH₃OH = 25). For its performances, this material represents an important breakthrough in this research field. At higher temperatures (>130°C), an increase in the formation of dimethyl ether as side product was observed mainly related to thermal decomposition of the formed dimethyl carbonate on the same basic/acid sites that have allowed its formation.⁵² The conversion to dimethyl carbonate at 130°C amounted to only 1.8 and 15.9% for the unsupported and supported mixed oxide, respectively.⁵² Both these values are still higher than those reported for all the previously reported heterogeneous catalysts for this reaction (about 1%).²²⁸ Stability of the catalyst up to 480 h was also reported.⁵² On further increasing of the temperature (175°C), dimethyl ether resulted the almost total product of the reaction (95%). This result is quite interesting too because, as stated in Section 2.2, dimethyl ether can directly substitute diesel oil in internal combustion engines.¹⁴

4.8. Silicates

Silicates are the largest group of mineral compounds. They constitutes well over the 90% of rocks forming minerals on the Earth's crust. Several synthetic structures have been also reported, belonging to the silicates group, further enlarging their number. Since their name it can be inferred as at the basis of their structures there is silicon that is present in [SiO₄]⁴⁻ tetrahedra. Because of the flatness of the energy potential surface on the rotation of two [SiO₄]⁴⁻ units, several structures can be obtained by using this tetrahedron as building unit (see for example zeolites, Section 4.8.1). In addition, in silicate structures other elements can be present, further enlarging the number of possible frameworks. Magnesium is often hosted in silicate frameworks, occupying the central position of octahedral building units (see Figure 17). Magnesium can be also present in silicates as an extraframework species as in zeolites and in clays, where it is hosted in the material pores, to counterbalance the negative charge of the frameworks. Silicates have been largely investigated for their affinity towards CO₂.^{55, 60, 229} The nature of

the interaction with CO₂ in sorption and separation process for silicate materials strongly depends on the subgroup considered, going from molecular adsorption in zeolites and clays materials (Sections 4.8.1 and 4.8.2) to chemical reaction (Sections 4.8.3).

4.8.1. Zeolites

Classically, zeolites are defined as aluminosilicate crystalline materials characterized by a permanent microporosity. Their three dimensional framework is obtained by linking corner-sharing [SiO₄]⁴⁻ tetrahedra. Being the conformational energy surface almost flat upon torsional rotation of two [SiO₄]⁴⁻ tetrahedra, a large variety of possible structures has been not only hypothesized but also observed (see Figure 16).²³⁰ Silicon substitution in the tetrahedra by other elements, e.g. Al³⁺, causes a lack of charge balance in the framework that it is compensated by ions (counterions) hosted in the zeolite pores. These ions are the basis of the large variability and flexibility of these materials for a great number of applications, going from gas separation to catalysis. The zeolites are then intrinsically characterized by acidic and basic properties and their properties can be tuned by changing: (i) the extraframework species, (ii) the framework composition (different Si/Al ratio, using Ti⁴⁺, P⁵⁺, B³⁺, ... as T-atoms); (iii) framework topology; (iv) introducing grafted species (as amines), or occluding species as metal/metal oxide particles in their pores; (v) introduction of mesopores during or by post-synthetic treatments. Recently it has also been shown as the aluminium distribution can be varied in the zeolites and that this has a direct effect on the CO₂ heat of adsorption.²³¹ Framework basicity can be tuned by selecting different frameworks, because different T-O-T angles can provide different acid-base properties to the zeolite. Among the different structures, faujasite has shown range of properties that may even extend from superacids to superbases.²⁰³ Basic functionalities can be inserted when the cations are weakly acidic or an even larger basicity can be introduced by occluded species. In particular, superbasicity properties can be provided by introduction of nanoclusters of basic oxides in the pores, such creating bifunctional zeolites. High chemical, pressure and thermal stabilities have made these materials largely used as adsorbents and catalysts in petrochemical industry, besides the large variety of other uses going from gas separation to additive to soaps. For what concerns CO₂ capture and separation, 13X (NaX) and NaY zeolites (FAU framework) are considered the reference materials in both adsorption and separation studies²³² for their high working capacities. CaA (LTA framework) is another material important in this field of study, having shown superior performances than Mg-IRMOF-74-I at 40°C up to 1 bar for both adsorption and separation.⁷⁶

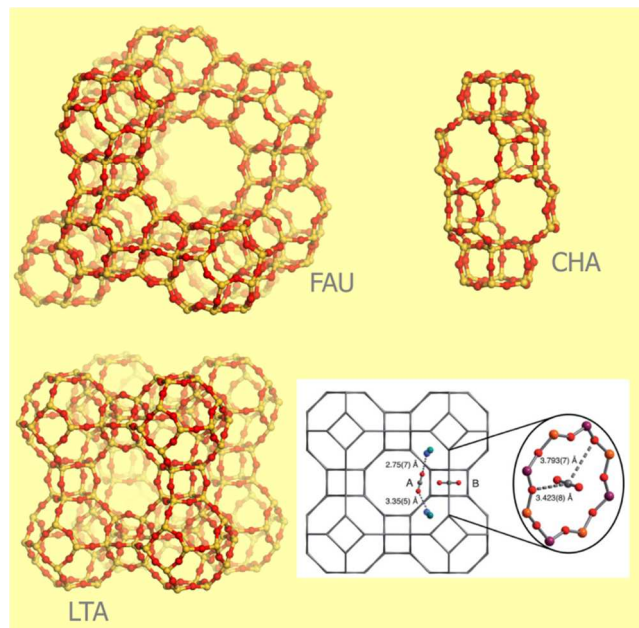


Figure 16. Zeolitic structures. The largest cavities (or supercages) of zeolite A (LTA framework), chabazite (CHA) and zeolite X or Y (FAU) are reported. The atoms are represented in the color code: oxygen (red), silicon/aluminium (yellow). The cations are omitted for clarity. In the scheme, the structures associated with CO₂ adsorption at two sites in zeolites Ca-A (A and B) are represented as determined from neutron powder diffraction measurements at 10 K. Gray, red, blue, green, orange, and purple spheres represent C, O, Na, Ca, Al, and Si atoms. Reproduced with permission from Ref. 76. Copyright 2013 Royal Society of Chemistry.

Zeolites having a porosity constituted by cavities with access apertures of 3.5-4.5 Å (that is close to the CO₂ kinetic diameter) yield the highest recorded selectivities for for both CO₂/N₂ and CO₂/CH₄ separation.^{78, 233} This pore dimension corresponds for example to siliceous 8-rings, that are typical of the CHA,²³⁴ LTA²³⁵ and KFI^{233, 236} frameworks. Because of their high working capacities, 13X (NaX) and NaY zeolites are considered the best CO₂ adsorbents but only when low pressure feed and low regeneration pressures are used.²³³ Nevertheless, because of their larger pore windows (12-rings) their CO₂/N₂ selectivity are not high enough to effectively adsorb CO₂ from a high purity CO₂ stream.²³³

Some of the magnesium zeolites studied in literature for CO₂ adsorption are listed in Table 7. It is evident that in the zeolite formula other cations than Mg are present. In fact, often zeolites are synthesized in their sodium form and the corresponding magnesium zeolite is obtained by cation exchange by stirring the zeolite in an aqueous solution of a magnesium salt. Exchange of monovalent with divalent cations is a quite difficult task resulting in general in a only partial exchanged zeolite. This fact has to be taken into account when comparison between different cations is considered. Another important information present in this table is the surface area of the materials that provides indication about the presence of defects in the structure, in particular about structure collapse due to improper synthetic or activation procedure. For what concerns Mg-exchanged zeolites, the activation temperature has another important effect: it is well known that Mg ions introduced by exchange in aqueous solution are at least in part in the form (Mg-OH)⁺.²⁰³ High activation temperatures (about

400°C) are then needed in order to completely dehydroxylate (Mg-OH)⁺ to form Mg²⁺.²³⁷

CO₂ affinity dependence upon different cations has been studied in literature in four different zeolitic frameworks: KFI (LS-KFI and Mg-ZK-5)^{233, 236}, CHA,²³⁴ LTA⁷⁶ and FAU (zeolite X)⁷⁶ zeolites. In these studies, the capacities of Mg-exchanged zeolites were compared to the ones obtained for the corresponding materials exchanged with other alkali and alkali earth cations. By comparing the results reported, the effect of the framework topology on the cation reactivity resulted to be important. This is a very well known matrix effect of zeolites and it is particularly important for an ion as Mg²⁺, having a very high charge/radius ratio. For that reason, a common trend cannot be evidenced for the different frameworks.

Different trends were also obtained for materials having the same framework topology but different Si/Al ratios. In LS-KFI materials (low silica KFI), the Mg-exchanged material showed the lowest CO₂ capacities in the 0-1 bar range than all the other LS-KFI frameworks considered (Li⁺, Na⁺, K⁺, Ca²⁺, Sr²⁺) likely because Mg²⁺ is more shielded than the other ions by the negative zeolite framework.²³⁶ Nevertheless, the low crystallinity of the Mg-KFI framework in this study is evident when comparing the surface areas for the different counterions, being for example Ca-KFI possessing a larger surface than Mg-KFI, otherwise than expected (337 vs. 358 m² g⁻¹, respectively).²³⁶ For what concerns separation, LS-Mg-KFI showed the larger selectivity at 308 K and 1 bar in a 50% CO₂/CH₄ flow (62), that is identical to NaX.²³⁶ The corresponding high silica material, Mg-ZK-5 showed the lower uptake for *p* < 0.3 bar with respect to other alkali and earth-alkali cations, ascribable also in this case to the low accessibility of the Mg²⁺ cations.²³³ This was confirmed by the low *q*_{iso} obtained also at the lowest CO₂ coverage (see Table 7). Nevertheless, at 1 bar an uptake comparable to NaY and Li-ZK-5 was obtained.²³³ Interestingly, the shape of Mg-ZK-5 isotherm, being less steep than Li-ZK-5 ones, indicates that larger working capacity would be possible by using this zeolite in PSA systems without the need of the more costly VSA systems, as for the other zeolites under study.²³³ For CO₂/N₂ flow of 10/90 in a PSA system working between 5 and 1 bar, Mg-ZK-5 resulted to have a decidedly higher selectivity with respect to 13X (121 vs. 37) and higher working capacities (2.05 vs. 1.44).²³³ Its higher working capacity is related to the lower CO₂ isosteric heat in Mg-ZK-5 with respect to 13X.²³³

In Mg-CHA zeolites, on the contrary, being the Mg ion more exposed, higher isosteric heat was obtained with respect to alkali and earth alkaline analogues, with corresponding poor performances as material for CO₂/N₂ separation.²³⁴ Energetic of interaction reported for LTA and FAU frameworks followed the same trend than in KFI framework, although likely slightly biased by a too low activation temperature of 250°C.⁷⁶ The reason of the low CO₂ isosteric heat in MgA has been explained on neutron diffraction basis and shows as the so called “framework shielding effect on the cation” can be more complicated than in general imagined.⁷⁶

Neutron diffraction studies evidenced as the Na⁺ cations occupies 6-ring and 8-ring in the LTA framework.²³⁸ A study conducted on CO₂ loaded LTA zeolites⁷⁶ evidenced as CO₂ has two preferential adsorption sites. In site (i), CO₂ interacts with two cations at the

same time through the oxygen atoms.⁷⁶ On the contrary, in site (ii) the carbon atom sites in the 8-ring plane, if free, to CO₂ contemporaneously interact with two oxygen atoms of the framework.⁷⁶ Between the two, site (ii) is the most energetic having a double occupancy with respect to (i).⁷⁶ This site would be at the basis of the particularly high isosteric heat registered for CaA (58 kJ mol⁻¹) with respect to other alkali and alkali earth

exchanged LTA.⁷⁶ For what concerns MgA, the unexpected lower q_{iso} measured with respect to Ca-A were explained by a partial blocking of 8-ring sites by Na⁺ due to a lower degree of exchange with respect to Ca-A or to a lower exposure of Mg²⁺.⁷⁶ Nevertheless, another explanation can rely in the low activation temperature adopted that would not allow a complete dehydroxylation of the (Mg-OH)⁺ species.

Table 7. Review of CO₂ adsorption on Mg-zeolites reporting the Si/Al atomic ratio, framework type according to IZA nomenclature, BET (S_{BET}) and Langmuir ($S_{Langmuir}$) surface area, pore volume (V_{por}), CO₂ capacity (n_{CO_2}) in different temperature and pressure conditions and isosteric heat of CO₂ adsorption (q_{iso}). Values for 13X and Mg(OH)₂ are also reported for comparison.

Material	Si/Al	Framework type	S_{BET} (m ² g ⁻¹) ^a	$S_{Langmuir}$ (m ² g ⁻¹) ^a	V_{por} (cm ³ g ⁻¹) ^a	$n_{CO_2}@P,T$ (mmol g ⁻¹) ^{b,c}	q_{iso} (kJ mol ⁻¹)	Ref.
LS Mg-KFI (Mg ₁₁ Li _{4.5} Na _{0.7} K _{2.8} ((CH ₃) ₄ N) ₆ [Si ₆₀ Al ₃₆ O ₁₉₂])	1.67	KFI	337 ^e	–	0.14 (micropore)	0.20@303 K and 0.9 mbar (vol) 3.09@303 K and 1 bar (vol) 3.64@303 K and 35 bar (vol)	–	236
Mg-ZK-5	4.7	KFI	–	–	0.21	4.43@303 K and 1 bar (vol)	30.8-34.7	233
Mg-CHA (Na _{3.3} Mg _{3.8} [Al _{10.9} Si _{25.1} O ₇₂])	2.4	CHA	–	–	–	4.28@273 K and 1.03 bar (vol)	30-41	234
MgCHA	2.4	CHA	503	–	0.38	4.57@298 K and 1 bar (vol)	–	217
CaCHA-Mg(OH) ₂ (15 wt%)	2.4	CHA	610	–	0.65	0.57@473 K and 1 bar (tga) ^f 1.14@473 K and 20 bar (ms) ^e	–	217
CaCHA(M)-Mg(OH) ₂ (Mg(OH) ₂ = 18wt%) ^g	2.4	CHA	173	–	0.57	0.45@473 K and 1 bar (tga) ^f 1.75@473 K and 20 bar (ms) ^e	–	217
Mg-A (Na _{0.48} Mg _{0.26} AlSiO ₄)	1.0	LTA	–	–	–	3.89@298 K and 1.03 bar (vol)	34-36	76
Mg-X (Na _{0.38} Mg _{0.31} AlSi _{1.18} O _{4.36})	1.1	FAU	–	–	–	5.00@298 K and 1.03 bar (vol)	33-40	76
13X-Mg(OH) ₂ (8wt%)	1.4	FAU	750	–	0.65	0.55@473 K and 1 bar (tga) ^f 2.11@473 K and 20 bar (ms) ^e	–	217
13X	1.4	FAU	804	–	0.39	5.9@298 K and 1 bar (vol) 0.48@473 K and 1 bar (tga) ^f 0.70@473 K and 20 bar (ms) ^e	49	76, 217
Mg(OH) ₂	–	–	~2	–	–	2.99@648 K and 0.5 bar	–	58

^aSurface area and pore volume as obtained from N₂ adsorption.

^bThe technique used for the measurement is indicated in parenthesis: vol = volumetry (static conditions), ms = mass spectroscopy, tga = thermal gravimetric analysis.

^cConversion from original data in wt% made on the assumption that wt% = CO₂ weight/(CO₂ weight+sample weight)*100, if not otherwise specified.

^dZeolite synthesized in presence of [3-(trimethoxysilyl)propyl]octadecyldimethylammonium chloride (TPOAC; 72%, Aldrich), a mesopore forming agent.

^emeasured in presence of water in the inlet gas (CO₂:N₂:H₂O = 3:6:1).

Metal organic frameworks are often seen as an evolution of zeolites, being MOFs in principle applicable to all the uses already covered by zeolites, with the advantage of the higher structure design flexibility, deeply described in Section 4.3. Nevertheless, at present, MOFs are in general seen as a laboratory curiosity more than materials that could have a real practical use. In fact at present MOFs cannot compete with zeolites because of the larger thermal, pressure and chemical stability and lower cost of zeolites. CO₂ separation from atmosphere and flue gases, nevertheless, is expected to be one field of exception.¹⁰ With respect to zeolites, MOFs have particular advantages, being CO₂

adsorption less affected by water than in zeolites^{129, 239} and being water more easily removed from MOFs than from zeolites.¹²⁹ For example IRMOF-74-I can be completely dehydrated for treatment at 200°C,¹⁴⁴ whereas for zeolites such a condition is reached only for temperatures of about 350-500°C.^{240, 241} MOFs moisture sensitivity, nevertheless, it is a strong disadvantage.

Amine grafting in zeolites has been proved to be a good strategy in order to enhance the water resistance of zeolites as CO₂ sorbents in CO₂/CH₄ separation, although a general lowering the CO₂ capacities is contemporaneously observed.¹⁰ This observation is analogue to what reported only recently for MOFs

(see Section 4.3). A new synthetic method²⁴² where the amine molecules (TEPA = tetraethylenepentamine) were introduced in zeolites during the synthesis seems to be particularly promising. In this case, an increase in the CO₂ uptake was observed. Nevertheless, the high environmental impact of amines indicates that they do not represent a possible solution on the base of the large scale of sorbents needed to sequester CO₂.⁶³ Clusters of MgO have been introduced in Y zeolites by heating Mg-exchanged Y zeolites,²⁰³ through their impregnation with magnesium dimethoxide^{203, 243} or by direct dispersion by microwave.²⁰¹ Strong basic sites are obtained only if ensembles of Mg and O form an MgO lattice.^{203, 243} In these cases, carbonates are formed very easily even from atmospheric CO₂.²⁰³ The presence of oxide clusters enhances the amount of CO₂ adsorbed and their affinity toward CO₂ allowing the atmospheric CO₂ sorption at RT.²⁰³ This observation is particularly important because these clusters could represent a possible alternative to amines. Some investigations on this topic are undergoing in our laboratory, showing actually as the presence of the MgO particles not only increases the water stability of the adsorbent but an increase of the CO₂ uptakes has been also observed.²⁴⁴ Zeolites have been also shown to be suitable supports for Mg(OH)₂ nanoparticles, allowing to enhance their CO₂ capacities up to the stoichiometric capacity (see Section 4.7.2).²¹⁷

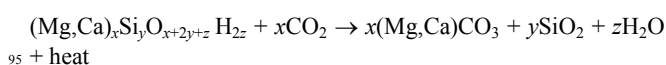
4.8.2. Clays

Clays are phyllosilicate materials, that is constituted by layers composed by different arrangements of tetrahedral and octahedral sheets (see Figure 17b).²⁴⁵ The tetrahedral sheets are composed by corner sharing [SiO₄]⁴⁻ tetrahedra and they are always bonded to an octahedral sheet through one of the corners of each [SiO₄]⁴⁻ unit. The octahedral sheets are formed from small cations, the most common being Al³⁺, Mg²⁺ or Fe^{2+/Fe³⁺}.²⁴⁵ The charge unbalance originating from the substitution in the tetrahedral sheet of Si⁴⁺ with Al³⁺ and the different charge of the cations in the octahedral sheets is in general compensated by extraframework cations hosted in the interlayer space.²⁴⁵ This is equivalent of what described for zeolites and LDH materials (see Sections 4.7.2 and 4.8.1). Analogously to zeolites, these counterions can be exchanged allowing to tailor clays affinity in relationship with the end use. Clays applications spread on the same range of zeolites, from catalysis to adsorption. Clays are naturally abundant materials²⁴⁶ and for this reason they have attracted interest as CO₂ sorbents. Nevertheless, clays are in general characterized by medium-low surface area at difference of what expected (<100 m² g⁻¹).^{247, 248} This is due to the inaccessibility of the interlayer space to molecules in the gas phase, at difference of what happens in liquids. For this reason, the CO₂ uptake of natural occurring clays are very low. In order to increase the surface area, a common strategy in layered materials science is to introduce species of appropriate size in the interlayer space (see also Section 4.7.2). The intercalation of those species can be obtained during the synthesis or by post-synthetic methods, the simplest of which is the ion exchange. In this way, the pore dimensions can be tuned up to the exfoliation of the material for very large species. Several solutions were proposed (aminopropyltrimethoxysilane, polyglycerol dendrimers, polyethylenimine, TEPA, ...).⁶³ Among them,

amines resulted to be the most suitable intercalated species for clays to be used as CO₂ scrubbers.⁶³ It is interesting to notice that the introduction of TEPA, analogously to what verified for zeolites and MOFs, allowed to strongly increase the CO₂ capacities of bentonite (a natural occurring material, mainly composed by montmorillonite clay, see Figure 17b). CO₂ capacities were increased from the negligible value reported for raw bentonite to up to 3.0 mmol g⁻¹ at 75°C and 1 bar.²⁴⁹ Also in this work, as for IRMOF-74-I, a bell bottomed dependence of the CO₂ capacity on the amine loading was observed,²⁴⁹ indicating as the amount of the harmful and costly amines have to be always optimized.

4.8.3. Carbonation

Mineral carbonation technology (MCT) is a process whereby stable carbonates are formed by CO₂ reaction with magnesium and calcium minerals or by the use of alkaline industrial waste.^{55, 60, 229} This approach is particularly appealing and among the few realistic, being the amount of materials already available exceeding the stoichiometric amount needed to fix the present CO₂ excess in the atmosphere.⁶⁰ A large amount of CO₂ is currently fixed in magnesium silicate by natural weathering: only in Oman, 10⁴-10⁵ tons per year of atmospheric CO₂ is fixed by carbonation of peridotite.²⁵⁰ In fact, magnesium silicates are abundant materials on Earth, and moreover constitute a large fraction of milling and mining waste in order of magnitude of the gigatons per mining site. Minerals as olivine,²⁵¹ pyroxene, serpentine,²⁴ lizardite,²⁵² antigorite²⁵³ and chrysotile²⁵⁴⁻²⁵⁶ have been studied for their carbonation properties for long term mitigation of anthropogenic emissions.^{55, 60} This is also related to the large CO₂ amounts that can be ideally stored in magnesium silicates: the maximal carbon fixation is 0.67 gCO₂ per gram of olivine and 0.5 gCO₂ in serpentine.⁶⁰ The general carbonation reaction for magnesium silicates is:⁶⁰



Carbonation of silicates is an exothermic reaction (see Table 1), although the heat released during carbonation is lower than MgO/CaO oxides.⁶⁰ Because of that, carbonation in magnesium silicate is a spontaneous process and, in fact, natural weathering is able to cause the carbonation of the fine-grained material on the surface of tailings pile with the formation of stable carbonate as magnesite (MgCO₃), hydromagnesite (Mg₅(CO₃)₄(OH)₂·4H₂O) and pyroaurite (Mg₆Fe₂(CO₃)(OH)₁₆·4H₂O) at atmospheric temperature and pressure conditions.^{254, 255}

It has been shown as in presence of mafic/ultramafic rocks (basic rocks, with a high Mg and Fe content), fixation of 1330 g C m⁻² y⁻¹ can be also reached, through natural weathering.²⁵⁵ Nevertheless, for what concerns bulky particles, instead, pretreating of the materials and high temperatures and pressures of reaction (>500°C, > 50 bar) are needed in order to obtain significant carbonation degrees, compromising the CO₂ efficiency and the cost of the whole process. The reaction is in fact characterized by slow reaction kinetics because of the low surface area and the rapid formation of passivative carbonate or

silica layers. Different routes for MCT have been then suggested, that can be divided in three main groups:⁶⁰ (i) ex situ MCT; (ii) in situ MCT; (iii) other MCT (e.g. natural processes as passive MCT and biomineralization). Ex situ MCT refers to the aboveground carbonation of natural minerals and industrial alkaline wastes with (indirect MCT) or without (direct MCT) previous extraction of Ca or Mg. The extraction procedure is aimed to the separation of iron and to the elimination of the siliceous part, that is inactive in the reaction and moreover brings to the formation of a passivating layer. The alkaline element is then extracted as oxide or hydroxide and used in the carbonation reaction. The reaction kinetics in indirect MCT are decidedly larger than in direct processes in milder conditions.⁶⁰ Moreover, a pure carbonate is

obtained as end-product. In situ MCT processes have been only recently developed and consist in geological storage conducted in optimized conditions (surface area, temperature, pH and CO₂ pressure) to accelerate the natural process.⁶⁰ In situ processes are cheaper than ex situ processes although still higher in cost with respect to geological storage in sedimentary basins and characterized by the same environmental problems. It is also important to remind that the amount of carbonate produced would be so high (see Figure 2c) that in order to lower the cost of production, applications of these products have to be addressed⁶⁰ or other motivations of the carbonation process, besides CO₂ capture itself, have to be envisaged.

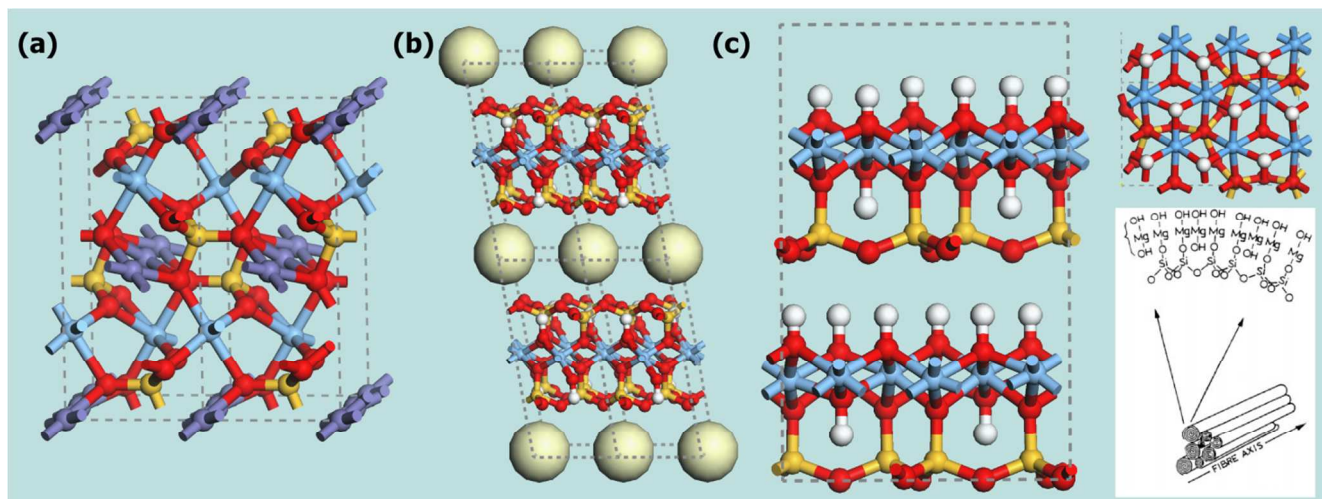


Figure 17. (a) Structure of olivine FeMgSiO_4 from Ref. 257. The atoms are represented according to following color code: hydrogen (white), oxygen (red), magnesium (light blue), silicon (yellow), iron (violet). (b) Structure of Cs-montmorillonite ($\text{Cs}_{0.62}[\text{Al}_{3.01}\text{Fe(III)}_{0.41}\text{Fe(II)}_{0.04}\text{Mg}_{0.54}](\text{Si}_{7.8}\text{Al}_{0.2})\text{O}_{20}(\text{OH})_4$) from Ref. 258. Tetrahedral atoms (silicon and aluminium) are represented as yellow sphere, whereas octahedral atoms (aluminium, iron and magnesium) are represented by light blue spheres. For the other elements, the following color code was used: hydrogen (white), oxygen (red), cesium (light yellow). (c) Chrysotile mineral description. From left to right: side and top view with respect to the brucite-like layers of the crystal ideal structure of chrysotile $[\text{Mg}_3\text{Si}_2\text{O}_5(\text{OH})_4]$; schematic representation of chrysotile asbestos fibres (Reproduced with permission from Ref. 259. Copyright 1999 Royal Society of Chemistry). The same color code as in part (a) was adopted.

Chrysotile. Chrysotile ($\text{Mg}_3\text{Si}_2\text{O}_5(\text{OH})_4$), the asbestiform polymorph of serpentine, is a phyllosilicate constituted by tetrahedral $[\text{SiO}_4]^{4-}$ sheets (T) and trioctahedral brucite-like $[\text{Mg}_3\text{O}_2(\text{OH})_4]^{2-}$ sheets (O) (see Figure 17c). Each T layer is chemically bounded to an O layer through the sharing of oxygens between Mg and Si. The TO couples are bounded to the other through hydrogen bonding between the hydroxyls of the O layer of one TO unit and the oxygen of the T sheet of another TO unit. The hydroxyls in the brucite-like layer are of two kinds: Si-O-Mg-OH and OH-Mg-OH. These species are alternating at the nanotube surface, as shown in the scheme reported in Figure 17c. As it is evident in this picture, one of the two hydroxyls of the OH-Mg-OH unit points towards the inner part of the TO sheet. The TO sheet lateral misfit is accommodated to a degree by a change in curvature resulting in various curved crystal shapes and sizes. The resulting material is composed by hollow nanotubes with an average diameter of 400 Å and inner diameter of 35 Å.²⁵⁴ As can be inferred from its tubular shape and composition, this mineral is an asbestos, that are well known carcinogenic agents. It is interesting to know, for example as chrysotile mining in the past has brought to the accumulation in Thetford Mines and Asbestos (Québec, Canada) of 2×10^9 tons of waste, rich in

chrysotile.²⁵⁶ Similar sites are present for example in Australia,²⁵⁵ Italy,²⁶⁰ United States of America and Brazil. The importance of reclaiming of the land by removing chrysotile is then evident. The presence of a brucite-like surface is expected to bring a strong ability to react with CO₂ to chrysotile. Nevertheless, in front of a 1:1 CO₂ to Mg molar ratio for the total conversion of chrysotile to hydromagnesite, only 0.01 was reached at about 130°C (CO₂ pressure of 31 bar, 1 bar H₂O) and 0.15 at 375°C (H₂O/CO₂/He = 10/90/50 ml/min). This was explained by the low surface area of the material (20 m² g⁻¹ for the raw chrysotile)²⁵⁴ and by an even closer atomic distances in the O layer with respect to brucite that would not allow an easy diffusion to CO₂ during the reaction. Alkali metal doping (10 wt%) was found to cause the increase in CO₂ fixation up to a factor of 3.²⁵⁴ Further improvements were obtained by the observation that the presence of water is beneficial on carbonation, likely because of the formation of meta-chrysotile ($\text{Mg}_3\text{Si}_2\text{O}_7$),²⁵⁶ characterized by an amorphous structure with tendency to crystallize in the less harmful forsterite (Mg_2SiO_4).²⁶¹ In particular, raw chrysotile was pretreated up to 700°C (100°C/min, isotherm for 20 min) to form meta-chrysotile²⁵⁶ before to be exposed to CO₂. At difference of the pristine chrysotile, this material was able to

strongly react with CO₂ in presence of steam for temperature between 100-160°C, with a peak of 0.7 mol CO₂/mol Mg at about 130°C (CO₂ pressure of 31 bar, 1 bar H₂O). This is a strong enhancement with respect to pristine chrysotile in the same conditions (1 mol%) and was observed only when water is present in the reaction vessel. XRD analysis indicated the formation of magnesite, while X-ray photoelectron spectra reveal the formation of both carbonate and bicarbonate species.²⁵⁶ The formation of this species was found to not be related to the presence of brucite or other impurities. This enhanced activity was explained by a rehydroxylation in steam accompanied by a strong increase in the surface area (13 and 147 m² g⁻¹ for meta chrysotile not exposed and exposed to steam, respectively). The formed species resulted to be highly stable, being decomposed only in the 400-600°C range.²⁵⁶

4.9. Hydrides

Hydrides are well-known reducing agent used in many chemical reactions for this purposes. As discussed in Section 2.2.1, hydrogenation of CO₂ would represent an advantageous method to obtain fuels having lower, if not negative, carbon footprints. In this respect, hydrides have been employed as (i) catalysts³⁵ in the CO₂ hydrogenation or as pure^{35, 262} or as supported species.^{14, 71} Moreover, their use as (ii) as co-reactants^{21, 263-265} has been also reported.

4.9.1. Mg₂NiH₄

The most common heterogeneous catalysts used for CO₂ methanation are supported transition metal ions (see Section 2.2.1 and 4.6).^{14, 71} Nevertheless, also intermetallic hydrides as LaNi₅²⁶⁶ and Mg₂Ni³⁵ can catalyze the hydrogenation of CO₂, CO and ethylene. This has been verified to happen through the disproportion of the RNi_x surface in a Ni layer covered by a layer of R oxide.^{35, 266} The ability to disproportionate at the surface of metal and complex hydrides is due to the difference in binding energies between constituents. Often an oxidic layer is present on the outer surface of hydrides, as result of the surface oxidation by impurities present in H₂ (i.e. O₂, H₂O, CO, CO₂). The passivation of hydride surfaces by the formation of this oxidic layer allows to protect the metal hydride from further oxidation. In the case of hydride reaction with CO₂, the oxide has not only the effect to protect the inner hydride from CO₂ but its presence is necessary for the activation of this molecule. In Figure 18a, a pictorial representation of the disproportionated surface of Mg₂NiH₄ catalyst is reported.³⁵ Mg₂NiH₄ structure is constituted by tetrahedral [NiH₄]²⁻ surrounded by Mg²⁺ cations (lower part of Figure 18a). This hydride is able to store 3.6 mass% of H₂ that can be fully released at 300°C with a full reversibility tested over 1500 cycles, if high purity hydrogen is used.²⁶⁷ Nevertheless, in presence of CO₂, also at atmospheric concentration, surface poisoning was observed with the formation of carbonates and CH₄.³⁵ In Ref. 35, Mg₂NiH₄ surface was characterized after several hydrogen absorption/desorption cycles, where the desorption was carried out in presence of a H₂/CO₂ flow. A reactant ratio H₂/CO₂ = 8 was used, being the one reported to allow the highest conversion rate for CO₂ methanation on Ni/MgO.⁷¹ Several techniques were employed as X-Ray photoelectron spectroscopy (XPS), scanning transmission

electron microscopy (STEM), electron energy loss (EELS) and time-of-flight secondary ion mass (ToF-SIMS) spectroscopies. The result of this characterization evidenced a material surface segregation in different phases (from the outer to the inner of the material): MgO, Ni, Mg₂Ni and Mg₂NiH₄ (see Figure 18a).³⁵ During the desorption, the external MgO layer is created by the dissociative adsorption of CO₂. The presence of MgO prevents Ni from oxidizing, Ni that can then dissociate the hydrogen molecules present in the flow, that are the species used in the reaction. The diffusion of H₂ to the underlying Ni layer is guaranteed by MgO/Ni interlayer mismatch. At the Ni layer, H₂ is dissociated and then spilled out toward the MgO layer where it happens the hydrogenation of CO and O surface species (originating by dissociation of CO₂ on edge species of the oxide layer).²⁶⁸⁻²⁷⁰ Reaction paths involving the formation of bicarbonate have been discarded being not energetically favorable.²⁷⁰ The formation of CH₄ and H₂O was observed only for $T > 330^\circ\text{C}$ in the first cycle (grey scatters in Figure 18b) with a slightly decrease in the activation temperature to 280°C and an increase in the catalyst activity toward methanation of CO₂ over cycles (black scatters).³⁵ This increase in activity over cycles is related to the formation of <20 nm Ni particles, avoided from aggregation by the presence of MgO. Actually, the true catalyst for CO₂ methanation is represented by the cycled hydride and not by the starting material.³⁵ In fact, during the reaction, the bulk of the hydride is essentially inactive, being the hydrogen used for CO₂ hydrogenation only the one present in the flow, as verified by using Mg₂NiD₄ as catalyst. The formation of MgH₂ at the interlayer could also be ruled out by the observation that cycling of MgH₂ under hydrogen atmosphere containing only 1.96% of CO₂ does not allow the evolution of CO, CH₄ or H₂O as verified in mass spectroscopy studies.²⁷¹ MgH₂ undergoes to a fast lowering of the kinetics and capacity in hydrogen in presence of CO₂ with the transformation in an MgO/MgCO₃ rich material.^{272, 273}

A closer glance to the disproportionate surface of Mg₂NiH₄ (Figure 18a) shows its essentially coincidence on the chemical point of view with the case of metal particles supported on metal oxide. It is interesting to notice as, in fact, only intermetallic hydrides constituted by a R component, which the correspondent oxide is able to allow an easy formation of carbonates, are active as catalysts in CO₂ hydrogenation. This is due to the fact that³⁵ in the CO₂ hydrogenation reaction, *the dissociation of the H₂ molecule is not the rate controlling step but the dissociative adsorption of CO₂ molecule on the hydride surface.*³⁵ The same results was reported for oxide catalyzed hydrogenation reactions. This coincidence could allow interesting perspective in the design of new optimized catalysts for CO₂ hydrogenation. Results and conclusions driven for one class of systems can be then applied to the other. This fact is in general not underlined in the literature on the subject. For example, the evidence that the rate controlling step in CO₂ methanation is the CO₂ dissociation is self-evident for hydride systems. Moreover, strategies for catalyst protections over poisoning could be straightforwardly driven from disproportioned hydride surfaces to supported metal particle systems. Use of this catalyst for dry methane reforming is expected to bring some improvements in the stability of Ni based catalysts especially for what concerns coke formation.

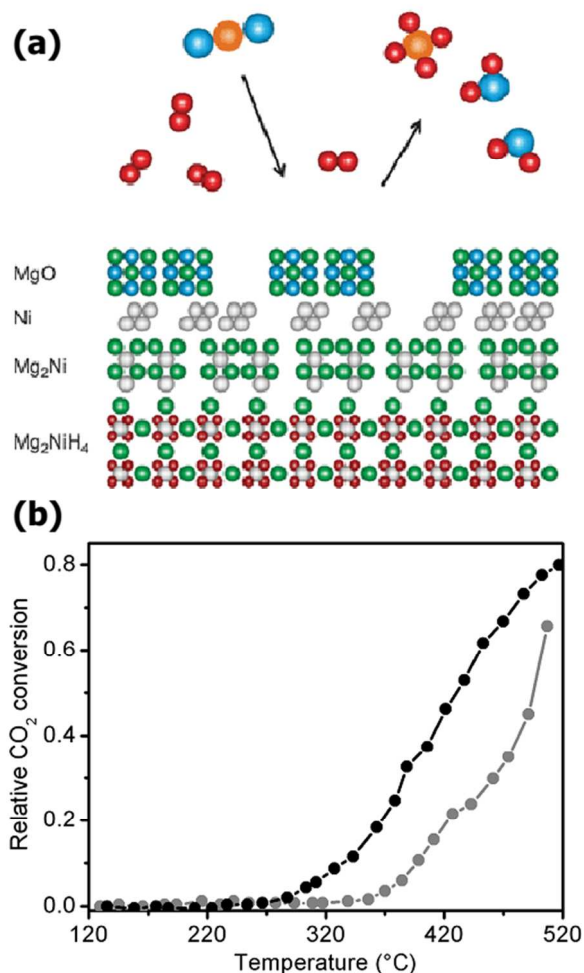


Figure 18. (a) The disproportionated surface of Mg₂NiH₄ (schematic representation). The metal hydride surface becomes catalytically active as Ni precipitates and converts CO₂ into CH₄ during hydrogen desorption (CO₂ + 4H₂ ⇌ CH₄ + 2H₂O). Reproduced with permission from Ref. 35. Copyright 2012 Royal Society of Chemistry. (b) The relative CO₂ conversion as function of the temperature (5°C min⁻¹) for CO₂ hydrogenation in a flow of CO₂ and H₂ (H₂/CO₂ = 8 with 50 ml min⁻¹ He at a total flow rate of 100 ml min⁻¹) on Mg₂NiH₄ for the first cycle (grey scatters) and after 18 cycles (black scatters). Data digitalized from Ref. 35.

4.9.2. Mg(BH₄)₂

Hydrides can also be used as co-reactants in reactions involving CO₂.^{21, 263-265} CO₂ reduction by BH₃NH₃, LiBH₄ and NaBH₄ was studied previously both theoretically²⁷⁴ and experimentally,²⁷⁵⁻²⁸³ as a method to enhance the thermolytic dehydrogenation of borohydride compounds^{275, 276, 283} or as a cheap method to obtain boron-doped carbons^{277, 278} or graphene oxide.²⁷⁹ It was also reported that sodium and lithium borohydrides react with CO₂ to give valuable chemical products as formic acid,²⁸² acyloxyborohydrides²⁸¹ and formatomethoxyborate or triformatoborohydride, depending on reaction conditions (temperature and solvents).²⁸⁰ The separation of the products from the reagents is possible by simply dissolving the material in a suitable solvent (e.g. water,²⁸¹ although this procedure can be safely adopted only after a high degree of CO₂ conversion has

been reached to avoid explosions due to the high exothermicity of unreacted borohydrides reaction with water).²¹ Nevertheless, the very low reaction rates at RT (1/90 molar ratio of reacted CO₂/BH₄ after 120 h),²⁸⁰ make unpractical its industrial application.

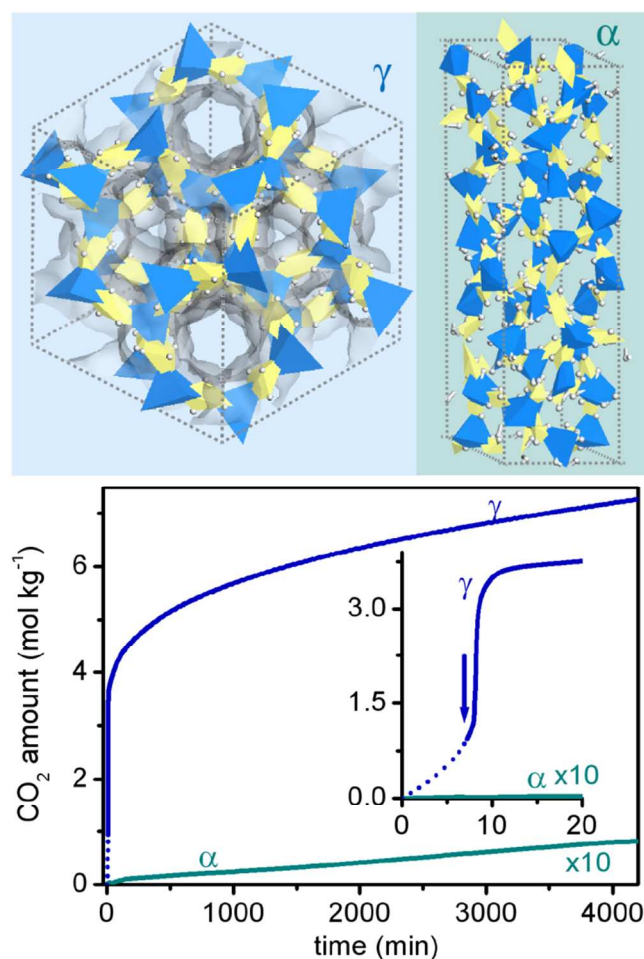


Figure 19. γ-Mg(BH₄)₂ and α-Mg(BH₄)₂ structures: Mg atoms are represented as light blue tetrahedra, B atoms as light yellow polyhedra and H atoms as spheres. The Connolly surface on γ-Mg(BH₄)₂ structure obtained by using a probe with radius of 1.82 Å is represented. a) Kinetic curve of CO₂ reaction with γ-Mg(BH₄)₂ at 30°C and 1 bar (blue curve). The inset shows the first 20 min of reaction (the arrow indicates the end of the CO₂ dosing procedure). The analogous curve obtained for α-Mg(BH₄)₂ is reported for comparison (dark cyan curve): the astonishing effect of the increased surface area on the reaction time is well evident. Data from Ref. 21.

Porous complex hydrides are a new class of materials in the panorama of metal hydrides.²⁸⁴ Among them, gamma phase of Mg(BH₄)₂ possesses the interesting peculiarity to show a large permanent porosity, accounting for about the 33% of the material volume (see Figure 19).²⁸⁴ Its structure is constituted by Mg²⁺ ions in tetrahedral coordination, linked through a shared [BH₄]⁻, giving rise to a highly 3D porous structure characterized by hexagonal overtures with a narrowest dimension of 5.95 Å (geometrical distance). Each hexagon, having a chair conformation, shares every Mg-BH₄-Mg side with a vicinal hexagon through a tetrahedral angle. The high surface of this material (1160 m² g⁻¹) makes it interesting as nanosponge for gas

adsorption and its ability to adsorb large quantities of molecular hydrogen was recently reported.²⁸⁴ This material, at difference of all the previously reported hydrides, is able to react fast with CO₂ at RT and for pressure close to the atmospheric CO₂ partial pressure. In Figure 19, the CO₂ reacted as function of time at 30°C and 1 bar is reported (blue curve), showing as 1 CO₂ reacts every 11 [BH₄]⁻ after only 11 min. The plateau value of 12 mol kg⁻¹ CO₂ was observed only after 7 days. Key role of the surface area was confirmed by comparison with data collected on its unporous isomorph α-Mg(BH₄)₂ (Figure 19, dark cyan line). The reaction products were analyzed by ¹³C-NMR and IR spectroscopies indicating as formate, methoxy and alkoxide species are formed, most of them bound to the boron atom. The reaction was monitored in time by IR spectroscopy, evidencing as all the products are formed at once (in the time needed for the spectra recording) and no evolution of the products towards more reduced CO₂ species was observed, at difference of ammonia borane studies.^{275, 276, 278, 279, 283} No evolution of gaseous reaction species (e.g. methane or CO) was also evidenced at 30°C and 1 bar.²¹ On the contrary, exposure to supercritical CO₂ (40°C and 90 bar for 1 h)²⁶³ allowed the formation of methane and methanol, further underlying the importance of the reaction conditions on the products that can be obtained in hydrogenation reactions of CO₂.

An important drawback of the use of hydrides as reactants is the impossibility to rehydrogenate them after reaction with CO₂.^{21, 263, 265} and γ-Mg(BH₄)₂ does not represent an exception, likely because of the higher CO₂ interaction energy with respect to H₂ and the large stability of the B-O bonds.²¹ If re-hydrogenable, γ-Mg(BH₄)₂ could be used as catalyst instead as reagent with performances in temperature and pressure conditions close to atmosphere not achieved by any other system. Nevertheless, this system remains very interesting. In fact, the very fast kinetics associated to the reaction provide to this hydride the peculiar characteristics to be able to couple in one step the separation and recycling of CO₂ in a wide temperature range (RT < T < 190°C) and pressures allowing to avoid the storage and transportation steps.²¹ The possibility to use γ-Mg(BH₄)₂ as co-reagents in other CO₂-based reactions to enlarge the number of obtainable products has been also proposed.²¹

Conclusions

In the present review, many of the different systems at work in both the natural and the artificial CO₂ cycle were described by using as *leitmotif* the presence of Mg in their structure. Although breakthrough results were reported recently for all the steps of the synthetic CO₂ cycle,^{52, 57, 147, 151} there is still large room for improvements.

For what concerns the *catalysis* research, among all the possible reactions involving CO₂, the synthesis of fuels has a principle role. This is appealing not only because it reduces the carbon footprint of fuels but also because it would allow to maintain the present existing infrastructure and the same quality of life, being most of the energetic alternatives to fossil fuels far to allow the same performances. In some applications (as plane propulsion), at present a reasonable substituent does not even exist.²⁸⁵ Considering the fact that 73.8% of the CO₂ emissions are related

to fossil fuels burning, it is clear that any strategy for CO₂ reduction will need to address also to: research on CCS and CCU, energy efficiency, and the use of less carbon intensive fuels such as CH₄ and other renewable energy sources.²⁸⁶ Coal-fired plants for example are characterized by a very low energetic efficiency (30%)⁵⁵ and they represent the most important CO₂ stationary sources. Their substitution has to envisaged by new coal-fired plants characterized by a more careful heat management⁵⁵ or by plants based on more efficient processes such as oxyfuel combustion coupled with CCS. Such changes can be addressed effectively only at the political level.

Coming back to CO₂ recycling, personally I consider the carboxylation of alcohols to fuels and the dry methane reforming as the most important reactions. The latter in particular, in combination with the Fisher-Tropsch process, has the advantage to transform the two most important greenhouse gases (CO₂ and CH₄) into hydrocarbons.²⁸ This technology is particularly promising for CO₂/CH₄ mixture deriving from fermentation and it does not require for CO₂ separation. In this field, the fast deactivation of industrial catalysts due to coke formation is the most important problem to overcome. A broader use of materials with high oxygen mobility such as perovskites is expected to bring benefits from this point of view.^{28, 40} Particularly interesting would be the testing of natural siliceous perovskites as (Mg,Fe)₂SiO₃, Al-(Mg,Fe)₂SiO₃. Carboxylation of methane, although more rarely studied, is another appealing reaction for valorization of biogas.¹²

Nevertheless, the availability of efficient catalytic processes is not enough to make CO₂ utilization feasible. In fact, the high cost of CO₂ separation makes it a costly feedstock, a fact that is at the basis of its low exploitation as a reagent in the industry.¹⁵ The drivers that can allow to reverse this situation are resources scarcity on one hand but also political and regulatory actions. The Kyoto protocol restrictions on CO₂ emissions can for example create a market for captured CO₂, aimed to compensate in part the cost of separation. On the other hand, reactions that allow to avoid the separation step have to be sought, like for example dry methane reforming and CO₂ hydrogenation by hydrides.^{21, 35, 263}

For what concerns separation, this is the field where improvements would be more urgently required, firstly to lower the energetic cost of CO₂ separation for the reasons discussed above and moreover to improve the purity of separated CO₂ (indispensable in many reactions).¹⁵ In this field the necessity of new materials is particularly urgent.⁶³ Among the different materials reported for low temperature separation, MOFs, because of their large flexibility in design, are particularly promising for improvements. The possibility to chemically alter the interior of MOFs to create pores analog to the enzyme pockets that can match target molecules is very promising.^{119, 287}

Flexible structures of MOFs able to respond to external stimuli of different nature (pressure, specific adsorbates, light, ...) have been also reported,^{81, 133, 287-289} materials that can bring some breakthrough in the separation field. Although the large selectivities and working capacities reported for some MOFs are very high (see Table 5), this class of materials suffers of two main problems: (i) high cost; (ii) water sensitivity. The low water resistance of MOFs does not only lower their performances as CO₂ scrubbers in presence of moisture as observed for zeolites,

but it undermines the stability of the materials themselves, besides some important exceptions.^{130, 153, 289-291} MOFs composites involving the presence of carbon, graphene oxide, aminated graphene oxide, nanotubes, etc., because of their hydrophobic nature, showed better anti-moisture performances than pure materials.²⁹²⁻²⁹⁴ Other strategies are represented by the introduction of hydrophobic groups, such as $-\text{CF}_3$.²⁹⁵ The best performances in CO_2 separation were observed for materials containing grafted alkylamines, in analogy to what reported for almost all the other classes of materials.^{63, 130, 147, 148, 296, 297}

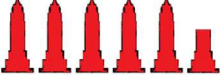
However, the amount of sorbents needed to address global scale CO_2 capture has to be so high that the choice of environmental benign compounds is mandatory.⁶³ Amines-based materials are lacking in this respect being corrosive and carcinogenic compounds.

MOFs are also materials characterized by a very high cost. Nevertheless, the cost of the material is in many cases only a small fraction of the cost of the CO_2 separation process, whose main contribution is energy consumption. Moreover, economical cost of CO_2 separation, although important, has to be compared with the corresponding cost due to climate change effects (e.g. drastic weather events, loss of fertile land and the reduction of Earth land surface due to sea level rising). Low cost materials for CO_2 capture exist and they are almost exclusively carbon based materials obtained from waste resources.^{63, 298} This solution has a double benefits allowing to reduce the waste (and also the biogas evolved from its fermentation) by creating an effective CO_2 sorbent that can be produced in the huge necessary amounts.²⁰⁰ In fact, 140 Gtons per year of biomass are produced from agriculture.²⁰⁰ These carbons are often nitrogen rich or contain nanodispersed basic oxides which improve their CO_2 sorption capacities.⁶³ Carbons obtained from poplar anthers are able to adsorb up to 51.3 mmol g^{-1} at 25°C and 50 bar.²⁹⁹ Although

carbons are good storage materials, they are in general characterized by very poor performances in separation processes.⁶³ An exception is represented by the MgO/C system reported in Ref. 200 able to capture significant CO_2 quantities also at 1 bar. Moreover this system was obtained by fast pyrolysis of biomass impregnated with sea salts.

Among separation processes, separation from the atmosphere is the one needing more improvements. Unfortunately, this is also the process for which the improvements are more urgent, being the drastic effects of the abnormal rise in CO_2 concentration in the atmosphere already visible and asking for an action that cannot be delayed further. Actually, few materials have been reported to date having significant CO_2 capacities at the very low partial CO_2 pressures at play (0.4 mbar). The best performing materials reported up to now are all amine containing structures (see for example Table 5). Nevertheless, the presence of amines still makes them unsuitable for a global use and production at least on the Mtons scale. The short list of materials can be enlarged by considering for example the possibility to compress air before capture. Normal compressors allow to reach pressures up to 35 bar. This would correspond to an increase in the CO_2 partial pressure up to 14 mbar, enabling the use of a broader range of existing capture materials. An increase of CO_2 partial pressure could be also reached through a two step separation process where the purity of separated CO_2 is increased stepwise. Being the amount of CO_2 to be handled so large, in order to be effective, an organized action at planetary level would have to consider no more than 2-3 ways to capture CO_2 from the atmosphere. In the choice, the energy and time needed to build the CCS infrastructure have to be considered. In the end, at present any synthetic material proposed so far does not constitute a reliable choice for CO_2 capture from the atmosphere.

Table 8. Qualitative and speculative comparison of different separation processes for CO_2 capture from atmosphere.

Process	product	Volume occupied (EB units) ^a	Time to complete separation (year) ^b	Characteristic storage time (year) ^c	Cost (USD ₂₀₁₀ ton ⁻¹ CO ₂) ^d	Air compression/intake
Separation through MOFs	liquid CO ₂		0.4	?	46-90	yes
Mineral carbonation	carbonate		1.24 - 61	> 10 ⁵	0-8	yes/no
Photosynthesis	wood		6 - 39	10-10 ² , > 10 ⁵	0-120	no

^aVolume normalized to the volume occupied by 900 metric Gton of liquid CO_2 to facilitate the comparison (see Figure 2).

^bComparative time calculated in the extreme hypothesis to completely cover a surface equal to the Earth land surface with: (i) 1 cm thick layer of IRMOF-74-Ilb-mmen (for liquid CO_2), (ii) mine tailings able to provide an average capture of $27\text{-}1330 \text{ g C m}^{-2} \text{ year}^{-1}$,²⁵⁵ and (iii) an hybrid poplar wood.³⁰⁰ For the MOF, the time necessary for the sorption/desorption cycle was underestimated and considered coincident twice the time needed for saturation of the material in 15% CO_2 atmosphere ($15 \cdot 2 = 30 \text{ min}$).¹⁴⁷ For the hybrid poplar wood, the growth factor was calculated from the values reported in Ref. 301. See ESI for further details.

^cValues from Ref. 55 and 300.

^dCost of the separation process with MOFs by considering it coincident with those reported for membrane post-combustion capture processes in Ref. 64. The cost of the material production (considering an operational time of the plant larger than 1 year and a market cost of $1 \text{ \$ kg}^{-1}$ for the scrubber) resulted negligible with respect to the separation process itself in the approximations adopted in this work ($< 1 \text{ \$ ton}^{-1} \text{ CO}_2$). On the contrary, the cost related to the air intake process have not been considered, although expected to be particularly important in air sequestration. At present such an infrastructure does not exist and then the cost of this process could be only of speculative nature. Mineral carbonation cost from Ref. 229. Upper limit for carbon fixation in plant estimated as the cost for wood production from Ref. 302.

Cite this: DOI: 10.1039/c0xx00000x

www.rsc.org/xxxxxx

REVIEW

For what concerns natural processes, two have shown to be able to allow significant carbon fixation from the atmosphere: natural weathering of silicates (Section 4.8.3) and photosynthesis (Section 4.2). In Table 8, a comparison between these two processes and a membrane capture plant based on one of the best performing material reported for CO₂ capture (IRMOF-74-Ilb-mm) is reported. The analysis presented there is far to be quantitative being based on rough assumptions. These assumptions have been adopted purposely in order to put on the same plane such different methods to roughly estimate the order of magnitude at play in term of time and cost. In fact, the estimate of times, precise or rough in nature, are completely lacking in the literature. For what concerns the photosynthetic and mineralization processes, data on carbon fixation are often normalized to the surface area occupied by the system. In order to compare MOFs with them, it has been considered the amount of IRMOF-74-Ilb-mm that would be necessary to cover with a thickness of 1 cm a certain surface. As surface, the total land surface has been considered. Although this option is far from being feasible, it can be thought as an upper limit. Among the several *plantae* existing, hybrid poplars have been considered here. In fact, they rank second among the fastest growing plants on Earth and they are not as strongly invasive and eco-system killers as the bamboo. Moreover, its wood is considered a medium high quality wood for combustion.³⁰³ For what concerns mineralization, on the contrary, the time for the completion of the process has been calculated considering the two limit carbon fixation rates reported for natural weathering in Ref. 255.

Surprisingly, the time estimated to complete the separation (in the rough approximation reported here) covers a few orders of magnitude. Actually, among the values in Table 8, the one reported for the artificial process is particularly low. Longer periods, although of only one order of magnitude larger, would be necessary to photosynthesis to fix the same amount of CO₂. For what concerns the separation cost, mineral carbonation remains the cheapest solution, having the photosynthetic and the MOF comparable cost. In the calculation of the data reported in Table 8, it is important to note that the time needed to construct the infrastructure necessary for each process has not been considered. This approximation is not very important for the two natural processes, being only an extension on the global scale of their already large exploitation. On the contrary, this is expected to strongly delaying the artificial process to start. The inertia in introducing new technologies is a well-known problem in this subject and their implementation can be driven only by policy makers or financial incentives.⁶³ Moreover the synthesis of the huge amount of sorbent necessary is not a trivial industrial pursuit.

Another important point to consider in this approximate comparison is the end product of the three separation processes. For what concerns the artificial process, pure CO₂ is obtained, which represents an interesting reagent and solvent, as discussed along this review. Nevertheless, besides the small part exploited

for this aim by industries, the most part of this amount would need to be stored in a long term disposal site (mineralization) increasing the cost and complexity of the process. Mineralization and photosynthetic end products represent themselves a solution for the long term storage of CO₂. Inorganic carbonates have the advantage to represent the ideal CO₂ disposal form, because of their high stability. Moreover, carbonates are considered valuable products, with uses in different fields from cosmetics, pharmaceuticals industry, paints, ceramics and cements. Magnesium bicarbonate is an important additive for desalinated and mineral water. A value of silicate carbonation would be added if this reaction would be used for land reclamation, as shown in the case of chrysotile (Section 4.8.3). On the other hand, for what concerns photosynthesis, a stable storage form is wood whose durability and inertness enable carbon storage over a relatively large timescale, comparable with that of carbonates.³⁰⁰ For this reason, it has been previously suggested that forestation can be an effective way to reduce global warming.³⁰⁰

Moreover, wood represents, among the three end products reported in Table 8, the one with the higher added value coupled with a significant chemical stability.³⁰⁰ By hypothesizing a correct exploitation of trees as carbon fixation systems (substitution of the trees each 3-5 years, appropriate storage conditions of wood, etc.), the use for this purpose of a surface corresponding to only 10% of the Earth land surface would allow to observe in 2050 the same atmospheric CO₂ concentration measured today. If combined with proper carbon sequestration at the larger stationary sources, in this optimistic view a deflection of the trend could be observed. Nevertheless, the forestation solution presents important drawbacks, essentially related to the necessity to exploit the same resources of agriculture: water and land surface. Actually, the first reason at the basis of deforestation is the conversion of forests in arable lands, because of the increasing food request. This means that such an action could have a direct and important effect on the price of food. For what concerns soil occupations, solutions not requiring the reconversion of arable lands to forests have to be considered. Possible solutions can be represented by a larger introduction of trees in urban areas or the use of reforestation as a mean for land reclamation of polluted arable lands. For what concerns the massive use of water, the optimization of the use of water in agriculture is at present largely studied. Large amounts of freshwater are commonly used also in material synthesis and CO₂ underground sequestration processes. A comparison of the three processes reported in Table 8 by LCA, comprehensive of these aspects, is at present not possible on the basis of the literature data. It would be particularly interesting if it would be addressed in future studies.

The most important advantage of photosynthesis is that, as also stated by Lackner,⁵⁵ seems currently the only practical form of air capture in the short middle term. It is interesting to note in this regard that this would have a precedent in the Earth's history. In fact, a particular algae species, the *Azolla filliculoides*, among the

fastest growing plants on Earth,³⁰⁴ was responsible of the strong decrease in the CO₂ level in the atmosphere about 48.5 million years ago, during the Eocene. This event goes under the name of the Azolla event.³⁰⁵ The massive proliferation of this freshwater fern in the Arctic region up to 4 × 10⁶ km² of covered surface (due to the mild temperature, to the presence of a freshwater surmountant layer in the oceans, and to the low presence of microorganisms for degradation) caused the decrease in CO₂ in the atmosphere from 3500 to 650 ppm in 800,000 years.^{90, 305} Several varieties of Azolla are still cultivated. Algae have in fact several uses as green manure, fodder for poultry,³⁰⁶ can be used as cosmetics, whole food ingredients, food integrators,³⁰⁷ for bulk chemicals, paper,^{308, 309} bio-ethanol^{309, 310} and biofuels production.³⁰⁷ Moreover, microalgae need for their cultivation only 3% of the area required by vegetation,^{307, 311} representing then an interesting alternative for CO₂ fixation. Nevertheless it is important to stress as the efficient CO₂ sequestration during Eocene was possible because of the absence of microorganisms responsible for fermentation of biomasses that exist nowadays. At present, the biogas that would be generated by putrefaction of microalgae, if not correctly handled, would cause a strong worsening of the greenhouse effects instead to be beneficial. The problem of degradation is only marginal in wood production but nevertheless it has to be properly addressed because of the large amounts of leaves and other waste products that would be produced.

An important point that is often forgotten is that any cultivation causes an important production of volatile organic compounds and in particular of isoprene.³¹² Hybrid poplars are not an exception. Isoprene is known to react with NO_x and radicals allowing a reduction of their concentration in the air.^{312, 313} In the reaction, ozone is released causing the reduction of the concentration of aerosol particles and pollutants in the air.³¹²⁻³¹⁴ This observation is important because indicates that the introduction of trees would be particularly beneficial in high polluted urban areas. Nevertheless, isoprene has been determined to critically influence the planet climate and then, careful modeling of any increase in its production have to be made. Moreover, ozone is a priority air pollutant causing about 22 000 excess deaths per year in Europe.³¹² For these reasons, all the possible parameters have to be carefully considered before a global action is started to address the problem of CO₂ excess in the atmosphere.

Like synthetic processes, also the photosynthetic one can be improved in efficiency. In fact, as stated in Section 4.1, Rubisco is the less efficient enzymes on Earth. For this reason, research is done extensively on how to increase crop yields by switching C3 plants to C4 ones (especially rice)^{87, 108, 315} or on increasing the Rubisco efficiency.^{84, 87, 102} This research is in primis aimed to decrease the world hunger. Nevertheless, besides the ethical and environmental concerns, a change in the carbon fixation rate is known to correspond to an alteration of the food nutritional parameters. An increase in the carbon dioxide fixation rates due to the increase in the atmospheric CO₂ concentration, for example, lower the quality of the wheat.⁹⁴⁻⁹⁶ This can be related to the fact that during photorespiration most of the nitrate/nitrogen assimilation happens, necessary for protein production.³¹⁶ In this way, faster growing plants would constitute a lower quality food. Moreover, accordingly to FAO one third of

global food is wasted, indicating as the world hunger problem could be solved by a more careful planned distribution of the food resources.

Nevertheless, this research can be beneficial to biofuels production and carbon fixation purposes.^{87, 101, 307, 309} Moreover, a deeper knowledge of the mechanisms and structural modifications in enzymatic reactions involving CO₂ can help in the design of new synthetic catalysts and sorbents.

It is interesting to remember as in many cultures there was the habit to plant a tree when a child was born. In China, an Empress tree has to be planted for any newborn girl. It is not surprising that this beautiful shrub is among the ten fastest growing plants on the planet.

Acknowledgments

Prof. Adriano Zecchina and Dr. Gabriele Ricchiardi are acknowledged for useful discussions on the global warming problem.

Notes and references

^a Department of Science and High Technology, Università dell'Insubria, Via Lucini 3, 22100 Como, Italy, Tel.: +39 031-2386614; Fax: +39 031-2386630; E-mail: jenny.vitillo@uninsubria.it.

† Electronic Supplementary Information (ESI) available: details of the calculations for the quantities reported in Figure 2 and in Table 8; comprehensive list of all the Mg-based metal organic frameworks reported in the literature. See DOI: 10.1039/b000000x/

- J. R. Petit, J. Jouzel, D. Raynaud, N. I. Barkov, J. M. Barnola, I. Basile, M. Bender, J. Chappellaz, M. Davis, G. Delaygue, M. Delmotte, V. M. Kotlyakov, M. Legrand, V. Y. Lipenkov, C. Lorius, L. Pepin, C. Ritz, E. Saltzman and M. Stievenard, *Nature*, 1999, **399**, 429-436.
- <http://www.esrl.noaa.gov/gmd/ccgg/trends/>, 2015.
- K. Sumida, D. L. Rogow, J. A. Mason, T. M. McDonald, E. D. Bloch, Z. R. Herm, T. H. Bae and J. R. Long, *Chem. Rev.*, 2012, **112**, 724-781.
- M. Mikkelsen, M. Jorgensen and F. C. Krebs, *Energy Environ. Sci.*, 2010, **3**, 43-81.
- J. D. Shakun, P. U. Clark, F. He, S. A. Marcott, A. C. Mix, Z. Liu, B. Otto-Bliesner, A. Schmittner and E. Bard, *Nature*, 2012, **484**, 49-54.
- Jet Propulsion Laboratory <http://sealevel.jpl.nasa.gov/>, 2015.
- D. A. King, *Science*, 2004, **303**, 176-177.
- D. W. Keith, *Science*, 2009, **325**, 1654-1655.
- F. Klein and T. M. McCollom, *Earth Planet. Sci. Lett.*, 2013, **379**, 137-145.
- Z. Zhang, Z.-Z. Yao, S. Xiang and B. Chen, *Energy Env. Sci.*, 2014, **7**, 2868-2899.
- D. M. D'Alessandro, B. Smit and J. R. Long, *Angew. Chem.-Int. Edit.*, 2010, **49**, 6058-6082.
- H. J. Freund and M. W. Roberts, *Surf. Sci. Rep.*, 1996, **25**, 225-273 and references therein.
- E. A. Quadrelli, G. Centi, J. L. Duplan and S. Perathoner, *Chem. Sus. Chem.*, 2011, **4**, 1194-1215.
- W. Wang, S. P. Wang, X. B. Ma and J. L. Gong, *Chem. Soc. Rev.*, 2011, **40**, 3703-3727.
- M. Aresta, in *Activation of Small Molecules*, Wiley-VCH Verlag GmbH & Co. KGaA, 2006, pp. 1-41.

16. A. Behr, *Carbon Dioxide Activation by Metal Complexes*, VCH Verlagsgesellschaft, Weinheim, 1988.
17. J. G. Vitillo, M. Savonnet, G. Ricchiardi and S. Bordiga, *Chem. Sus. Chem.*, 2011, **4**, 1281-1290.
18. J. M. Weber and H. Schneider, *J. Chem. Phys.*, 2004, **120**, 10056-10061.
19. R. Vaidhyanathan, S. S. Iremonger, G. K. H. Shimizu, P. G. Boyd, S. Alavi and T. K. Woo, *Science*, 2010, **330**, 650-653.
20. X. Kong, E. Scott, W. Ding, J. A. Mason, J. R. Long and J. A. Reimer, *J. Am. Chem. Soc.*, 2012, **134**, 14341-14344.
21. J. G. Vitillo, E. Groppo, E. G. Bardaji, M. Baricco and S. Bordiga, *Phys. Chem. Chem. Phys.*, 2014, **16**, 22482-22486.
22. G. Busca and V. Lorenzelli, *Mater. Chem.*, 1982, **7**, 89-126.
23. B. Bonelli, B. Civalieri, B. Fubini, P. Ugliengo, C. Otero Areán and E. Garrone, *J. Phys. Chem. B*, 2000, **104**, 10978-10988.
24. M. Werner, S. Hariharan and M. Mazzotti, *Phys. Chem. Chem. Phys.*, 2014, **16**, 24978-24993.
25. K. Teramura, T. Tanaka, H. Ishikawa, Y. Kohno and T. Funabiki, *J. Phys. Chem. B*, 2003, **108**, 346-354.
26. M. M. Halmann, *Chemical Fixation of Carbon Dioxide : Methods of Recycling CO2 into Useful Products*, CRC Press, Boca Raton, Florida, 1993.
27. G. A. Olah and Á. Molnár, *Hydrocarbon Chemistry*, John Wiley & Sons, 2003.
28. D. Pakhare and J. Spivey, *Chem. Soc. Rev.*, 2014, **43**, 7813-7837.
29. Q. Cai, B. Lu, L. Guo and Y. Shan, *Catal. Commun.*, 2009, **10**, 605-609.
30. R. V. Siriwardane and R. W. Stevens, *Ind. Eng. Chem. Res.*, 2009, **48**, 2135-2141.
31. K. S. Lackner, C. H. Wendt, D. P. Butt, E. L. Joyce Jr and D. H. Sharp, *Energy*, 1995, **20**, 1153-1170.
32. J.-N. Park and E. W. McFarland, *J. Catal.*, 2009, **266**, 92-97.
33. J. Mascetti, F. Galan and I. Pápai, *Coord. Chem. Rev.*, 1999, **190-192**, 557-576.
34. D. E. Peebles, D. W. Goodman and J. M. White, *J. Phys. Chem.*, 1983, **87**, 4378-4387.
35. S. Kato, A. Borgschulte, D. Ferri, M. Biemann, J.-C. Crivello, D. Wiedenmann, M. Parlinska-Wojtan, P. Rossbach, Y. Lu, A. Remhof and A. Zuttel, *Phys. Chem. Chem. Phys.*, 2012, **14**, 5518-5526.
36. S. Yokota, K. Okumura and M. Niwa, *Catal. Lett.*, 2002, **84**, 131-134.
37. J. R. Rostrup-Nielsen, K. Pedersen and J. Sehested, *Appl. Catal. A*, 2007, **330**, 134-138.
38. G. Du, S. Lim, Y. Yang, C. Wang, L. Pfefferle and G. L. Haller, *J. Catal.*, 2007, **249**, 370-379.
39. P. J. Lunde and F. L. Kester, *Ind. Eng. Chem. Process Des. Dev.*, 1974, **13**, 27-33.
40. H. Zhan, F. Li, P. Gao, N. Zhao, F. Xiao, W. Wei, L. Zhong and Y. Sun, *J. Power Sources*, 2014, **251**, 113-121.
41. D. Scarano, S. Bertarione, F. Cesano, J. G. Vitillo and A. Zecchina, *Catal. Today*, 2006, **116**, 433-438.
42. A. Parmaliana, F. Arena, F. Frusteri, S. Coluccia, L. Marchese, G. Martra and A. L. Chuvilin, *J. Catal.*, 1993, **141**, 34-47.
43. B. Nematollahi, M. Rezaei, E. N. Lay and M. Khajenoori, *J. Nat. Gas Chem.*, 2012, **21**, 694-702.
44. D. Pakhare, C. Shaw, D. Haynes, D. Shekhawat and J. Spivey, *J. CO2 Utilization*, 2013, **1**, 37-42.
45. A. Erdohelyi, J. Cserenyi and F. Solymosi, *J. Catal.*, 1993, **141**, 287-299.
46. P. Ferreira-Aparicio, M. Fernandez-Garcia, A. Guerrero-Ruiz and I. Rodriguez-Ramos, *J. Catal.*, 2000, **190**, 296-308.
47. M. C. J. Bradford and M. A. Vannice, *Catal. Rev.*, 1999, **41**, 1-42.
48. J. H. Bitter, K. Seshan and J. A. Lercher, *Top. Catal.*, 2000, **10**, 295-305.
49. S. M. Stagg, E. Romeo, C. Padro and D. E. Resasco, *J. Catal.*, 1998, **178**, 137-145.
50. M. Garcia-Dieguez, I. S. Pieta, M. C. Herrera, M. A. Larrubia, I. Malpartida and L. J. Alemany, *Catal. Today*, 2010, **149**, 380-387.
51. Y. Ono, *Appl. Catal. A*, 1997, **155**, 133-166.
52. D. C. Stoian, E. Taboada, J. Llorca, E. Molins, F. Medina and A. M. Segarra, *Chem. Commun.*, 2013, **49**, 5489-5491.
53. D. Delledonne, F. Rivetti and U. Romano, *Appl. Catal. A*, 2001, **221**, 241-251.
54. K. Tomishige, Y. Ikeda, T. Sakaihorii and K. Fujimoto, *J. Catal.*, 2000, **192**, 355-362.
55. K. S. Lackner, *Science*, 2003, **300**, 1677-1678.
56. G. Xiao, R. Singh, A. Chaffee and P. Webley, *Int. J. Greenhouse Gas Control*, 2011, **5**, 634-639.
57. E. J. Swanson, K. J. Fricker, M. Sun and A.-H. A. Park, 2014, **16**, 23440-23450.
58. D. P. Butt, K. S. Lackner, C. H. Wendt, S. D. Conzone, H. Kung, Y.-C. Lu and J. K. Bremser, *J. Am. Ceram. Soc.*, 1996, **79**, 1892-1898.
59. S. Wang, S. Yan, X. Ma and J. Gong, *Energy Environ. Sci.*, 2011, **4**, 3805-3819.
60. A. A. Olajire, *J. Petrol. Sci. Eng.*, 2013, **109**, 364-392.
61. A. Aroux and A. Gervasini, *J. Phys. Chem.*, 1990, **94**, 6371-6379.
62. C. Pighini, T. Belin, J. Mijoin, P. Magnoux, G. Costentin and H. Lauron-Pernot, *Appl. Surf. Sci.*, 2011, **257**, 6952-6962.
63. J. Wang, L. Huang, R. Yang, Z. Zhang, J. Wu, Y. Gao, Q. Wang, D. O'Hare and Z. Zhong, *Energy Environ. Sci.*, 2014, **7**, 3478-3518.
64. M. Zhao, A. I. Minett and A. T. Harris, *Energy Environ. Sci.*, 2013, **6**, 25-40.
65. K. Vatopoulos and E. Tzimas, *J. Cleaner Prod.*, 2012, **32**, 251-261.
66. Y. Liang, D. P. Harrison, R. P. Gupta, D. A. Green and W. J. McMichael, *Energy Fuels*, 2004, **18**, 569-575.
67. S. C. Lee, B. Y. Choi, T. J. Lee, C. K. Ryu, Y. S. Ahn and J. C. Kim, *Catal. Today*, 2006, **111**, 385-390.
68. P. Gélin and M. Primet, *Appl. Catal. B*, 2002, **39**, 1-37.
69. V. C. Menon and S. Komarneni, *J. Porous Mat.*, 1998, **5**, 43-58.
70. S. Ma, D. Sun, J. M. Simmons, C. D. Collier, D. Yuan and H.-C. Zhou, *J. Am. Chem. Soc.*, 2007, **130**, 1012-1016.
71. T. Nakayama, N. Ichikuni, S. Sato and F. Nozaki, *Appl. Catal. A*, 1997, **158**, 185-199.
72. L.-C. Lin, A. H. Berger, R. L. Martin, J. Kim, J. A. Swisher, K. Jariwala, C. H. Rycroft, A. S. Bhowm, M. Deem, M. Haranczyk and B. Smit, *Nature Mater.*, 2012, **11**, 633-641.
73. M. Tagliabue, D. Farrusseng, S. Valencia, S. Aguado, U. Ravon, C. Rizzo, A. Corma and C. Mirodatos, *Chem. Eng. J.*, 2009, **155**, 553-566.
74. H. Furukawa, N. Ko, Y. B. Go, N. Aratani, S. B. Choi, E. Choi, A. Ö. Yazaydin, R. Q. Snurr, M. O'Keeffe, J. Kim and O. M. Yaghi, *Science*, 2010, **329**, 424-428.

75. C. A. Grande and A. E. Rodrigues, *Int. J. Greenhouse Gas Control*, 2008, **2**, 194-202.
76. T.-H. Bae, M. R. Hudson, J. A. Mason, W. L. Queen, J. J. Dutton, K. Sumida, K. J. Micklash, S. S. Kaye, C. M. Brown and J. R. Long, *Environ. Sci.*, 2013, **6**, 128-138.
77. S. Xiang, Y. He, Z. Zhang, H. Wu, W. Zhou, R. Krishna and B. Chen, *Nature Commun.*, 2012, **3**.
78. R. Krishna and J. M. van Baten, *J. Membr. Sci.*, 2010, **360**, 323-333.
79. M. P. Allen and D. J. Tildesley, *Computer simulation of liquids*, Clarendon Press, 1989.
80. A. Boutin, S. Couck, F.-X. Coudert, P. Serra-Crespo, J. Gascon, F. Kapteijn, A. H. Fuchs and J. F. M. Denayer, *Micropor. Mesopor. Mater.*, 2011, **140**, 108-113.
81. F.-X. Coudert, C. Mellot-Draznieks, A. H. Fuchs and A. Boutin, *J. Am. Chem. Soc.*, 2009, **131**, 11329-11331.
82. P. A. Frey and A. D. Hegeman, *Enzymatic Reaction Mechanisms*, Oxford University Press, New York, 2007.
83. S. R. Caskey, A. G. Wong-Foy and A. J. Matzger, *J. Am. Chem. Soc.*, 2008, **130**, 10870-10871.
84. S. M. Whitney, R. L. Houtz and H. Alonso, *Plant Physiol.*, 2011, **155**, 27-35.
85. A. R. Portis and M. A. J. Parry, *Photosynth. Res.*, 2007, **94**, 121-143.
86. B. Kannappan and J. E. Gready, *J. Am. Chem. Soc.*, 2008, **130**, 15063-15080.
87. C. C. Mann, *Science*, 1999, **283**, 314-316.
88. I. Andersson, *J. Molec. Biol.*, 1996, **259**, 160-174.
89. R. A. Berner, *Science*, 1997, **276**, 544-546.
90. P. N. Pearson and M. R. Palmer, *Nature*, 2000, **406**, 695-699.
91. R. F. Sage, T. L. Sage and F. Kocacinar, *Ann. Rev. Plant Biol.*, 2012, **63**, 19-47.
92. R. Chollet, J. Vidal and M. H. O'Leary, *Ann. Rev. Plant Physiol. Plant Molec. Biol.*, 1996, **47**, 273-298.
93. C. Peterhansel and V. G. Maurino, *Plant Physiol.*, 2011, **155**, 49-55.
94. B. A. Kimball, C. F. Morris, P. J. Pinter, G. W. Wall, D. J. Hunsaker, F. J. Adamsen, R. L. LaMorte, S. W. Leavitt, T. L. Thompson, A. D. Matthias and T. J. Brooks, *New Phytol.*, 2001, **150**, 295-303.
95. F.-W. Badeck, F. Rizza, C. Maré, L. Cattivelli, A. Zaldei and F. Miglietta, XVI convegno nazionale di Agrometeorologia, Firenze, 2013.
96. D. W. Lawlor and R. A. C. Mitchell, *Plant Cell Environ.*, 1991, **14**, 807-818.
97. P. M. Drennan and P. S. Nobel, *Plant Cell Environ.*, 2000, **23**, 767-781.
98. A. G. Eric and S. N. Park, *J. Exp. Botany*, 1996, **47**, 61-69.
99. M. Calvin, *Angew. Chem. Int. Ed.*, 1962, **1**, 65-75.
100. *Jmol: an open-source Java viewer for chemical structures in 3D*. <http://www.jmol.org/>
101. B. Stec, *Proc. Natl. Acad. Sci. U.S.A.*, 2012, **109**, 18785-18790.
102. M. M. El-Hendawy, N. J. English and D. A. Mooney, *J. Molec. Mod.*, 2013, **19**, 2329-2334.
103. Y. Kai, H. Matsumura and K. Izui, *Arch. Biochem. Biophys.*, 2003, **414**, 170-179.
104. I. P. Ting, *Ann. Rev. Plant Physiol.*, 1985, **36**, 595-622.
105. A. S. Raghavendra and R. F. Sage, *C4 Photosynthesis and Related CO2 Concentrating Mechanisms*, Springer Science & Business Media, 2010.
106. R. F. Sage, *New Phytol.*, 2004, **161**, 341-370.
107. H. Matsumura, Y. Xie, S. Shirakata, T. Inoue, T. Yoshinaga, Y. Ueno, K. Izui and Y. Kai, *Structure*, 2002, **10**, 1721-1730.
108. J. K. Paulus, D. Schlieper and G. Groth, *Nature Commun.*, 2013, **4**, 1518.
109. I. P. Ting and C. B. Osmond, *Plant. Physiol.*, 1973, **51**, 448-453.
110. Y. Kai, H. Matsumura, T. Inoue, K. Terada, Y. Nagara, T. Yoshinaga, A. Kihara, K. Tsumura and K. Izui, *Proc. Natl. Acad. Sci.*, 1999, **96**, 823-828.
111. O. E. Bläsing, P. Westhoff and P. Svensson, *J. Biol. Chem.*, 2000, **275**, 27917-27923.
112. C. P. Osborne and D. J. Beerling, *Philos. Trans. R. Soc. Lond. B Biol. Sci.*, 2006, **361**, 173-194.
113. V. Grignard, *Compt. Rend.*, 1900, **130**, 1322-1325.
114. M. Orchin, *J. Chem. Educ.*, 1989, **66**, 586.
115. A. V. Nemukhin, I. A. Topol and F. Weinhold, *Inorg. Chem.*, 1995, **34**, 2980-2983.
116. R. W. Hoffmann and B. Holzer, *Chem. Commun.*, 2001, 491-492.
117. F. Blasberg, M. Bolte, M. Wagner and H.-W. Lerner, *Organometallics*, 2012, **31**, 1001-1005.
118. A. M. Fracaroli, H. Furukawa, M. Suzuki, M. Dodd, S. Okajima, F. Gándara, J. A. Reimer and O. M. Yaghi, *J. Am. Chem. Soc.*, 2014, **136**, 8863-8866.
119. H. Furukawa, K. E. Cordova, M. O'Keeffe and O. M. Yaghi, *Science*, 2013, **341**.
120. O. M. Yaghi, M. O'Keeffe, N. W. Ockwig, H. K. Chae, M. Eddaoudi and J. Kim, *Nature*, 2003, **423**, 705-714.
121. V. Guillermin, F. Ragon, M. Dan-Hardi, T. Devic, M. Vishnuvarthan, B. Campo, A. Vimont, G. Clet, Q. Yang, G. Maurin, G. Férey, A. Vittadini, S. Gross and C. Serre, *Angew. Chem.*, 2012, **51**, 9267-9271.
122. Y. Fu, D. Sun, Y. Chen, R. Huang, Z. Ding, X. Fu and Z. Li, *Angew. Chem. Int. Ed.*, 2012, **51**, 3364-3367.
123. D. Saha, T. Maity, S. Das and S. Koner, *Dalton Trans.*, 2013, **42**, 13912-13922.
124. H. X. Deng, S. Grunder, K. E. Cordova, C. Valente, H. Furukawa, M. Hmadeh, F. Gandara, A. C. Whalley, Z. Liu, S. Asahina, H. Kazumori, M. O'Keeffe, O. Terasaki, J. F. Stoddart and O. M. Yaghi, *Science*, 2012, **336**, 1018-1023.
125. H. Li, M. Eddaoudi, M. O'Keeffe and O. M. Yaghi, *Nature*, 1999, **402**, 276-279.
126. O. K. Farha, I. Eryazici, N. C. Jeong, B. G. Hauser, C. E. Wilmer, A. A. Sarjeant, R. Q. Snurr, S. T. Nguyen, A. Ö. Yazaydin and J. T. Hupp, *J. Am. Chem. Soc.*, 2012, **134**, 15016-15021.
127. H. Furukawa, Y. B. Go, N. Ko, Y. K. Park, F. J. Uribe-Romo, J. Kim, M. O'Keeffe and O. M. Yaghi, *Inorg. Chem.*, 2011, **50**, 9147-9152.
128. A. C. Kizzie, A. G. Wong-Foy and A. J. Matzger, *Langmuir*, 2011, **27**, 6368-6373.
129. J. Liu, P. K. Thallapally, B. P. McGrail, D. R. Brown and J. Liu, *Chem. Soc. Rev.*, 2012, **41**, 2308-2322.
130. Y. K. Hwang, D. Y. Hong, J. S. Chang, S. H. Jung, Y. K. Seo, J. Kim, A. Vimont, M. Daturi, C. Serre and G. Férey, *Angew. Chem.-Int. Edit.*, 2008, **47**, 4144-4148.
131. C. E. Wilmer, M. Leaf, C. Y. Lee, O. K. Farha, B. G. Hauser, J. T. Hupp and R. Q. Snurr, *Nature Chem.*, 2012, **4**, 83-89.
132. A. L. Dzubak, L.-C. Lin, J. Kim, J. A. Swisher, R. Poloni, S. N. Maximoff, B. Smit and L. Gagliardi, *Nature Chem.*, 2012, **4**, 810-816.

- 133.X. Q. Kong, H. X. Deng, F. Y. Yan, J. Kim, J. A. Swisher, B. Smit, O. M. Yaghi and J. A. Reimer, *Science*, 2014, **341**, 882-885.
- 134.D. Banerjee and J. B. Parise, *Cryst. Growth Des.*, 2011, **11**, 4704-4720 and references therein.
- 5 135.M. Dinča and J. R. Long, *J. Am. Chem. Soc.*, 2005, **127**, 9376-9377.
- 136.L. Han, L. Qin, X. Z. Yan, L. P. Xu, J. L. Sun, L. Yu, H. B. Chen and X. D. Zou, *Cryst. Growth Des.*, 2013, **13**, 1807-1811.
- 137.Y. Liu, Y.-P. Chen, T.-F. Liu, A. A. Yakovenko, A. M. Raiff and H.-C. Zhou, *Cryst. Eng. Comm.*, 2013, **15**, 9688-9693.
- 10 138.D. Britt, H. Furukawa, B. Wang, T. G. Glover and O. M. Yaghi, *Proc. Natl. Acad. Sci.*, 2009, **106**, 20637-20640.
- 139.J. G. Vitillo, L. Regli, S. Chavan, G. Ricchiardi, G. Spoto, P. D. C. Dietzel, S. Bordiga and A. Zecchina, *J. Am. Chem. Soc.*, 2008, **130**, 8386-8396.
- 15 140.C. Prestipino, L. Regli, J. G. Vitillo, F. Bonino, A. Damin, C. Lamberti, A. Zecchina, P. L. Solari, K. O. Kongshaug and S. Bordiga, *Chem. Mat.*, 2006, **18**, 1337-1346.
- 141.P. D. C. Dietzel, V. Besikiotis and R. Blom, *J. Mater. Chem.*, 2009, **19**, 7362-7370.
- 20 142.W. L. Queen, C. M. Brown, D. K. Britt, P. Zajdel, M. R. Hudson and O. M. Yaghi, *J. Phys. Chem. C*, 2011, **115**, 24915-24919.
- 143.W. Zhou, H. Wu and T. Yildirim, *J. Am. Chem. Soc.*, 2008, **130**, 15268-15269.
- 144.L. Valenzano, B. Civalieri, S. Chavan, G. Turnes Palomino, C. Otero 25 Areán and S. Bordiga, *J. Phys. Chem. C*, 2010, **114**, 11185-11191.
- 145.A. Pulido, M. R. Delgado, O. Bludsky, M. Rubes, P. Nachtigall and C. O. Arean, *Environ. Sci.*, 2009, **2**, 1187-1195.
- 146.Y. F. Chen, A. Nalaparaju, M. Eddaoudi and J. W. Jiang, *Langmuir*, 2012, **28**, 3903-3910.
- 30 147.T. M. McDonald, W. R. Lee, J. A. Mason, B. M. Wiers, C. S. Hong and J. R. Long, *J. Am. Chem. Soc.*, 2012, **134**, 7056-7065.
- 148.S. Choi, T. Watanabe, T.-H. Bae, D. S. Sholl and C. W. Jones, *J. Phys. Chem. Lett.*, 2012, **3**, 1136-1141.
- 149.J. Yu and P. B. Balbuena, *J. Phys. Chem. C*, 2013, **117**, 3383-3388.
- 35 150.Y. E. Cheon, J. Park and M. P. Suh, *Chem. Commun.*, 2009, 5436-5438.
- 151.Y. Cao, F. Song, Y. Zhao and Q. Zhong, *J. Environ. Sci.*, 2013, **25**, 2081-2087.
- 152.T. M. McDonald, J. A. Mason, X. Kong, E. D. Bloch, D. Gygi, A. 40 Dani, V. Crocella, F. Giordanino, S. O. Odoh, W. S. Drisdell, B. Vlaisavljevich, A. L. Dzubak, R. Poloni, S. K. Schnell, N. Planas, K. Lee, T. Pascal, L. F. Wan, D. Prendergast, J. B. Neaton, B. Smit, J. B. Kortright, L. Gagliardi, S. Bordiga, J. A. Reimer and J. R. Long, *Nature*, 2015, accepted.
- 45 153.D.-Y. Hong, Y. K. Hwang, C. Serre, G. Férey and J.-S. Chang, *Adv. Funct. Mater.*, 2009, **19**, 1537-1552.
- 154.A. Demessence, D. M. D'Alessandro, M. L. Foo and J. R. Long, *J. Am. Chem. Soc.*, 2009, **131**, 8784-8785.
- 155.J. C. Hicks, J. H. Drese, D. J. Fauth, M. L. Gray, G. G. Qi and C. W. 50 Jones, *J. Am. Chem. Soc.*, 2008, **130**, 2902-2903.
- 156.J. Ethiraj, E. Albanese, B. Civalieri, J. G. Vitillo, F. Bonino, S. Chavan, G. C. Shearer, K. P. Lillerud and S. Bordiga, *Chem. Sus. Chem.*, 2014, **7**, 3382-3388.
- 157.K. L. Gurunatha, K. Uemura and T. K. Maji, *Inorg. Chem.*, 2008, **47**, 55 6578-6580.
- 158.A. Rossin, A. Ienco, F. Costantino, T. Montini, B. Di Credico, M. Caporali, L. Gonsalvi, P. Fornasiero and M. Peruzzini, *Cryst. Growth Des.*, 2008, **8**, 3302-3308.
- 159.J. A. Rood, B. C. Noll and K. W. Henderson, *Inorg. Chem.*, 2006, **45**, 5521-5528.
- 60 160.A. Mallick, S. Saha, P. Pachfule, S. Roy and R. Banerjee, *Inorg. Chem.*, 2011, **50**, 1392-1401.
- 161.A. Rossin, M. R. Chierotti, G. Giambastiani, R. Gobetto and M. Peruzzini, *Cryst. Eng. Comm.*, 2012, **14**, 4454-4460.
- 65 162.A. Mallick, S. Saha, P. Pachfule, S. Roy and R. Banerjee, *J. Mater. Chem.*, 2010, **20**, 9073-9080.
- 163.P. D. C. Dietzel, R. Blom and H. Fjellvåg, *Eur. J. Inorg. Chem.*, 2008, **2008**, 3624-3632.
- 164.Z. R. Herm, J. A. Swisher, B. Smit, R. Krishna and J. R. Long, *J. Am. 70 Chem. Soc.*, 2011, **133**, 5664-5667.
- 165.J. M. C. Plane and C. L. Whalley, *J. Phys. Chem. A*, 2012, **116**, 6240-6252.
- 166.J. J. Olivero and G. E. Thomas, *Adv. Space Res.*, 2001, **28**, 931-936.
- 167.J. M. C. Plane, *Chem. Rev.*, 2003, **103**, 4963-4984.
- 75 168.N. McBride, S. F. Green and J. A. M. McDonnell, *Adv. Space Res.*, 1999, **23**, 73-82.
- 169.B. Mason, *Handbook of elemental abundances of the elements in meteorites*, Gordon and Breach, Newark, NJ, 1971.
- 170.W. Swider, *Planet. Space Sci.*, 1984, **32**, 307-312.
- 80 171.M. Scharringhausen, *Investigation of Mesospheric and Thermospheric Magnesium Species from Space*, VDM Verlag Dr. Mueller e. K, Saarbrücken, Germany, 2007.
- 172.J. M. C. Plane, C. S. Gardner, J. Yu, C. Y. She, R. R. Garcia and H. C. Pumphrey, *J. Geophys. Res.*, 1999, **104**, 3773-3788.
- 85 173.S. Campbell, P. Hollins, E. McCash and M. W. Roberts, *J. Electron Spectrosc. Relat. Phenom.*, 1986, **39**, 145-153.
- 174.R. G. Copperthwaite, P. R. Davies, M. A. Morris, M. W. Roberts and R. A. Ryder, *Catal. Lett.*, 1988, **1**, 11-19.
- 175.M. B. Jensen, L. G. M. Pettersson, O. Swang and U. Olsbye, *J. Phys. 90 Chem. B*, 2005, **109**, 16774-16781.
- 176.H. Kawakami and S. Yoshida, *J. Chem. Soc., Faraday Trans.*, 1984, **80**, 921-932.
- 177.L. Hopkinson, P. Kristova, K. Rutt and G. Cressey, *Geochim. Cosmochim. Acta*, 2012, **76**, 1-13.
- 95 178.B.-J. Kim, K.-S. Cho and S.-J. Park, *J. Colloid Interface Sci.*, 2010, **342**, 575-578.
- 179.W. H. Cheng and H. H. Kung, *Surf. Sci.*, 1981, **102**, L21-L28.
- 180.E. N. Gribov, S. Bertarione, D. Scarano, C. Lamberti, G. Spoto and A. Zecchina, *J. Phys. Chem. B*, 2004, **108**, 16174-16186.
- 100 181.G. Spoto, E. N. Gribov, G. Ricchiardi, A. Damin, D. Scarano, S. Bordiga, C. Lamberti and A. Zecchina, *Progr. Surf. Sci.*, 2004, **76**, 71-146.
- 182.M.-L. Bailly, G. n. Costentin, H. I. n. Lauron-Pernot, J. M. Krafft and M. Che, *J. Phys. Chem. B*, 2004, **109**, 2404-2413.
- 105 183.C. Chizallet, G. Costentin, M. Che, F. Delbecq and P. Sautet, *J. Phys. Chem. B*, 2006, **110**, 15878-15886.
- 184.E. Knözinger, K.-H. Jacob, S. Singh and P. Hofmann, *Surf. Sci.*, 1993, **290**, 388-402.
- 185.C. Chizallet, G. Costentin, M. Che, F. Delbecq and P. Sautet, *J. Am. 110 Chem. Soc.*, 2007, **129**, 6442-6452.

- 186.Y. Fukuda and K. Tanabe, *Bull. Chem. Soc. Jpn.*, 1973, **46**, 1616-1619.
- 187.R. A. Robie, B. S. Hemingway and J. R. Fisher, "*Thermodynamic properties of minerals and related substances at 298.15 K and 1 bar (10⁵ pascals) pressure and at high temperatures*", Bulletin 1452, U.S. Geological Survey, Washington DC, 1984.
- 188.K. Nakagawa and T. Ohashi, *J. Electrochem. Soc.*, 1998, **145**, 1344-1346.
- 189.R. V. Siriwardane, *Regenerable Sorbents for CO₂ Capture from Moderate and High Temperature Applications*, 2008, U.S. Patent 7,314,847.
- 190.J. Roggenbuck, G. Koch and M. Tiemann, *Chem. Mater.*, 2006, **18**, 4151-4156.
- 191.J. Roggenbuck and M. Tiemann, *J. Am. Chem. Soc.*, 2005, **127**, 1096-1097.
- 192.K. K. Han, Y. Zhou, Y. Chun and J. H. Zhu, *J. Hazard. Mater.*, 2012, **203**, 341-347.
- 193.Z. Zhao, H. Dai, Y. Du, J. Deng, L. Zhang and F. Shi, *Mater Chem Phys*, 2011, **128**, 348-356.
- 194.S. Utamapanya, K. J. Klabunde and J. R. Schlup, *Chem. Mat.*, 1991, **3**, 175-181.
- 195.R. Das, P. Pachfule, R. Banerjee and P. Poddar, *Nanoscale*, 2012, **4**, 591-599.
- 196.S.-W. Bian, J. Baltrusaitis, P. Galhotra and V. H. Grassian, *J. Mater. Chem.*, 2010, **20**, 8705-8710.
- 197.M. Bhagiyalakshmi, J. Y. Lee and H. T. Jang, *Int. J. Greenh. Gas Control*, 2010, **4**, 51-56.
- 198.K. K. Han, Y. Zhou, W. G. Lin and J. H. Zhu, *Micropor. Mesopor. Mater.*, 2013, **169**, 112-119.
- 199.H. N. Li, L. Zhang, H. X. Dai and H. He, *Inorg. Chem.*, 2009, **48**, 4421-4434.
- 200.W.-J. Liu, H. Jiang, K. Tian, Y.-W. Ding and H.-Q. Yu, *Environ. Sci. Technol.*, 2013, **47**, 9397-9403.
- 201.Y. Wang, J. H. Zhu, J. M. Cao, Y. Chun and Q. H. Xu, *Micropor. Mesopor. Mater.*, 1998, **26**, 175-184.
- 202.J. H. Zhu, Y. Wang, Y. Chun, Z. Xing and Q. H. Xu, *Mater. Lett.*, 1998, **35**, 177-182.
- 203.D. Barthomeuf, *Catal. Rev.*, 1996, **38**, 521-612.
- 204.Y. L. Wei, Y. M. Wang, J. H. Zhu and Z. Y. Wu, *Adv. Mater.*, 2003, **15**, 1943-1945.
- 205.J. C. Mabry and K. Mondal, *Environ. Technol.*, 2011, **32**, 55-67.
- 206.X. C. Yan, H. Guo, D. J. Yang, S. L. Qiu and X. D. Yao, *Curr. Org. Chem.*, 2014, **18**, 1335-1345.
- 207.Z. Kowalczyk, K. Stolecki, W. Rarog-Pilecka, E. b. Miskiewicz, E. Wilczkowska and Z. Karpinski, *Appl. Catal. A*, 2008, **342**, 35-39.
- 208.H. Y. Kim, H. M. Lee and J.-N. Park, *J. Phys. Chem. C*, 2010, **114**, 7128-7131.
- 209.S. Mori, W. C. Xu, T. Ishidzuki, N. Ogasawara, J. Imai and K. Kobayashi, *Appl. Catal. A*, 1996, **137**, 255-268.
- 210.J. Rostrup-Nielsen, U.S. Pat., 3,791,993, 1974.
- 211.J. Zhang, H. Wang, C. Xi, M. Shakouri, Y. Hu and A. K. Dalai, in *Nanocatalysis for Fuels and Chemicals*, American Chemical Society, 2012, vol. 1092, pp. 195-221.
- 212.H. Y. Wang and E. Ruckenstein, *Appl. Catal. A*, 2000, **204**, 143-152.
- 213.K. Nagaoka, M. Okamura and K.-I. Aika, *Catal. Commun.*, 2001, **2**, 255-260.
- 214.A. Ballarini, F. Basile, P. Benito, I. Bersani, G. Fornasari, S. de Miguel, S. C. P. Maina, J. Vilella, A. Vaccari and O. A. Scelza, *Appl. Catal. A-Gen.*, 2012, **433**, 1-11.
- 215.L. Desgranges, G. Calvarin and G. Chevrier, *Acta Cryst.*, 1996, **52**, 82-86.
- 216.M. Bellotto, B. Rebours, O. Clause, J. Lynch, D. Bazin and E. Elkaïm, *J. Phys. Chem.*, 1996, **100**, 8527-8534.
- 217.S.-H. Hong, M.-S. Jang, S. J. Cho and W.-S. Ahn, *Chem. Commun.*, 2014, **50**, 4927-4930.
- 218.G. R. Williams and D. O'Hare, *J. Mater. Chem.*, 2006, **16**, 3065-3074.
- 219.V. Rives and S. Kannan, *J. Mater. Chem.*, 2000, **10**, 489-495.
- 220.Q. Wang, H. H. Tay, Z. Zhong, J. Luo and A. Borgna, *Energy Environ. Sci.*, 2012, **5**, 7526-7530.
- 221.G. Fetter, M. T. Olguán, P. Bosch and S. Bulbulian, *J. Porous Mater.*, 2000, **7**, 469-473.
- 222.A. Garcia-Gallastegui, D. Iruretagoyena, V. Gouvea, M. Mokhtar, A. M. Asiri, S. N. Basahel, S. A. Al-Thabaiti, A. O. Alyoubi, D. Chadwick and M. S. P. Shaffer, *Chem. Mater.*, 2012, **24**, 4531-4539.
- 223.S. Choi, J. H. Drese and C. W. Jones, *Chem. Sus. Chem.*, 2009, **2**, 796-854.
- 224.E. Ochoa-Fernandez, H. K. Rusten, H. A. Jakobsen, M. Ronning, A. Holmen and D. Chen, *Catal. Today*, 2005, **106**, 41-46.
- 225.C. T. Yavuz, B. D. Shinall, A. V. Iretskii, M. G. White, T. Golden, M. Atilhan, P. C. Ford and G. D. Stucky, *Chem. Mat.*, 2009, **21**, 3473-3475.
- 226.A. F. Lucredio, J. M. Assaf and E. M. Assaf, *Appl. Catal. A-Gen.*, 2011, **400**, 156-165.
- 227.Y. Gao, Z. Zhang, J. Wu, X. Yi, A. Zheng, A. Umar, D. O'Hare and Q. Wang, *J. Mater. Chem. A*, 2013, **1**, 12782-12790.
- 228.D. Aymes, D. Ballivet-Tkatchenko, K. Jeyalakshmi, L. Saviot and S. Vasireddy, *Catal. Today*, 2009, **147**, 62-67.
- 229.A. Sanna, M. Uibu, G. Caramanna, R. Kuusik and M. M. Maroto-Valer, *Chem. Soc. Rev.*, 2014, **43**, 8049-8080.
- 230.H. Gies and H. van Koningsveld, *Catalog of Disorder in Zeolite Frameworks*, <http://www.iza-structure.org/databases/>.
- 231.P. Nachtigall, L. Grajciar, J. Perez-Pariente, A. B. Pinar, A. Zukal and J. Cejka, *Phys. Chem. Chem. Phys.*, 2012, **14**, 1117-1120.
- 232.F. Su and C. Lu, *Energy Env. Sci.*, 2012, **5**, 9021-9027.
- 233.Q. Liu, T. Pham, M. D. Porosoff and R. F. Lobo, *Chem. Sus. Chem.*, 2012, **5**, 2237-2242.
- 234.J. Zhang, R. Singh and P. A. Webley, *Micropor. Mesopor. Mater.*, 2008, **111**, 478-487.
- 235.M. Palomino, A. Corma, F. Rey and S. Valencia, *Langmuir*, 2009, **26**, 1910-1917.
- 236.T. Remy, S. A. Peter, L. Van Tendeloo, S. Van der Perre, Y. Lorgouilloux, C. E. A. Kirschhock, G. V. Baron and J. F. M. Denayer, *Langmuir*, 2013, **29**, 4998-5012.
- 237.S. Y. Zhang, O. Talu and D. T. Hayhurst, *J. Phys. Chem.*, 1991, **95**, 1722-1726.
- 238.J. J. Pluth and J. V. Smith, *J. Am. Chem. Soc.*, 1980, **102**, 4704-4708.
- 239.J. Liu, Y. Wang, A. I. Benin, P. Jakubczak, R. R. Willis and M. D. LeVan, *Langmuir*, 2010, **26**, 14301-14307.
- 240.O. Zavorotynska, J. G. Vitillo, G. Spoto and A. Zecchina, *Int. J. Hydrogen Energy*, 2011, **36**, 7944-7950.

- 241.C. Pazé, S. Bordiga, C. Lamberti, M. Salvalaggio, A. Zecchina and G. Bellussi, *J. Phys. Chem. B*, 1997, **101**, 4740-4751.
- 242.Y.-K. Kim, Y.-H. Mo, J. Lee, H.-S. You, C.-K. Yi, Y. C. Park and S.-E. Park, *J. Nanosci. Nanotechnol.*, 2013, **13**, 2703-2707.
- 5 243.H. Tsuji, F. Yagi, H. Hattori and H. Kita, in *Studies in Surface Science and Catalysis*, eds. L. Guzzi, F. Solymosi and P. Tétényi, Elsevier, Budapest, 1993, vol. 75, pp. 1171-1183.
- 244.J. G. Vitillo et al., *J. Mater. Chem.*, 2015, in preparation.
- 245.F. Bergaya, B. K. G. Theng and G. Lagaly, *Developments in Clay Science in Handbook of clay science*, Elsevier, Oxford, 2006.
- 10 246.C. Chen, D.-W. Park and W.-S. Ahn, *Appl. Surf. Sci.*, 2013, **283**, 699-704.
- 247.F. Bardelli, C. Mondelli, M. Didier, J. G. Vitillo, D. R. Cavicchia, J.-C. Robinet, L. Leone and L. Charlet, *Appl. Geochem.*, 2014, **49**, 168-177.
- 15 248.C. Mondelli, F. Bardelli, J. G. Vitillo, M. Didier, J. Brendle, D. R. Cavicchia, J.-C. Robinet and L. Charlet, *Int. J. Hydrogen Energy*, 2015, **40**, 2698-2709.
- 249.W. Wang, X. Wang, C. Song, X. Wei, J. Ding and J. Xiao, *Energy Fuels*, 2013, **27**, 1538-1546.
- 20 250.P. B. Kelemen and J. r. Matter, *Proc. Natl. Acad. Sci. U. S. A.*, 2008.
- 251.W. K. O'Connor, D. C. Dahlin, G. E. Rush, C. L. Dahlin and W. K. Collins, *Miner. Metall. Proc.*, 2002, **19**, 95-101.
- 252.S. J. Gerdemann, W. K. O'Connor, D. C. Dahlin, L. R. Penner and H. Rush, *Envir. Sci. Techn.*, 2007, **41**, 2587-2593.
- 25 253.M. J. McKelvy, A. V. G. Chizmeshya, J. Diefenbacher, H. Béarat and G. Wolf, *Envir. Sci. Techn.*, 2004, **38**, 6897-6903.
- 254.F. Larachi, I. Daldoul and G. Beaudoin, *Geochim. Cosmochim. Acta*, 2010, **74**, 3051-3075.
- 255.H. C. Oskierski, B. Z. Dlugogorski and G. Jacobsen, *Chem. Geol.*, 30 2013, **358**, 156-169.
- 256.F. Larachi, J. P. Gravel, B. P. A. Grandjean and G. Beaudoin, *Int. J. Greenh. Gas Control*, 2012, **6**, 69-76.
- 257.S. Chatterjee, S. Sengupta, T. Saha-Dasgupta, K. Chatterjee and N. Mandal, *Phys. Rev. B*, 2009, **79**.
- 35 258.D. Gournis, A. Lappas, M. A. Karakassides, D. Töbrens and A. Moukarika, *Phys. Chem. Minerals*, 2008, **35**, 49-58.
- 259.B. Fubini and C. Otero Areal, *Chem. Soc. Rev.*, 1999, **28**, 373-381.
- 260.F. Turci, M. Tomatis, S. Mantegna, G. Cravotto and B. Fubini, *J. Environ. Monitor.*, 2007, **9**, 1064-1066.
- 40 261.R. Lafay, G. Montes-Hernandez, E. Janots, R. Chiriach, N. Findling and F. Toche, *Chem. Eur. J.*, 2013, **19**, 5417-5424.
- 262.A. K. Chakraborty, K. B. Bischoff, G. Astarita and J. R. Damewood, *J. Am. Chem. Soc.*, 1988, **110**, 6947-6954.
- 263.N. P. Stadie, E. Callini, B. Richter, T. R. Jensen, A. Borgschulte and 45 A. Züttel, *J. Am. Chem. Soc.*, 2014, **136**, 8181-8184.
- 264.B. T. Thompson, T. N. Gallaher and T. C. DeVore, *Polyhedron*, 1983, **2**, 619-621.
- 265.C. L. Hugelshofer, A. Borgschulte, E. Callini, S. K. Matam, J. Gehrig, D. T. Hog and A. Züttel, *J. Phys. Chem. C*, 2014, **118**, 15940- 50 15945.
- 266.H. Ando, M. Fujiwara, Y. Matsumura, H. Miyamura, H. Tanaka and Y. Souma, *J. Alloy. Compd.*, 1995, **223**, 139-141.
- 267.E. Akiba, Y. Y. Ishido, H. Hayakawa, S. Shin and K. Nomura, *Z. Phys. Chemie*, 1989, **164**, 1319-1324.
- 55 268.A. A. Peterson, F. Abild-Pedersen, F. Studt, J. Rossmeisl and J. K. Nørskov, *Energy Environ. Sci.*, 2010, **3**, 1311-1315.
- 269.K. J. Williams, A. B. Boffa, M. Salmeron, A. T. Bell and G. A. Somorjai, *Catal. Lett.*, 1991, **9**, 415-426.
- 270.J. Ye, C. Liu and Q. Ge, *J. Phys. Chem. C*, 2012, **116**, 7817-7825.
- 60 271.M. Tian, Master Thesis, University of East Anglia, 2010.
- 272.S. Bouaricha, J. Huot, D. Guay and R. Schulz, *Int. J. Hydrogen Energy*, 2002, **27**, 909-913.
- 273.A. S. Pedersen and B. Larsen, *Int. J. Hydrogen En.*, 1993, **18**, 297-300.
- 65 274.P. M. Zimmerman, Z. Zhang and C. B. Musgrave, *Inorg. Chem.*, 2010, **49**, 8724-8728.
- 275.J. Zhang, Y. Zhao, D. L. Akins and J. W. Lee, *J. Phys. Chem. C*, 2011, **115**, 8386-8392.
- 276.R. Xiong, J. S. Zhang and J. W. Lee, *J. Phys. Chem. C*, 2013, **117**, 70 3799-3803.
- 277.J. S. Zhang and J. W. Lee, *Carbon*, 2013, **53**, 216-221.
- 278.J. S. Zhang, A. Byeon and J. W. Lee, *J. Mater. Chem. A*, 2013, **1**, 8665-8671.
- 279.J. S. Zhang, Y. Zhao, X. D. Guan, R. E. Stark, D. L. Akins and J. W. 75 Lee, *J. Phys. Chem. C*, 2012, **116**, 2639-2644.
- 280.T. Wartik and R. K. Pearson, *J. Inorg. Nuclear Chem.*, 1958, **7**, 404-411.
- 281.G. W. Gribble and C. F. Nutaitis, *Org. Prep. Proced. Int.*, 1985, **17**, 317-384.
- 80 282.J. G. Burr, W. G. Brown and H. E. Heller, *J. Am. Chem. Soc.*, 1950, **72**, 2560-2562.
- 283.R. Xiong, J. Zhang, Y. Zhao, D. L. Akins and J. W. Lee, *Int. J. Hydrogen En.*, 2012, **37**, 3344-3349.
- 284.Y. Filinchuk, B. Richter, T. R. Jensen, V. Dmitriev, D. Chernyshov 85 and H. Hagemann, *Angew. Chem. Int. Ed.*, 2011, **50**, 11162-11166.
- 285.A. Züttel, *Proceedings of the MH2014 Conference*, 2014, Manchester, UK.
- 286.N. Armaroli and V. Balzani, *Angew. Chem. Int. Ed.*, 2007, **46**, 52-66.
- 287.J. Rabone, Y. F. Yue, S. Y. Chong, K. C. Stylianou, J. Bacsa, D. 90 Bradshaw, G. R. Darling, N. G. Berry, Y. Z. Khimiyak, A. Y. Ganin, P. Wiper, J. B. Claridge and M. J. Rosseinsky, *Science*, 2010, **329**, 1053-1057.
- 288.A. Schneemann, V. Bon, I. Schwedler, I. Senkovska, S. Kaskel and R. A. Fischer, *Chem. Soc. Rev.*, 2014, **43**, 6062-6096.
- 95 289.T. Loiseau, C. Serre, C. Huguénard, G. Fink, F. Taulelle, M. Henry, T. Bataille and G. Férey, *Chem. Eur. J.*, 2004, **10**, 1373-1382.
- 290.M. Kandiah, M. H. Nilsen, S. Usseglio, S. Jakobsen, U. Olsbye, M. Tilset, C. Larabi, E. A. Quadrelli, F. Bonino and K. P. Lillerud, *Chem. Mater.*, 2010, **22**, 6632-6640.
- 100 291.C. Volkringer, M. Meddouri, T. Loiseau, N. Guillou, J. Marrot, G. Férey, M. Haouas, F. Taulelle, N. Audebrand and M. Latroche, *Inorg. Chem.*, 2008, **47**, 11892-11901.
- 292.C. Petit, J. Burress and T. J. Bandoz, *Carbon*, 2011, **49**, 563-572.
- 293.C. Petit and T. J. Bandoz, *Adv. Funct. Mater.*, 2011, **21**, 2108-2117.
- 105 294.Y. Zhao, M. Seredych, Q. Zhong and T. J. Bandoz, *RSC Adv.*, 2013, **3**, 9932-9941.
- 295.L. Hou, W.-J. Shi, Y.-Y. Wang, Y. Guo, C. Jin and Q.-Z. Shi, *Chem. Commun.*, 2011, **47**, 5464-5466.
- 296.C. Chen, S. T. Yang, W. S. Ahn and R. Ryoo, *Chem. Commun.*, 110 2009, 3627-3629.
- 297.T. M. McDonald et al., *Nature*, 2015, accepted.

- 298.G. K. Parshetti, S. Chowdhury and R. Balasubramanian, *RSC Adv.*, 2014, **4**, 44634-44643.
- 299.J. Song, W. Shen, J. Wang and W. Fan, *Carbon*, 2014, **69**, 255-263.
- 300.S. H. Lamtom and R. A. Savidge, *Biomass Bioen.*, 2003, **25**, 381-388.
301. http://www.extension.org/pages/70456/poplar-populus-spp-trees-for-biofuel-production#.VGfRr_mG98F, 2013.
302. http://www.arsia.toscana.it/UserFiles/File/Woodland/Risultati_di_un_progetto_triennale_finanziato_dalla_CCIAA_di_Padova.pdf, 2014.
- 303.A. Brunori, *Legno ed energia: come produrre energie con le biomasse agricole (in italian)*, Il Sole 24 Ore Edagricole, 2008.
- 304.E. N. Speelman, M. M. L. Van Kempen, J. Barke, H. Brinkhuis, G. J. Reichart, A. J. P. Smolders, J. G. M. Roelofs, F. Sangiorgi, J. W. De Leeuw, A. F. Lotter and J. S. Sinninghe Damsté, *Geobiol.*, 2009, **7**, 155-170.
- 305.H. Brinkhuis, S. Schouten, M. E. Collinson, A. Sluijs, J. S. S. Damsté, G. R. Dickens, M. Huber, T. M. Cronin, J. Onodera, K. Takahashi, J. P. Bujak, R. Stein, J. van der Burgh, J. S. Eldrett, I. C. Harding, A. F. Lotter, F. Sangiorgi, H. v. K.-v. Cittert, J. W. de Leeuw, J. Matthiessen, J. Backman, K. Moran and S. the Expedition, *Nature*, 2006, **441**, 606-609.
- 306.D.-J. Shi and D. Hall, *Bot. Rev.*, 1988, **54**, 353-386.
- 307.M. S. A. Rahaman, L.-H. Cheng, X.-H. Xu, L. Zhang and H.-L. Chen, *Renew. Sustain. Energy Rev.*, 2011, **15**, 4002-4012.
- 308.Y.-B. Seo, Y.-W. Lee, C.-H. Lee and H.-C. You, *Biores. Technol.*, 2010, **101**, 2549-2553.
309. <http://theazollafoundation.org/>, 2014.
- 310.M. H. Yoon, Y. W. Lee, C. H. Lee and Y. B. Seo, *Biores. Technol.*, 2012, **126**, 198-201.
- 311.A. J. Ragauskas, C. K. Williams, B. H. Davison, G. Britovsek, J. Cairney, C. A. Eckert, W. J. Frederick, J. P. Hallett, D. J. Leak, C. L. Liotta, J. R. Mielenz, R. Murphy, R. Templer and T. Tschaplinski, *Science*, 2006, **311**, 484-489.
- 312.K. Ashworth, O. Wild and C. N. Hewitt, *Nature Clim. Change*, 2013, **3**, 492-496.
- 313.D. Taraborrelli, M. G. Lawrence, J. N. Crowley, T. J. Dillon, S. Gromov, C. B. M. Grosz, L. Vereecken and J. Lelieveld, *Nature Geosci.*, 2011, **5**, 190-193.
- 314.A. T. Archibald, *Nature Geosci.*, 2011, **4**, 659-660.
- 315.S. von Caemmerer, W. P. Quick and R. T. Furbank, *Science*, 2012, **336**, 1671-1672.
- 316.S. Rachmilevitch, A. B. Cousins and A. J. Bloom, *Proc. Natl. Acad. Sci. U.S.A.*, 2004, **101**, 11506-11510.

45